UNIVERSIDAD
DE LA REPUBLICA
URUGUAY

Air quality evaluation in Uruguayan operating rooms

Evaluation of parameters, practices and measures associated with air quality in Uruguayan hospitals using air quality reports and computational fluid mechanics

Federico Hugo Licandro Errazola

Postgraduate program in Maestría en Ingeniería Mecánica
Facultad de Ingeniería
Universidad de la República

Montevideo – Uruguay
September of 2024

UNIVERSIDAD
DE LA REPUBLICA
URUGUAY

Air quality evaluation in Uruguayan operating rooms

Evaluation of parameters, practices and measures associated with air quality in Uruguayan hospitals using air quality reports and computational fluid mechanics

Federico Hugo Licandro Errazola

Master's Thesis submitted to the Postgraduate Program in Maestría en Ingeniería Mecánica, Facultad de Ingeniería of the Universidad de la República, as part of the necessary requirements for obtaining the title of Master in Maestría en Ingeniería Mecánica.

Director:
Ph.D. Ing. Federico Favre

Co-advisor:
M.Sc. Ing. Ana Urquiola

Academic director:
Ph.D. Ing. Federico Favre

Montevideo – Uruguay
September of 2024

Licandro Errazola, Federico Hugo

Air quality evaluation in Uruguayan operating rooms / Federico Hugo Licandro Errazola. - Montevideo: Universidad de la República, Facultad de Ingeniería, 2024.

XVII, 94 p.: il.; 29, 7cm.

Director:

Federico Favre

Co-advisor:

Ana Urquiola

Academic director:

Federico Favre

Tesis de Maestría – Universidad de la República, Program in Maestría en Ingeniería Mecánica, 2024.

Bibliography: p. 89 – 94.

1. Infección perioperatoria, 2. Sala de operación, 3. Material particulado, 4. Dinámica de fluidos computacional, 5. Calidad de aire. I. Favre, Federico, *et al.* II. Universidad de la República, Postgraduate Program in Maestría en Ingeniería Mecánica. III. Title

MEMBERS OF THE THESIS DEFENSE COURT

Ph.D. Ing. Santiago Corzo

Ph.D. Ing. Pedro Galione

Ph.D Ing. Mariana Mendina

Montevideo – Uruguay
September of 2024

Agradecimientos

Quisiera agradecer a mis tutores Ana y Fede por depositar su confianza y acompañarme durante el proceso de mi maestría. Al IIMPI y a todos los compañeros de trabajo con los que compartí durante este proceso, por el muy agradable ambiente laboral que se ha logrado, mención especial para quienes me tuvieron que soportar en la oficina 314 durante este proceso. A los compañeros del CTTC de la Universidad Politécnica de Cataluña por recibirme en Terrassa, especialmente a Eugenio, muchas gracias por toda la ayuda y la guía con el proceso de simulación.

También quiero agradecer a la ANII por hacer posible este proceso, a CSIQ y al grupo de termodinámica aplicada (GTA) por hacer posible mi estancia en la Universidad Politécnica, al Fondo Nacional de Recursos por permitir la investigación y al CENAQUE por poner a disposición sus instalaciones.

Por último, pero sin menos importancia, quiero agradecer a mi familia y amigos, por todo el apoyo, la paciencia y la compañía; ninguno de mis logros es posible sin ustedes, y ninguno tendría sentido. En este sentido, soy una persona muy afortunada, son mi inspiración, muchísimas gracias.

ABSTRACT

This thesis evaluates air quality in Uruguayan operating rooms, focusing on both general air quality principles and a specific case study of a surgical room. The work is divided into three main parts. The first part presents a literature review on air quality, covering key parameters such as temperature, humidity, ventilation, differential pressure, and particulate concentration. It also discusses national and international air quality standards, ventilation systems (TMA and LAF), and associated maintenance practices. Additionally, air quality evaluations from 41 operating rooms in Uruguayan hospitals are analyzed using air quality reports. The results reveal a general lack of knowledge about ventilation and differential pressure management, specially for TMA rooms, despite the similar risks presented by the more controlled LAF-operated rooms. The second part focuses in the design and validation of a computational fluid dynamics code implemented in openFOAM for air quality evaluation in indoor environments. The code is validated using reference experiments. The third part focuses on a case study involving a specific OR with LAF ventilation. The CFD model is implemented to assess the impact of a partial separation wall between the air supply inlet and ceiling exhaust outlets. Three scenarios are simulated: with the separation wall installed, with a shorter wall, and without the wall. Results indicate that the partial wall improves air quality across the entire room, reducing contaminant concentration by 10.7% and increasing ventilation efficiency from 41.7% to 51.5%. Near the patient area, contaminant levels decrease by 8.32% compared to the scenario without the wall.

Keywords:
Surgical site infection, Operating Room, Particulate Matter, Computational Fluid Dynamics, Air Quality.

RESUMEN

Esta tesis evalúa la calidad del aire en salas de operación en Uruguay, enfocándose tanto en los principios generales de calidad del aire como en un caso de estudio específico. El trabajo se divide en tres partes principales. La primera parte presenta una revisión de la literatura sobre la calidad del aire, abarcando parámetros clave como la temperatura, la humedad, la ventilación, la presión diferencial y la concentración de partículas. También se discuten normativas de calidad de aire a nivel nacional e internacional, sistemas de ventilación (TMA y LAF) y las prácticas de mantenimiento asociadas. Se analizan evaluaciones de calidad de aire en 41 salas de operación de hospitales uruguayos utilizando informes de calidad del aire. Los resultados revelan un desconocimiento general sobre la gestión de la ventilación, especialmente en las salas TMA, a pesar de los riesgos similares que presentan las salas con LAF, que están más controladas. La segunda parte se centra en el diseño y validación de un código de dinámica de fluidos computacional implementado en OpenFOAM para la evaluación de la calidad del aire en ambientes interiores. El código se valida mediante experimentos de referencia. La tercera parte se enfoca en un caso de estudio que involucra una sala de operaciones con ventilación LAF. Se implementa el modelo CFD para evaluar el impacto de una pared de separación parcial entre la inyección y las salidas de techo. Se simulan tres escenarios: con la pared instalada, con una pared más corta y sin la pared. Los resultados indican que la pared parcial mejora la calidad del aire en toda la sala, reduciendo la concentración de contaminantes en un 10.7% y aumentando la eficiencia de la ventilación del 41.7% al 51.5%. Cerca del área del paciente, los niveles de contaminantes disminuyen en un 8.32% en comparación con el escenario sin la pared.

Palabras claves:
Infección perioperatoria, Sala de operación, Material particulado, Dinámica de fluidos computacional, Calidad de aire.

List of Figures

List of Tables

List of symbols

Lista de los símbolos más relevantes de la tesis.

Pr_t Heat turbulent Prandlt Number 33
C Scalar concentration of particls $(\mu g/m^3)$ 34
C_c Cunningham correction coefficient 35
D_b Brownian diffusion coefficient (m^2/s) 34
ϵ_p Turbulent diffusion coefficient (m^2/s) 34
$\hat{i}$ Directional versor 1 33
$\hat{j}$ Directional versor 2 33
$\hat{k}$ Directional versor 3 33
Sc Schmidt number 34
σ_ϵ Turbulence dissipation rate turbulent Prandlt Number 33
σ_k Turbulence kinetic energy turbulent Prandlt Number 33
σ_τ Air age turbulent Prandlt Number 33
Stk Stokes Number 31
τ Air age (s) 33
$\vec{n}$ Normal versor 36
β Volumetric thermal expansion coefficient $(1/K)$ 34
μ Density at reference temperature (kg/m^3) 31
ρ_0 Dynamic viscosity (kg/ms) 34
ρ Density (kg/m^3) 31, 33
$\vec{g}$ Gravitational acceleration (m/s^2) 34
A Implicit coefficient matrix 36
b Explicit coefficient vector 36
Φ Solution vector to the linear system 36
λ Mean free path (m) 35
p Air dynamic pressure (m^2/s^2) 33

c_p Specific heat coefficient (W/kgK) 33

T Temperature (K) 33

T_0 Reference temperature (K) 34

ϵ Turbulence dissipation rate (m^2/s^3) 33

k Turbulence kinetic energy (m^2/s^2) 33

G Turbulence generation (m^2/s^2) 34

$\vec{v}$ Velocity Vector (m/s) 33

u $\hat{i}$ Component of the velocity vector (m/s) 33

v $\hat{j}$ Component of the velocity vector (m/s) 33

w $\hat{k}$ Component of the velocity vector (m/s) 33

ν Cinematic viscosity (m^2/s) 33

ν_t Turbulent cinematic viscosity (m^2/s) 33, 34

α Heat diffusion coefficient (m^2/s) 33

$\vec{F}$ Volumetric forces (N/m^3) 33

g_0 Volumetric heat generation (W/m^3) 33

Acronyms

Lista de siglas

ACH Air Change per Hour 8
AHU Air Handling Unit 14
CENAQUE "*Centro nacional de Quemados*" 26, 58
CFD Computational Fluid Dynamics 1, 27, 31
CFU Colony Forming Units 10
DIN Deutsches Institut für Normung 13
FING Facultad de Ingeniería (Engineering faculty) 20
FNR Fondo Nacional de Recursos (national resources found) 19
HEPA High-Efficiency Particle Absorbing 9
HLAF Horizontal Laminar Airflow 57
HVAC Heating Ventilation and Air Conditioning 3, 11
IIMPI Instituto de Ingeniería Mecánica y Producción Industrial (mechaninal engineering and insdustrial production institute) 19
LAF Laminar Airflow 17
OR Operating Room 1, 4, 5
PC Particle Count 13
PISO Pressure-Implicit with Splitting of Operators 39
RANS Reynolds Averaged Navier-Stokes 34
RH Relative Humidity 7
SCU Sociedad de Cirugía del Uruguay (Uruguayan society of surgeons) 19
SSI Surgical Site Infection 1, 4
TCAF Temperature Controlled Airflow 17
TMA Turbulent Mixing Airflow 17
USA United States of America 4
UdelaR Universidad de la República 20

VLAF Vertical Laminar Airflow 12

WHO World Health Organization 3, 4

Contents

Chapter 1

Introduction

Maintaining high air quality standards is important in Operating Room (OR) to minimize the risk of infections and ensure a safe environment for both patients and healthcare workers. Air quality control in these environments is particularly important due to the vulnerability of patients during surgeries, and the healthcare impacts of the Surgical Site Infection (SSI). This thesis focuses on evaluating the air quality in operating rooms using Computational Fluid Dynamics (CFD). CFD allows for the analysis of air quality without interrupting the normal functioning of the operating room. The main objectives of this work can be divided into four key points: (1) Identify the factors that define air quality in operating rooms. The factor identification process includes: identification of key air quality parameters, analysis of national and international standards, identification of ventilation systems and schemes used in OR environments (2) Select a relevant and feasible case study to analyze air quality using computational fluid dynamics (CFD). Case study selection should contemplate the national situation in relation to air quality inside ORs, and the data availability for the study scenario. (3) Develop and validate a mathematical-numerical model capable of evaluating indoor air quality parameters in indoor environments. (4) Simulate fluid dynamics and other critical air quality parameters for the selected case study.

The thesis is structured into three main chapters, and a brief conclusion chapter, it's contents are distributed as follows:

Chapter 2 *"Air quality in Uruguayan operating rooms"* reviews controlled air

parameters in hospitals, with a focus ORs. It provides an overview of various ventilation system designs and operational practices, as well as a summary of relevant regulations. Finally, it presents a state-of-the-art analysis of air quality control in Uruguayan ORs, guided by a set of reference questions. Also, a case study is selected from the state-of-the-art analysis.

Descrpition and validation of the mathematical-numérical model is described in Chapter 3 *"Numerical-Mathematical model and validation"*. The equation solving algorithm is defined and evaluated. Model validation is carried out comparing with two reference experiments,the "Heated Cavity" by Limane et al., 2015 and the "Two-Zone Chamber" by Lu et al., 1996.

Chapter 4 *"Case study: effect of the partial wall at ceiling level."* applies the designed CFD model to an operating room where a partial separation wall was recently installed between the ceiling-level outlet and inlet. Three scenarios are simulated and compared: (1) with the partial wall, (2) with a shorter partial wall, and (3) without the partial wall. Differences in airflow patterns and air quality parameters are analyzed across these scenarios.

Finally, Chapter 5 *"Conclusions"* summarizes the main conclusions drawn from this thesis.

Chapter 2

Air quality in operating rooms

2.1. Introduction

Primum non nocere, when applied to infection control in hospitals, could be interpreted as: "The first requirement of a hospital is that it should do the sick no harm," as famously stated by Nightingale, 1863. Although the concept of "bad air" and infections due to poor hygiene had been acknowledged since ancient times, it was not until the late 19th century that a deeper understanding of infection mechanisms emerged, along with strategies to mitigate them. This progress was driven by ideas from figures like Florence Nightingale, who demonstrated the importance of proper ventilation through statistical data showing improved hospital outcomes, and Joseph Lister, who introduced handwashing before surgery for the first time. Additionally, scientific advancements in microbiology by researchers like Koch and Pasteur significantly contributed to this evolving knowledge.

During the 20th century, advancements in filtration technology, mechanical ventilation, and Heating Ventilation and Air Conditioning (HVAC) systems, along with a broader understanding of infections, significantly improved air quality in hospitals. Concurrently, the introduction of chemical disinfectants and the development of antibiotics revolutionized infection control practices.

Despite the advances made since the 19th century, HAIs remain a significant global issue. According to the World Health Organization (WHO) infection prevention and control guidelines (World Health Organization, 2022), out of

every 100 patients in intensive care hospitals, between 7 and 15 (depending on the country's level of development) acquire at least one infection during their hospital stay. Furthermore, the emergence of multidrug-resistant bacteria has made HAIs one of the most critical public health threats today (Barrasa-Villar et al., 2017; Cornejo-Juárez et al., 2015). The rise in antibiotic resistance, combined with recent airborne transmission outbreaks (such as SARS-CoV-19), has underscored the importance of effective ventilation systems in hospitals.

In comparison, we define the air quality of a given space as higher than another (or a reference) when its conditions—temperature, humidity, particle concentration, and airflow—better support the activities performed in that space. In a room where invasive surgical procedures take place, such as an OR, the air must ensure both the comfort of the occupants and the protection of the surgical team and patient from potential infections.

An infection that occurs at the site of a surgical incision is known as a SSI. Most SSIs become evident within 30 days of the procedure, except for those associated with prosthetic implants, which affect deeper tissue layers (National Collaborating Centre for Women's and Children's Health (UK), 2008). According to the WHO Global Guidelines for the Prevention of Surgical Site Infection (World Health Organization, 2018), SSIs are the most common type of hospital-acquired infection in low- and middle-income countries, affecting up to one-third of patients, and the second most frequent in Europe and the United States of America (USA). SSIs can have severe consequences for both patients and healthcare providers.

For patients, the consequences of contracting an SSI can vary significantly depending on the severity of the infection and individual risk factors. An SSI may prolong hospitalization, delay recovery, increase healthcare costs, lead to scarring and disfigurement, cause chronic pain, necessitate re-operation, result in systemic infections, and even lead to death (National Collaborating Centre for Women's and Children's Health (UK), 2008).

For healthcare providers, potential consequences include increased costs, prolonged patient stays, and reputational damage (Brewster et al., 2016; de Lissovoy et al., 2009). A study by de Lissovoy et al., 2009 conducted in the

USA found that, on average, SSIs extended hospital stays by 9.7 days and increased costs by $ 20,842 per admission.

SSIs can be attributed to various factors, including the presence of pathogens on the patient's skin or surgical instruments. Airborne transmission of bacteria should not be underestimated; Whyte et al., 1982 found that, in the absence of proper ventilation systems, 98% of the bacteria present in patient wounds originate directly or indirectly (via instruments or surfaces) from airborne transmission.

Primarily, two types of microorganisms can become airborne in an adequately ventilated OR: bacteria and fungi. Although viruses can also become airborne when healthcare providers or patients cough, talk, or exhale, their presence in the OR is related to the viral load of individuals present. While fungi can become airborne on their own as spores, bacteria and viruses use airborne particulate matter (PM), such as respiratory droplets, skin flakes, aerosols, and dust, to spread through the air.

This Chapter reviews controlled air parameters in hospitals, with a focus on ORs. It provides an overview of various ventilation system designs and operational practices, as well as a summary of relevant regulations. Finally, it presents a state-of-the-art analysis of air quality control in Uruguayan ORs, guided by a set of reference questions.

2.2. Air Quality Parameters

Airborne contaminants can be generated within the room or enter from the outside. Sources of contamination may include patient and surgical team skin scales or flakes, respiratory aerosols, and aerosols produced by surgical procedures (Armellino, 2017). External contaminants or particulate matter (PM) can be introduced into the OR through the ventilation system or from adjacent areas via doors and door gaps. Factors that affect the risk of airborne transmission inside the OR include air temperature and humidity, ventilation, pressure differences between the room and adjacent Areas, and filtering.

2.2.1. Temperature

The air temperature inside the OR impacts thermal comfort, the risk of infection, and airflow conditions. Thermal comfort is defined as *"that condition of mind which expresses satisfaction with the thermal environment"* (Gaever et al., 2014). The conditions required to achieve thermal comfort differ between the patient and various members of the surgical team. For example, the thermal comfort needs of the surgeon and the anesthetist differ due to their varying levels of physical activity. Achieving thermal comfort is crucial for ensuring optimal performance of the surgical team and for safeguarding the health of both the patient and the team members.

Even though technical standards state that thermal comfort must be achieved for everyone inside the OR, Gaever et al., 2014 has found that the recommended temperatures do not guarantee thermal comfort for the entire surgical team. Furthermore, the differences in clothing and metabolic activity between the patient and the surgeon place them in opposing thermal conditions. Comfort temperatures for the surgeon can be unhealthy for the patient, while comfort temperatures for the patient can induce thermal stress on the surgeon, potentially harming their performance (Angelova and Velichkova, 2020).

Heat sources such as the surgical light, patient, and surgical team locally heat the air, generating currents due to buoyant forces, known as thermal plumes. In ORs designed for "laminar" flow distributions (see Section 2.4), thermal plumes can increase the risk of SSI (Liu et al., 2022). Therefore, it is imperative that the air enters the room with sufficient inertia so as not to be affected by thermal plumes.

Temperatures above 24^{o}C tend to reduce the survival of airborne pathogens, specifically bacteria and viruses (Tang, 2009). Most airborne viruses and bacteria are exhaled with a layer of saliva or mucus, which evaporates at a faster rate when the OR temperature is higher.

Generally, the temperature of the OR is determined as a compromise between the comfort of the surgical team and the patient. Most standards and guidelines recommend temperatures between 20^{o}C and 24^{o}C for adult operations,

and slightly higher for pediatric operations, due to the patient's greater risk of hypothermia (Balaras et al., 2007). Furthermore, some specific procedures may require specific temperature ranges, such as the treatment of burned skin, as stated by NHS England, 2021 and Ferguson and Martin, 1991.

2.2.2. Humidity

Humidity, generally expressed through Relative Humidity (RH), measures the concentration of water vapor in the air. Specifically, relative humidity varies from 0% to 100%, from completely dry air to saturated air at a given temperature. As the saturation pressure of vapor in air increases with temperature, the same RH value represents higher absolute humidity in the air at higher temperatures.

Like temperature, humidity plays an important role in the thermal comfort of the patient and the surgical team. However, unlike temperature, the RH values associated with the comfort of different actors are not contradictory. Very low RH favors dehydration of the skin, irritation, and blood coagulation (Balaras et al., 2007), while high RH slows down the evaporation of sweat, impairing the body's natural cooling process and thus increasing the thermal sensation, which can lead to discomfort (Djamila et al., 2014).

Humidity affects the various pathogens present in the OR differently. Tang, 2009 highlighted that high relative humidity favors the growth of bacteria and fungi, with bacteria being the most common pathogen inside ORs. Furthermore, the aerial survival of bacteria increases with relative humidity, as the evaporation of droplets slows down (Balaras et al., 2007). On the other hand, the survival of airborne viruses is minimized at medium levels of humidity (40%-70%) (Tang, 2009).

In conclusion, medium levels of relative humidity are recommended to avoid blood coagulation, ensure skin moisturization, prevent electrical discharges, limit the growth and survival of bacteria, and reduce thermal discomfort. There is little disagreement in humidity range recommendations between different guidelines and standards, as further discussed in Section 2.3. A recommended RH range of 45% to 55% is generally agreed upon.

2.2.3. Ventilation and particle control

Ventilation control in an OR includes several factors, such as the filtering system, total and outdoor Air Change per Hour (ACH), pressure relationship with adjacent areas or differential pressure, and control over airflow distribution. Furthermore, a lack of control over the amount of air supplied to the room may result in a loss of control over the distribution of temperature and humidity (thermal comfort). Control over the ventilation of the OR influences both thermal comfort and infection prevention.

The easiest way to keep the air inside the OR in good condition is to constantly replace it with clean, thermally conditioned air. This can be achieved using either outdoor air or recirculated air. Recirculated air has already been conditioned, typically resulting in lower energy consumption, as explained by ASHRAE, 2021 and U S Department of Health and Human Services and Centers for Disease Control, 2019. However, it is crucial that a portion of the ACH comes from outdoor sources to sustain oxygen levels and decrease the concentration of gaseous contaminants such as anesthetic gases, which cause discomfort and long-term health problems for surgical teams due to continuous exposure, as well as odors, as discussed by Memarzadeh and Manning, 2002, Whyte et al., 1982, Balaras et al., 2007.

Contamination from the outside of the OR can be reduced through Appropriate filter arrangement. Filters are installed to reduce the entrance of fungal spores and PM that may be contaminated or become contaminated inside the room. An adequate arrangement of filters for an OR includes at least two filtering stages (three for more intrusive interventions).

The first filtering stage (or prefilter) is carried out with a filter equivalent to a Class F5 or higher. The prefilter is responsible for retaining large particles and is mainly placed to protect other higher-efficiency filters and mechanical equipment. Therefore, it is installed upstream of turbomachines, heat exchangers, higher-efficiency filters, and other conditioning equipment. In addition to protecting the most sensitive and expensive components, Balaras et al., 2007 proposes that proper maintenance of prefilters can reduce the generation of bacteria inside the ventilation system. Since prefilters are inexpensive and

easy to replace, it is usual to replace them routinely, without the need for testing, on a monthly or bimonthly scale.

For the second filtering stage, high-efficiency filters, with above 80%-90% retention (Class C) are used, such as Class F7 or F9 or equivalent filters. In addition to the particles that pass the first filtering stage, second-stage filters should retain contaminants generated inside the ventilation system and its components (such as the temperature controlling coils), thus second stage filters should be installed downstream of air conditioning systems. Studies have shown that about 99.9% of all bacteria present in hospitals are retained in 90-95% efficient filters (Balaras et al., 2007). The high-efficiency filter could be final for a room where low-risk procedures are performed; in such cases, it should be installed as close to the OR as possible to avoid contamination generation between the final filter inlet and the OR. As high-efficiency filters retain particles, the effective area for air passage through the filter decreases, leading to an increase in pressure drop. To mitigate the reduction in airflow, pressure drop tests are conducted approximately every six months, and the filters are replaced when the pressure drop is deemed significant enough to warrant replacement.

In rooms where higher-risk interventions are carried out, second-stage filters are followed by the terminal High-Efficiency Particle Absorbing (HEPA) filter. HEPA filters are installed as close as possible to the room air inlet to retain particulate matter generated in the supply duct. Their efficiency exceeds 99.97% for particles with a diameter of $D = 0.3\mu m$. To ensure proper ventilation, pressure drop and integrity of HEPA filters must be tested approximately every year. Upstream filtration stages reduce the amount of PM that reaches the HEPA filter bank, reducing its replacement rate, which is very advantageous because HEPA filters are more expensive. Proper maintenance of the filter bank can nearly eliminate external contamination from the ventilation system.

External contaminants could enter the OR from adjacent Areas through gaps or when the door is opened. To mitigate the risk of infection via this mechanism, ORs normally work with positive differential pressure. The exception to this rule is when the patient has a contagious disease; in these cases, ORs

should operate under negative differential pressure conditions to prevent the disease from spreading. Desired differential pressures are achieved by properly choosing the fan positions and airflow supply. When installed upstream from the room and with enough air supply, differential pressure is positive. The amount of air supplied and extracted from the room determines the pressure. When the air supply exceeds the extraction, the pressure is positive; otherwise, it is negative, given that a positive pressure difference implies that the flow through door gaps or similar openings moves from inside to outside, and the opposite occurs for negative pressure..

Even when contamination from the outside is completely avoided, the risk of airborne transmission remains due to the generation of potentially contaminated particles within the OR, as discussed earlier in this section. In addition to reducing the rate of particle suspension through disinfection and surgical clothing, ventilations systems are designed to reduce the presence of suspended particles near the surgical team and the patient (critical zone).

There are two general approaches for contaminant concentration reduction in the critical zone. The first approach is based on diluting the contaminants throughout the volume of the room, while the second approach pushes airflow away from the critical zone, "sweeping" the contaminants into the periphery of the room. For either approach, the flow distribution is determined by the geometry of the room and the volume of air displaced. The number, shape, size, and position of air inlets and outlets are determined by the design flow distribution. Ventilation approaches are discussed in more depth in Section 2.4.

In order to determine the number of ACH, the ventilation strategy, operating costs, thermal comfort, and pressure ratio must be taken into account. Studies have shown that the concentration of both gaseous contaminants (Y. Zhang et al., 2020) and Colony Forming Units (CFU) (Alsved et al., 2018; Vonci et al., 2019) decrease as ACH increases, but higher ACH is related to increased energy consumption and discomfort, as stated by Mičko et al., 2023. A minimum of 20 ACH is generally recommended; most studied standards agree with this recommendation (further discussed in Section 2.3).

2.3. Standards

Standards and guidelines regarding ventilation and air quality for health care facilities are constantly in development around the world. Health care center ventilation and HVAC standards aim to control air quality, which includes odors, sepsis, and comfort. ASHRAE, 2021 defines its purpose as: *"The purpose of this standard is to define ventilation system design requirements that provide environmental control in health care facilities."* Despite the universality of standard purpose and objectives, Nastase et al., 2016 found that there is a lack of specifications and uniformity in the existing standards. Table 2.1 presents the limits for temperature, differential pressure, minimum ventilation, and minimum outdoor air for ORs in accordance with different standards, such as anesthetic gases.

Table 2.1: Recommended ranges for air quality parameters inside the OR according to the following international standards: ASHRAE, 2021, Asociación Española de Normalización, 2005, Asociación Española de Normalización, 2020, DIN, 2008, and NHS England, 2021.

Standard	T (ºC)	RH (%)	Ventilation	Out. Air	p (Pa)
ASHRAE 170	20-24	20-60	20 ACH	4 ACH	2.5[1]
DIN 1964-08	19-26	-	-	1200 $\frac{m^3}{h}$	> 0
UNE 100713 A	22-26	44-55	3600 $\frac{m^3}{h}$ & 20 ACH	1200 $\frac{m^3}{h}$	> 0
UNE 100713 B	22-26	44-55	2400 $\frac{m^3}{h}$ & 20 ACH	1200 $\frac{m^3}{h}$	> 0
UNE 171340	20-26	40-60	20 ACH	20 ACH	20
HTM 03-01	18-25	35-60	22 ACH	4.4 ACH[2]	25

The lack of uniformity found by Nastase et al., 2016 is evident in the parameters of the standards, particularly in the temperature range. The temperature ranges established by the revised standards vary from 19-26ºC (DIN) or 18-25ºC (HTM) to 20-24ºC (ASHRAE) or 22-26ºC (UNE 100713). Intersecting all recommended temperature ranges results in a common range of 22-24ºC; however, this range could be narrowed when considering other standards. Since the temperature set point within the OR is a compromise between several factors, the differences in the temperature ranges imposed by the standards may reflect the varying emphasis placed by each regulatory body on quality of care parameters, such as comfort, sepsis prevention, and airflow distribution.

Standards for relative humidity (RH) are more consistent across different

guidelines compared to temperature ranges. The RH ranges specified in the standards fall between 20% and 60%, representing medium levels of humidity. As discussed in Section 2.2, medium RH levels support environmental sepsis and reduce the risk of fire due to electrical discharges, among other factors. It is important to note that RH, along with temperature, is crucial for thermal comfort. Consequently, the variations in RH ranges among standards may be related to the temperature ranges set by each standard.

Minimum ventilation recommendations do not vary much between standards; those listed in Table 2.1 define a minimum of 20 ACH (ASHRAE and UNE) and 22 ACH (HTM). In addition to the minimum ACH requirements, the UNE specifies a minimum flow rate in m^3/h depending on the type of room. Establishing minimum flow rates ensures adequate oxygen concentration and helps dissipate odors and gaseous contaminants. Standards also specify differential pressure relations. For instance, ASHRAE 170 and HTM 03-01 set minimum differential pressure values (2.5 and 25 Pa, respectively), while other standards merely require the differential pressure to be positive (with reversed requirements for rooms treating infectious patients).

Standards such as ASHRAE, 2021 and NHS England, 2021 03-01 also provide inlet velocity specifications. For example, ASHRAE 170-2021 recommends an average inlet velocity range of 25-35 cfm/ft^2 (approximately 0.126-0.178 m/s). These velocity specifications are related to Vertical Laminar Airflow (VLAF) ventilation systems. VLAF ventilation cleans the room by sweeping contaminants from the center toward the periphery. Effective contaminant removal requires an orderly, unidirectional airflow with enough inertia to overcome thermal plumes and other adverse pressure gradients. The recommended velocity ranges are based on the study by Memarzadeh and Manning, 2002, ensuring an effective flow pattern as detailed in Section 2.4.

Another way for standards to promote protective spaces for OR occupants is to impose a maximum number of PCs when the OR is unoccupied (at-rest conditions). Unlike the imposition of the ventilation system and ASHRAE 170 flow rate range, limiting the maximum PC makes the protection of the OR independent of the ventilation system. Making the protection of the OR independent of the ventilation system may be desirable since, although stud-

ies carried out by Memarzadeh and Manning, 2002, T.-T. Chow and Yang, 2004, and Liu et al., 2021 show that under theoretical operating conditions the VLAF system generates a protective environment, however, studies such as that of Brandt et al., 2008 did not find evidence that the presence of a VLAF system reduces the patient's risk of contracting an SSI.

There are different ways to restrict Particle Count (PC) within the OR; the most universal way is using the ISO 14644-1 classes for clean rooms. The standard allows the room to be classified into 9 classes, with class 1 being the cleanest and class 9 the least clean. For each class, the ISO standard defines a maximum cumulative concentration of particles of different maximumn sizes (0.1, 0.2, 0.3, 0.5, 1, and 5 μm). The certification of the type of room is carried out using reports of particle counts of different representative sizes at different points inside the room (the amount and location of measurement points is established by ISO), where concentrations lower than those demanded by the class to be certified are demonstrated. In order to ensure the certified ISO class, particle count reports must be performed recurrently.

The UNE 173140 standard is an example of OR protection using ISO classes. Generally, the objective degree of protection (equivalent to ISO class) is determined by the severity of the procedures carried out in the room. Specifically, the UNE 173140 standard separates the procedures into 5 groups according to the degree of risk: very risky, risky, medium, moderate, and light, for which it defines a minimum ISO class, from ISO 5 for very risky procedure rooms (at rest conditions), up to ISO 8 for light risk rooms. The ISO class is not the only requirement that changes depending on the OR group; the minimum renewals, minimum differential pressure, and filtration system also vary.

Separating hospital zones according to the air quality requirement is common in regulations; some examples are presented in Table 2.2. ORs are grouped in the two most stringent categories for the evaluated standards.

Deutsches Institut für Normung (DIN) 1964-08 limits particle concentration through a parameter called "degree of protection" SG (DIN, 2008). The degree of protection is calculated with Equation 2.1 and measures the logarithmic ratio of particle concentration against a reference of $C_{ref} = 35.3 \times 10^6$ P/m^3.

It is stated that a degree of protection equal to or greater than 4 is required for class Ia ORs ($C_p \leq 35.3 \times 10^2$ P/m^3), and a degree of protection equal to or greater than 2 for class Ib ORs ($C_p \leq 35.3 \times 10^4$ P/m^3).

$$SG = log\left(\frac{C_{ref}}{C_p}\right) \tag{2.1}$$

Area classification also dictates the minimum filtering requirements for differ-

Table 2.2: Space or air classification according to international standards.

Standard	Class name	Description
DIN 1964-0	Class Ia	ORs with LAF.
	Class Ib	ORs without LAF.
	Class II	Every room that is not an OR.
UNE 173140	1. Very risky	Protected zone of ORs with LAF.
	2. Risky	Peryphery of ORs with LAF, ORs without LAF.
	3. Medium	Eg. Protective isolation rooms.
	4. Moderate	Eg. Infectious isolation rooms.
	5. Light	Eg. Emergency Blocks.
UNE 100713	OR class A	ORs for high risk surgery.
	OR class B	Every other OR.
HTM 03-01	Ultra clean	With LAF; less than 10 cfu/m^3.
	Conventional	Every other OR.

ent areas. OR inflow is typically filtered in at least three stages, including a HEPA/ULPA filter that achieves a particle removal efficiency of over 99.97% for particles with a diameter of 0.3 μm (the most challenging to filter). The specifics of filtering stages are discussed further in Section 2.4.

2.4. Ventilation systems

Proper design, coordination with adequate maintenance, and proper operation of ventilation systems are expected to improve air quality inside ORs. Most OR mechanical ventilation systems use an Air Handling Unit (AHU) to condition outdoor air and inject it into the OR. The AHU takes outdoor air at ambient conditions and makes it "suitable" for supply into the room.Air is deemed suitable for entry into the room when its parameters meet specific criteria, ensuring that the conditions in the OR achieve the predefined design set points. Upon entering the room, the air quality parameters change with

respect to the AHU exhaust conditions, due to particles becoming airborne and thermal and humidity loads, as shown in Figure 2.1, therefore AHU exhaust conditions such as temperature and RH differ from the OR set points. It is common for a portion of the air exhausted from the room to be reused for energy-saving purposes, as its temperature and humidity may be closer to the thermal or humidity design points than the outdoor air. Since the quality parameters of the expelled air differ from the AHU's set points, it must be conditioned again before re-entering the room.

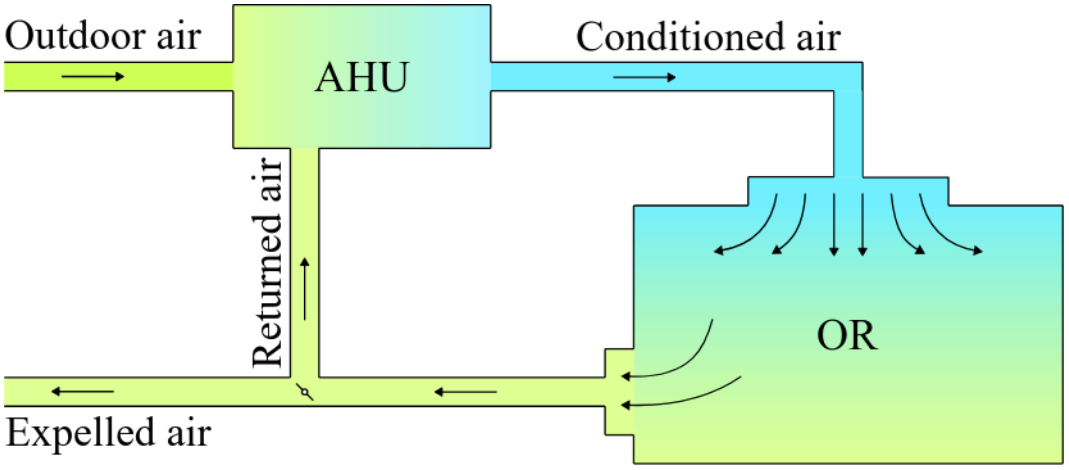

Figure 2.1: OR ventilation system general scheme. Sky blue air represents air with good air quality and yellow represents air with lesser air quality.

The most basic AHU for a surgical room should, firstly, ensure the necessary ventilation and differential pressure, and secondly, regulate the temperature, humidity, and degree of cleanliness required. Consequently, the unit must have at a minimum a fan, heating and cooling coils, a humidifier, and the required filters, as shown in Figure 2.2. The fan generates ventilation and affects the partial pressure in the room. Cooling and heating coils are used for temperature regulation, with the cooling coil also capable of reducing air humidity. The installed filter arrangement reduces the concentration of particulate matter in the airflow, either before the air is injected into the room or before the next filtering stage (terminal HEPA filter).

Sensors can be installed in the AHU to control temperature, humidity, and ventilation. Control can be either automatic, using a building management system, or manual, adjusted by personnel. Regardless of the control method-

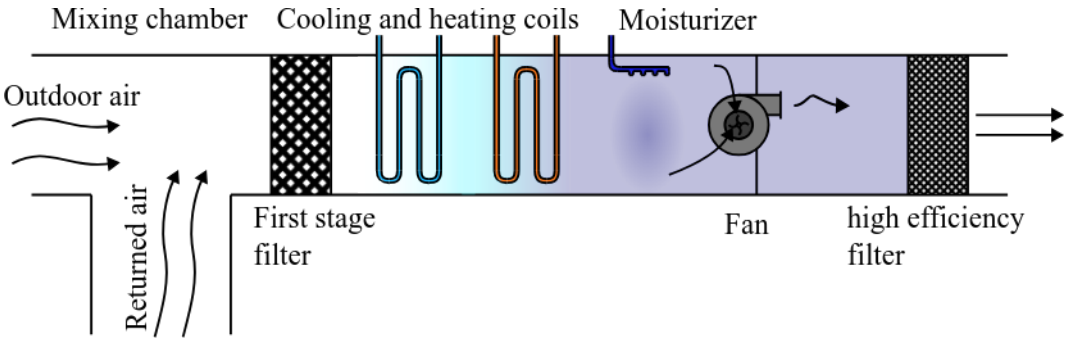

Figure 2.2: Air handling unit components.

ology, the objective is to achieve the set points for airflow, temperature, and humidity. Set points depend on the specific operation being carried out in the room and may vary from procedure to procedure. AHU temperature and humidity exhaust conditions differ from the OR set point due to thermal and humidity loads inside the room, such as those caused by people or electronic equipment.

Ventilation control is typically achieved by adjusting dampers to regulate the amount of air entering the OR. If the air temperature is below the set point, the heating coil is used to raise it. Conversely, if the temperature is above the set point, the cooling coil lowers it. Humidity control is managed through a combination of the humidifier and temperature-controlling coils. If humidity needs to be increased, the humidifier adds moisture to the airflow by releasing dry steam. To decrease humidity, the airflow is cooled, causing water to condense and subsequently reducing humidity. After this process, the heating coil adjusts the temperature to the desired level.

After being conditioned in the AHU, air is injected into the OR through an inlet array. The installation location, shape, and number of inlet and exhaust grills, as well as other room elements such as the operating lamp or table, influence the velocity field inside the room. Consequently, the configuration of inlets, outlets, and other elements may vary from room to room according to the design flow distribution. Terminal HEPA filter banks are installed upstream of the inlet array in ORs with higher air quality demands. Clean and thermally conditioned air removes particles, heat, and moisture from the OR and is exhausted through the outlet grills.

Even though contamination from the outside can be minimized through proper filtering, sources of contamination exist inside the OR. Evacuating contamination generated within the room and reducing its concentration near the incision area can help minimize the risk of SSI. Therefore, significant attention has been given to the velocity field within the OR.

Ventilation configurations inside the room can be categorized into two main types: Laminar Airflow (LAF), which could be horizontal (HLAF) but is predominately vertical (VLAF), and Turbulent Mixing Airflow (TMA). In VLAF systems, airflow moves from the ceiling towards the operating table, maintaining parallel streamlines. Contamination is swept away by the inertial force of the stream, from the table to the exhaust grilles positioned around the periphery of the room, and sometimes in the ceiling if there is a physical separation from the air injection. HLAF configurations are based in the same principle, but airflow is injected horizontally. TMA systems reduce contamination concentration near the patient and staff by diluting contaminants. The turbulent airflow in TMA systems mixes and disperses airborne particles throughout the entire room volume, ss shown in Figure 2.3b, thereby lowering local concentrations near the surgical wound.

Both airflow distributions have been thoroughly investigated and are considered effective at reducing contamination concentration in the OR, as stated by Liu et al., 2021. Studies by Liu et al., 2021 and C. Wang et al., 2018b provide evidence that VLAF configurations are more effective at reducing particle counts close to the operating table compared to TMA airflow. TMA systems are less expensive and their working conditions are less likely to be disrupted (DIN, 2008); therefore, when higher levels of air pollution are deemed acceptable (as discussed in subSection 2.3), TMA systems may be installed in the OR. Other possible OR ventilation systems have been studied in recent years such as Temperature Controlled Airflow (TCAF) by Liu et al., 2021, C. Wang et al., 2018b and Alsved et al., 2018. TCAF separates air injection in two separated arrays. Cool air flows through the central array, and warmer through the peripheral array, as air density decreases with temperature, the peripheral flow functions as a ceiling for the central air. The airflow distribution is in result similar to VLAF ventilation system, as shown in Figure 2.4. TCAF

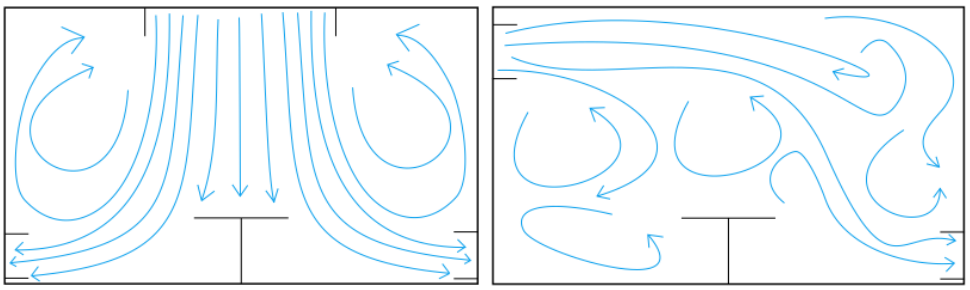

(a) VLAF streamline scheme **(b)** TMA streamline scheme

Figure 2.3: Airflow distribution for (a) VLAF, (b) TMA systems.

Systems have been found to reduce concentration similar to VLAF systems by C. Wang et al., 2018b Alsved et al., 2018, while reducing energy consumption.

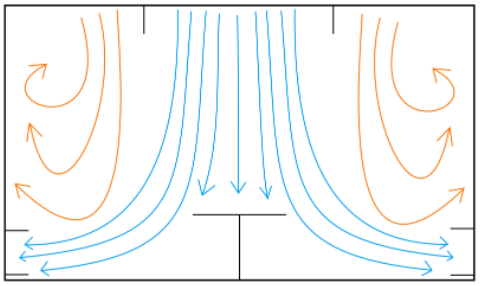

Figure 2.4: TCAF streamline scheme

Downstream of the OR, the air is expelled from the hospital. Since the air being expelled was previously conditioned, it is common to recirculate a portion of it to save energy. Although it may be energetically optimal to recirculate all the air leaving the room, a minimum fraction of outdoor air must always be maintained to keep oxygen concentrations at acceptable levels, evacuate odors and anesthetic gases, among other considerations (see Section 1.2). In most cases where air is recirculated, a dedicated AHU must be installed for each OR to avoid mixing pathogens. However, in special cases, such as rooms intended for the same procedures, the same AHU can supply air (with a recirculated air fraction) to several rooms. Another alternative for improving energy efficiency is the installation of an air pre-heater (usually a plate heat exchanger between the injection and exhaust air).

Other ventilation system design alternatives include installing fans and filters downstream of the room, which are commonly used for ORs with patients

who have contagious diseases. By placing the fan downstream of the room, negative differential pressure can be generated, which helps reduce the probability of disease transmission. Additionally, filters are installed in the air outlet duct to minimize the risk of contagion spreading outside the hospital.

2.5. Air quality control in Uruguay

Records of surgical procedures in Uruguay date back to around 1840, during a period known as the "tiempo de los franceses," which was marked by significant French emigration between 1830 and 1840. By 1843, the surgical team at the French Legion Hospital had assisted 2,363 patients in their first four years. In 1847, Maciel Hospital performed the first generalized anesthesia with ether in all of South America. In 1920, the Sociedad de Cirugía del Uruguay (Uruguayan society of surgeons) (SCU) was established, becoming one of the oldest surgical societies on the continent. Prior to the SCU, there were four surgical clinics at the National School of Medicine, operating independently within Maciel Hospital with no scientific exchange between them. The SCU's goal was to promote scientific exchange among different surgical teams and staff. The first OR with LAF ventilation in South America was inaugurated at the Banco de Prótesis in 1976.

Despite the country's rich clinical history, national indicators of operative results were not found during this research. The indicators of the Fondo Nacional de Recursos (national resources found) (FNR) can be used as a reference, as shown in Table 2.3. The FNR is a public entity that finances various specialized medical procedures through Institutes of Highly Specialized Medicine, or "Institutos de Medicina Altamente Especializada" (IMAE). The indicators presented by the FNR suggest that the maximum risk corresponds to the annual mortality rate for hip arthroplasty (fracture), which reached 19.5% of the procedures evaluated between 2018 and 2021. The re-entry rate for cardiac surgery is also relatively high at 5.78% in 2021. Additionally, the operative mortality rates are significant for cardiac surgeries (6.46%), percutaneous coronary interventions (4.26%), and hip arthroplasty (9.01% combining fracture and teoarthritis).

In February 2018, an agreement was signed between the Instituto de In-

Table 2.3: FNR Indicators.

Indicator	Type of procedure	Nº Proc.	Val. (%)	Period
Re-entry	cardiac surgery	1574	5.78	2021
Operative Mortality	Knee arthroplasty	6552	0.17	2018-2021
	Percutaneous coronary interventions	4226	4.26	2021
	Cardiac surgery	1564	6.46	2021
	Hip arthroplasty (fracture)	3864	4.1	2018-2021
	Hip arthroplasty (osteoarthritis)	5360	0.19	2018-2021
Anual Mortality	knee arthroplasty	6552	1.21	2018-2021
	Hip arthroplasty (fracture)	3864	19.5	2018-2021
	Hip arthroplasty (osteoarthritis)	5360	1.45	2018-2021

geniería Mecánica y Producción Industrial (mechanincal engineering and insdustrial production institute) (IIMPI) from the Facultad de Ingeniería (Engineering faculty) (FING) of the Universidad de la República (UdelaR) and the FNR. The objective of the agreement is for the IIMPI team to collaborate with the FNR in auditing the air conditioning systems of IMAEs. The audits aim to evaluate air quality conditions and the management and maintenance practices related to air conditioning in various ORs used by the different IMAEs. The goal is to improve service quality by aligning with good practices and international regulations, given the scarcity of enforceable national standards (as discussed in Section 2.3). Under this agreement, audits have been conducted at IMAEs across over twenty health centers.

From the year 2021 onwards, the evaluation methodology has been standardized according to the questionnaire outlined in the FNR handbook Gambogi et al., 2020. The updated report uses the questions form Table 2.4 as guidance in order to Section information about air quality parameters and practices. The inspection of an IMAE results in the generation of a report, where the questions are answered for the relevant ORs. Although the questions are designed to elicit Yes or No answers, it is common to include observations in cases where the information is unclear or when specifications are met to a certain degree or in a manner different from what is recommended by the FNR, but

still valid according to other regulations.

Questions can be categorized into two groups. Following the order of pre-

Table 2.4: Guiding questions for evaluation of air conditioning systems of the FNR-FNR agreement.

Number	Question
1	Has an institutional manager or air management company; contracted, registered, qualified and with suitable responsible.
2	It has a documented procedure to carry out the control of the air system.
3	Mechanical maintenance of the facilities and the cleaning of ducts and grilles, others, are verified.
4	The types of filters used are those required for the class of air to be achieved according to the service
5	Standardized criteria is utilized for filter exchange according to the filter type
6	Filter exchange dates are registered as is established by the procedure
7	Temperature and relative humidity are monitored; requirements are met for the different areas.
8	Pressure requirements are met according to type of areas.
9	Air renovation requirements are met.
10	Particle count is measured annually and after maintenance, reparations or in critical situations.
11	Air class requirements are met according to area type.
12	Terminal filter integrity is monitored accordingly.
13	Control equipment is calibrated

sentation, questions 1 through 6, along with questions 12 and 13, directly evaluate administrative and system management aspects of the room. Questions 7 through 11 assess air quality and ventilation parameters. The answers to these questions for 41 ORs—7 with VLAF ventilation systems and 34 with TMA systems—are presented below to provide a framework for air quality in ORs nationwide. All reports evaluated are from the initial audit of the rooms. Figures 2.5 to 2.8 graphically represent responses regarding air quality and ventilation parameters. In these figures, light green *"O.Y."* stands for *"observed yes"*, yellow *"Inc."* stands for *"inconclusive"*, orange *"O.N."* stands for *"observed no"*, and grey *"N.D."* stands for *"no data"*.

Despite most rooms conducting real-time measurements and meeting temper-

ature and humidity criteria, approximately 27% do not satisfactorily answer the question, as shown in Figure 2.5. The primary reason for the unsatisfactory responses to question 7 is the lack of temperature and, particularly, humidity measurement equipment. Although more ORs lack real-time measurement capabilities, they do have punctual, satisfactory measurements of temperature and humidity obtained through specific tests. Audited ORs that record these parameters meet the recommended temperature and humidity levels. Rooms lacking temperature and/or humidity sensors should incorporate a thermo-hygrometer for real-time control of these parameters. Question 8,

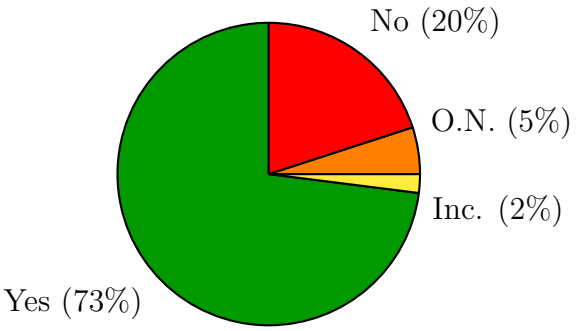

Figure 2.5: Temperature and Relative Humidity monitoring and requirement satisfaction

which addresses pressure requirements in the room, shows the lowest degree of absolute satisfaction, with approximately 29% answering "Yes." The distribution of answers can be visualized in Figure 2.6. In several instances, although there is no direct control over the room's differential pressure, a positive differential pressure can be inferred from the difference between the extraction and injection flow rates. When these differences are sufficiently large, the response is marked as "Observed yes."

In cases where the inferred difference is not large enough, the answer is "Inconclusive." An inconclusive answer is also given when there is no pressure gauge in the room, but positive differential pressure can be verified by observing the direction of the air flows in the room door gap. "Observed no" is recorded when the differential pressure is measured, is positive, but does not meet the minimum requirements of 5-10 Pa (depending on the type of room).

The answer is "No" when there is no pressure meter in the room and differential pressure cannot be confirmed as positive, or when a negative pressure

difference relative to the adjacent rooms is registered. The lack of control over the air pressure in the room can be concerning, as maintaining relative positive pressure to adjacent rooms reduces the amount of external contaminants, as explained in Section 2.2. Differential pressure deficits can be addressed by checking filters, reducing adjacent area ventilation, increasing room ventilation, or fixing air leakages.

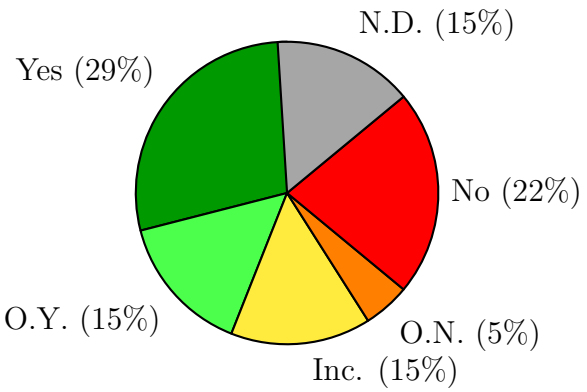

Figure 2.6: Pressure requirement satisfaction

Question 9 is the one with the most missing data, as shown in Figure 2.7. The lack of real-time ventilation control is a common issue among audited ORs, with outdated punctual measurements being another significant reason for the "No data" responses. Total ventilation recommendations are met for 51% of the audited ORs, while they are not met for 12% of them.

The availability of information and the frequency of satisfaction for the question decrease when considering the minimum outdoor air requirements. These requirements are separated into two conditions: minimum outdoor ACH (4 ACH), which addresses oxygen concentration, odor dissipation, and other air cleanliness aspects, and minimum airflow for anesthetic gases (1200 m^3/h). Separating outdoor airflow requirements into these two conditions allows for comparison between them. The minimum outdoor airflow of 1200 m^3/h for anesthetic gases is proportionally less met than the 4 ACH requirement (44% of the audited rooms meet the 4 ACH requirement, while 32% meet the 1200 m^3/h requirement), as presented in Figures 2.7b and 2.7c. This difference is expected, given that the volume of air inside the audited rooms is less than 300 m^3, which corresponds to $m^3/h = 4$ ACH.

Annual or post-maintenance particle count evaluations are not a generalized

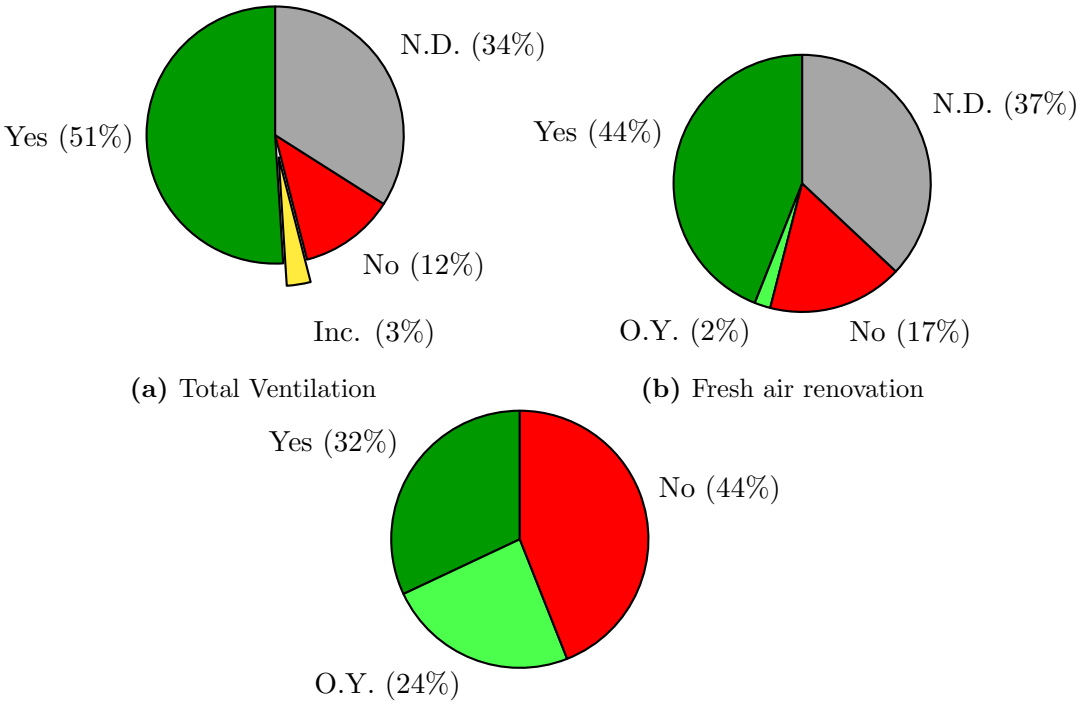

(a) Total Ventilation

(b) Fresh air renovation

(c) Anesthesia gases requirement.

Figure 2.7: Ventilation requirements, (a) Total Ventilation, (b) Fresh air renovation, (c) Anesthesia gases requirement satisfaction.

practice for OR management, as shown in Figure 2.8a. Figure 2.8b indicates that there are no particle reports available for approximately 27% of the audited ORs. Including ORs where particle counts are conducted irregularly (commonly, only one outdated particle report for ISO certification), 42% of the rooms lack annual particle reports. Responses labeled *"Observed yes"* refer to ORs where air quality is monitored using alternative criteria, such as microbiological controls. The *"Inconclusive"* responses correspond to rooms where evidence from particle count reports is missing.

It is observed that particle counts are reported annually (or at least systematically) for all ORs with VLAF ventilation systems. Although the sample size of VLAF-equipped ORs is small, a trend towards prioritizing particle counting in these rooms is evident. VLAF systems are typically installed in rooms where superior air quality is desired, as they are used for higher-risk operations that warrant a higher ISO classification (between 5 and 6 for ORs). This preference

for particle counting in VLAF-equipped rooms may reflect their intended use. However, there are also ORs with TMA ventilation systems where procedures as invasive as those in VLAF rooms are conducted. Even though SSI risk is lower in rooms where less invasive procedures are performed (less demanding in terms of PC limits), reaching the appropriate air quality standard in these rooms is equally important.

Given that the reports evaluated are based on initial audits and the subsequent conclusions presented to the IMAEs, it is expected that the frequency of particle count evaluations in less demanding rooms will progressively increase.

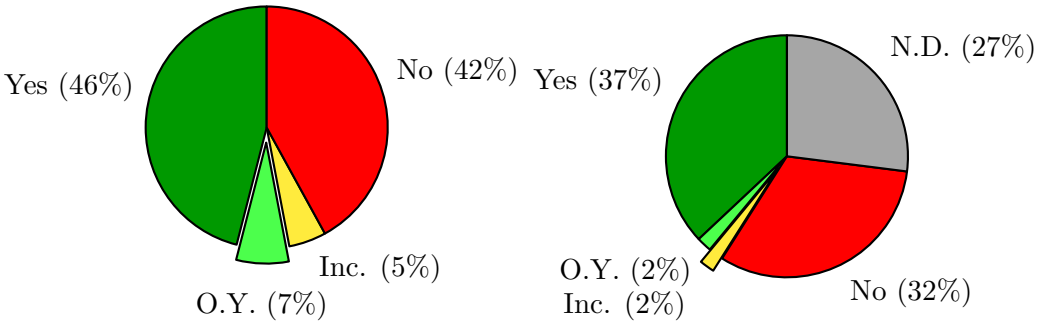

(a) About particle count practices **(b)** about particle count requirements.

Figure 2.8: Answer distribution for question 10 (a), about particle count practices and question 11 (b), about particle count requirements.

Approximately 37% of the ORs meet the ISO class recommended by the IIMPI for the procedures performed in the room. For question 11, the answer "Yes, observed" indicates rooms where particle counts are evaluated at fewer points than established by ISO. In cases where rooms with VLAF ventilation systems reported particle counts only below the injection area, the answer is *"Inconclusive"* due to the lack of information from the room periphery.

In general, a lack of information about air quality and ventilation parameters is evident in a portion of audited ORs, despite the presence of institutional managers in most cases. When separating ORs with VLAF systems from those with TMA ventilation, it is observed that ORs with TMA systems exhibit a higher degree of non-compliance and less information than those with VLAF systems. Rooms with TMA ventilation have about 21% of non-satisfactory answers (no, observed no, and inconclusive) and lack information for 19% of

the questions. In contrast, ORs with VLAF ventilation show about 15% non-satisfactory answers, with missing information for only 4% of the questions. Given that most ORs have a responsible person in charge, it is expected that, as audits continue, the understanding of facility operations and air quality parameters will improve.

Audit result analysis reveals that several factors may be affecting air quality in the room and, consequently, the quality of surgical services. For instance, inadequate control over airflow, room temperature, and supply temperature can alter the velocity field, potentially making it unsuitable for the operations being performed. This issue may be more pronounced in rooms with LAF (Vertical Laminar Airflow) systems, as suggested by Ufat et al., 2018. Additionally, rooms with insufficient differential pressure pose a higher risk of outside contamination when the door is opened, as noted by Zhou et al., 2018.

Although audit reports provide information about air quality inside the room, flow distribution is often only roughly monitored. During visits to ORs as part of the audits, significant deviations from theoretical configurations were observed. For example, in some rooms, air extraction vents were partially or completely obstructed by instrument tables or other equipment. Another issue was found in rooms modified from their original design. Specifically, in ORs with VLAF systems designed to work with a curtain separating the center of the room from the periphery, the curtains had been removed to facilitate procedures and improve staff comfort. Since VLAF ventilation sweeps contaminants from the operating area (center) to the periphery, the absence of the curtain allows contaminants to re-enter the working area when personnel move around the room. Additionally, air outlets at ceiling level are now directly in contact with the injection air, which may cause the air to 'short-circuit' from the injection to the ceiling outlets, thereby reducing the effective ACH (Air Changes per Hour) and disrupting the airflow distribution.

Such is the case with the OR used for burn treatment at the "*Centro nacional de Quemados*" (CENAQUE). This OR previously had a physical separation between the center and the periphery of the room. The separation was removed, which likely disrupted the ventilation design and caused air to short-circuit. After auditing this room, the IIMPI team recommended using a

partial separation between the inlet and ceiling-level outlets, such as an acrylic partial wall or curtain. Scenarios where the room operates with and without the partial separation are further explored in Chapter 4, using CFD to evaluate the impact of installing a partial wall and its length.

2.6. Conclusions

In this chapter, the mechanisms, technologies, practices, and regulations for controlling air quality in ORs are studied. The air quality inside an OR is considered better when it optimally supports the comfort and asepsis of its occupants. Air quality in ORs depends on several factors. The best way to ensure adequate air quality is through proper design, maintenance, and use of all associated elements (room, instruments, equipment, etc.).

The main air quality parameters for an OR are identified as temperature, relative humidity, particle concentration, ventilation (total and air exchanges), and pressure differential.

The temperature set point inside the OR must take into account the comfort and sepsis of those who occupy it. As the comfort conditions of the surgeon (which greatly influence performance) and the patient (which affects the probability of contracting SSIs) fall within different temperature ranges, the design temperature ends up being a compromise between the two, around 22–24°C (unless the procedures require different temperature values, such as for burn treatments). Relative humidity also affects thermal comfort due to sweat evaporation and wet bulb temperature, as well as air sepsis, since many bacteria travel in suspended liquids. It is concluded that a medium relative humidity range (30–60%) is recommended to prevent infections due to bacteria suspended in the air, among other factors.

To control the risk of infection within the OR, the number of suspended particles must be managed. Since bacteria cannot travel through the air on their own, both direct and indirect airborne transmission occur through particles (PM) acting as vehicles for bacterial spread.

The amount of air injected into the OR is crucial for maintaining cleanli-

ness. When the filter system is adequate, the air entering the OR is almost completely clean and is capable of dragging contaminants generated inside the room to the outside. The required airflow depends on the cleaning mechanism employed by the ventilation system—whether it is sweeping (LAF) or diffusion (TMA). LAF systems, which move large masses of air to achieve sweeping effects, generally require greater airflow compared to TMA systems.

A minimum injection of outdoor air (air changes) must always be ensured to dissipate odors, gaseous contaminants, and maintain breathable oxygen levels. Ventilation also affects differential pressure; ORs must maintain a positive pressure difference relative to all adjacent spaces to prevent the ingress of outside contaminants, unless the patient has an infectious disease.

OR ventilation systems can be categorized into two main groups: conventional, diffusive flow systems (TMA) and sweep systems (LAF). Studies have shown that LAF systems are more effective at creating a protective area within the OR, making them the preferred choice for ORs performing higher-risk procedures. In contrast, TMA systems are less complex to operate and require less ventilation, making them suitable for ORs where a lower level of air cleaning is adequate.

AHUs are responsible for supplying airflow with adequate temperature, relative humidity, and particle concentration. Each AHU should include at least two stages of filtration: a pre-filter and a high-efficiency filter, which typically removes about 90-95% of particulates, as well as temperature and RH controlling systems, such as heating and cooling coils. When additional filtration is required beyond what the AHU provides, air should be injected into the room through a terminal HEPA filter to ensure higher air quality.

At national level, there are no specific regulations for the operation and maintenance of ORs. Recently, organizations such as the FNR have begun monitoring air quality in rooms used by associated IMAEs. Analysis of reports generated by the IIMPI team for 41 rooms used by IMAEs reveals that key air quality parameters such as total ACH, outdoor ACH, temperature, humidity, and differential pressures are not commonly known by ventilation system supervisors. As interactions between the IMAEs, the FNR, and the room managers con-

tinue, it is anticipated that information on these air quality parameters will become more widely available.

On the other hand, while the reports used to analyze air quality control provides a general overview, it may not capture specific nuances of each room. For instance, in a room dedicated to burn patients, a total separation previously existed between the center and the periphery of the room. The removal of this separation may have caused air to short-circuit, diminishing the sweeping effect of the VLAF system. Installing a partial separation between the inlet and ceiling-level outlets could potentially improve airflow conditions without disrupting OR practices. This scenario is further explored using CFD in the following chapters. Chapter 3 develops and evaluates a mathematical and numerical model for contaminant transport, while Chapter 4 uses this model to assess the impact of the partial separation, comparing it with a scenario lacking such separation.

Chapter 3

Numerical-Mathematical model and validation

3.1. Introduction

Chapter 2 provides a bibliographic analysis of air quality and thermal comfort parameters, ventilation systems for ORs, and international standards, along with a survey on the management of ORs in Uruguayan hospitals. So far, air quality and ventilation inside ORs have been evaluated broadly, considering aspects such as management, ventilation, and maintenance, using the questionnaire in Table 2.4 as a reference. However, certain situations or aspects of air quality control are not covered by the questionnaire.

To evaluate specific situations or measure the impact of air quality improvement suggestions in ORs, two primary tools are generally used. The first tool involves direct corroboration through measurements. While this approach can directly confirm the effectiveness of various measures, its disadvantage is that it often requires halting the operation of the room, which conflicts with the emergency nature of the service, making it difficult to justify. Some parameters, such as temperature, humidity, pressure differential, and airflow, can be measured at specific points in real time while the room is in operation. However, additional measurements are typically only justified during scheduled maintenance.

The second method for evaluating specific air quality situations or modifi-

cations inside the OR is through modeling physical phenomena using mathematical equations. The complexity of the model depends on the desired level of precision, but generally, it includes fluid dynamics, including turbulence, which is modeled as non-linear and chaotic. Consequently, the most common way to solve the resulting mathematical systems involves numerical solutions, which are typically solved using computers. Airflow inside the OR can be modeled using CFD without interrupting OR operations.

When dealing with CFD, turbulence modeling is one of the main challenges. There are three primary approaches to turbulence modeling: Direct Numerical Simulation (DNS), which simulates both large and small vortices; Large Eddy Simulation (LES), which simulates larger vortices and models smaller ones; and Reynolds-Averaged Navier-Stokes (RANS, or URANS when unsteady), which models turbulence as "turbulent diffusion." For ORs, $k-\varepsilon$ RANS simulations are widely used (Memarzadeh and Manning, 2002, Z. Zhang and Chen, 2006, T. T. Chow and Wang, 2012, Cho, 2019, Balocco and Petrone, 2015, Yang et al., 2015, Liu et al., 2022, among others) and have produced satisfactory results, offering lower computational costs compared to DNS and LES models.

This work focuses on representing air quality by examining the concentration of airborne contaminants and ventilation quality. The presence of suspended solids (such as airborne contaminants) in the air can influence both air velocity and turbulence fields due to the principle of action and reaction. However, given the minimal number and small size of these particles, their impact on air dynamics is considered negligible.

Particle concentration is mainly modeled in two ways, using the Euler-Euler model, or the Euler-Lagrange model. The Euler-Euler or passive scalar model treats the concentration of particles as a scalar field, while the Euler-Lagrange or Lagrange transport model studies the trajectories of the particles individually through motion laws. The selection of the particle transport model to use depends on the Stokes number Stk calculated as shown in Equation 3.1, where the p subindex indicates particle property, u_0 is a reference speed magnitude and d the diameter, ρ is the density and μ the dinamic viscosity of the medium.

$$Stk = \frac{\rho_p d_p u_0}{18\mu} \tag{3.1}$$

For low Stokes numbers, the Euler-Euler model can be used with greater precision, while for high values of Stk, the Euler-Lagrange model offers better accuracy. As explained in Chapter 2, during an operation, the majority of BCPs consist of skin flakes or originate from the respiratory tract; these particles are typically represented as particulate matter between $1 - 10\mu m$. Figure 3.1 presents a model-selection diagram for airborne particle motion (Schillaci et al., 2022). According to Figure 3.1, the appropriate particle transport modeling method for OR BCPs remains unclear.

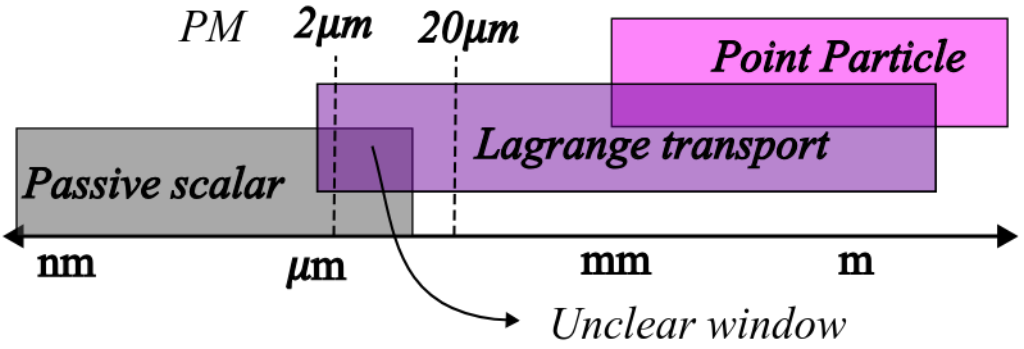

Figure 3.1: Particle motion model-selection diagram.

Most OR BCP simulations use Lagrangian transport modeling, as it has shown better results than the passive scalar approach (Memarzadeh and Manning, 2002; C. Wang et al., 2018a; F. Wang et al., 2021; Zhou et al., 2018, as examples). However, the computational cost of the Lagrangian transport model is higher than that of the passive-scalar approach, as a higher degree of post-processing is required to obtain concentration fields. An alternative approach, suggested by Chen et al., 2006 and adopted in this work, involves modifying the passive-scalar model to include the particle settling speed for the convective term (see Section 3.2).

Furthermore, room ventilation is evaluated through it's **Air age** (or age of air) τ. The age of air quantifies how much time has the air at certain point and time spent inside the operating room. This metric can be used to identify stagnation areas, evaluate the "freshness" of air exiting through different room outlets, and compare these conditions with reference scenarios.

The simulations are implemented in OpenFOAM software, which stands for Open Field Operation And Manipulation. OpenFOAM uses finite volume methods to solve partial differential equations, including non-linear equations such as the Navier-Stokes equations.

From this point onward, the study focuses on evaluating the effect of suggestions on BCP concentration. The case study is further discussed in Chapter 4. Chapter 3 describes and validates the mathematical model and numerical implementation, which are applied to the case study in Chapter 4.

3.2. Mathematical model

The scalar transport equation (Equation 3.2) is used to calculate the velocity field, temperatures, air age, turbulence kinetic energy, and turbulence dissipation rate. The parameters ϕ, Γ_ϕ, and S_ϕ take values from Table 3.1 depending on the equation, ρ is the air density, and $\vec{v} = (u,v,w)$ is the average velocity field. The Navier-Stokes equations are derived by projecting the scalar transport equation with $\phi = \vec{v}$ in each primary direction $(\hat{i},\hat{j},\hat{k})$.

$$\frac{\partial \phi}{\partial t} + \nabla.(\vec{v}\phi) = \nabla.(\Gamma_\phi \nabla \phi) + S_\phi \tag{3.2}$$

Table 3.1: Scalar transport equation parameters.

Equation	ϕ	Γ_ϕ	S_ϕ
Mass Conservation	ρ	0	0
Momentum	$\vec{v}$	$\nu + \nu_t$	$-\frac{1}{\rho}\nabla p + \vec{F}$
Energy	T	$\alpha + \nu_t/Pr_t$	$g_0/\rho c_p$
Air Age	τ	$\nu + \nu_t/\sigma_\tau$	1
Turb. Kinetic Energy	k	$\nu + \nu_t/\sigma_k$	$G - \frac{2}{3}\nabla \cdot (\vec{v}k) - \varepsilon$
Turb. Dissipation Rate	ϵ	$\nu + \nu_t/\sigma_\varepsilon$	$C_1 \left(\frac{\varepsilon}{k}G - \frac{2}{3}\nabla \cdot (\vec{v}\varepsilon)\right) - C_2\frac{\varepsilon^2}{k}$

Where ν is the cinematic viscosity of the fluid, ν_t is the turbulent cinematic viscosity, p is the pressure field, $\vec{F}$ is the volume forces, α is the thermal heat diffusion coefficient, c_p is the heat coefficient of air at constant pressure, g_0 is the volumetric heat generation, Pr_t, σ_τ, σ_k and σ_ϵ are correction factors

($Pr_t = 0.85$, $\sigma_\tau = 1.0$, $\sigma_k = 1.0$, $\sigma_\varepsilon = 1.3$), G is the turbulent kinetic energy production rate due to the anisotropic part of the Reynolds-stress tensor, $C_1 = 1.44$, $C_2 = 1.92$.

Air inside the OR is modeled as incompressible, as the overall cooling load is relatively low (T. T. Chow and Wang, 2012). Buoyancy forces are accounted for using the Boussinesq approximation (Equation 3.3), where T_0 is the reference temperature ($T_0 = 293.15$ K), ρ_0 is the air density at T_0, p_d is the dinamic pressure, z is the vertical location component, β is the volumetric thermal expansion coefficient ($\beta = 1/T_0$), and $\vec{g}$ is the gravitational acceleration ($\vec{g} = -9.81\hat{k}\ m/s^2$).

$$-\frac{1}{\rho}\nabla p + \vec{F} = -\frac{1}{\rho}\nabla(p_d - \rho_0\vec{g}z) + \vec{F} \approx -\frac{1}{\rho}\nabla p_d + \beta(T - T_0)\vec{g} \tag{3.3}$$

Reynolds Averaged Navier-Stokes (RANS) $k-\varepsilon$ turbulence models are widely used and have shown accurate results in OR simulations, as discussed in Section 3.1. Turbulence is modeled through the turbulent kinetic energy (k) and the turbulence dissipation rate (ε). The standard $k-\varepsilon$ model is implemented, and the corresponding equations can be derived from Table 3.1 and Equation 3.2. The effects of turbulence are incorporated into the Navier-Stokes equations through the turbulent viscosity ν_t, as defined in Equation 3.4, where $C_\mu = 0.09$. For other variables, such as temperature and air age, the turbulent diffusion coefficients are calculated using turbulent Prandtl numbers, as indicated in Table 3.1.

$$\nu_t = C_\mu \frac{k^2}{\varepsilon} \tag{3.4}$$

As particle forces' effect on airflow is neglected, the air velocity field can be calculated independently from particle motion. Particle transport is modeled using an Euler-Euler approach based on an alternative implementation by Chen et al., 2006, T. T. Chow and Wang, 2012 and Balocco and Petrone, 2015, which modifies the scalar transport equation by changing the advective transport term to include the deposition velocity of the particles. This approach is known as the modified drift-flux model (Equation 3.5), where $\vec{v_s}$ represents the settling speed of the particles, C is the particle concentration, D_b is the Brownian diffusion coefficient, and ϵ_p is the turbulent diffusion coefficient of the particles, $\varepsilon_p = \nu_t/Sc_t$, with Sc as the turbulent Schmidt number. This

method aims to reduce computational cost while accounting for the particle size effect on particle distributions.

$$\frac{\partial C}{\partial t} + \nabla.((\vec{v} + \vec{v}_s)C) = \nabla.((D_b + \varepsilon_p)\nabla C) + S_C \tag{3.5}$$

To estimate the settling speed, particles are modeled as perfect spheres. By developing the Navier-Stokes equation for a sphere falling under the effects of a gravitational field, Equation 3.6 is obtained. In this equation, C_c represents the Cunningham correction coefficient, calculated using Equation 3.7 (Davies, 1945), where λ is the mean free path.

$$\vec{v}_s = \frac{C_c \rho_p d_p^2}{18\mu}\vec{g} \tag{3.6}$$

$$C_c = 1 + \frac{2\lambda}{d_p}(1.257 + 0.4e^{-0.55\frac{d_p}{\lambda}}) \tag{3.7}$$

For this simulation, the mean free path was calculated using the ideal gas approximation. The settling speed depends quadratically on the particle diameter, which means that the solution of Equation 3.2 diverges from the scalar transport solution as the size of the modeled particles increases.

3.3. Numerical Implementation

Approximated solutions for Equation 3.2 and Equation 3.5 can be obtained from computational simulations. The software used for the simulations in this work is OpenFOAM v2306 ("OpenFOAM", n.d.). OpenFOAM (Open Field Operation And Manipulation) is a free-access CFD software based on the finite volume method for approximating systems of partial differential equations. This method discretizes the equations, space, and time of the problem. The space where the equations are to be solved is discretized into computational meshes, generating contiguous non-overlapping elements that completely fill the domain (cells). Dependent variables and properties (such as temperature) are primarily stored in the cell centroid but can also be stored in cell faces and vertices. Time is broken into a set of timesteps Δt, which can vary depending on the Courant number (Greenshields and Weller, 2022). The integral form of

the scalar transport Equation 3.8 is then solved for each cell.

$$\underbrace{\frac{\partial}{\partial t}\int_D \rho\phi dV}_{\text{Accumulation term}} + \underbrace{\int_{\partial D} \rho\phi\vec{v}.\vec{n}dS}_{\text{Advective term}} = \underbrace{\int_{\partial D} \Gamma_\phi \nabla\phi.\vec{n}dS}_{\text{Diffusive term}} + \underbrace{\int_D S\_\phi dV}_{\text{Source term}} \tag{3.8}$$

3.3.1. Equation discretization

When discretized and linearized, the equations adopt the form shown in Equation 3.9.

$$A.\Phi = b \tag{3.9}$$

Where A is a coefficient matrix, Φ= $(\Phi_1, ..., \Phi_n)$ is the dependent variable for every cell centroid (Φ_i corresponds to cell i), and b is the independent term. Every term can provide an explicit and implicit component. Explicit components are independent of the variable Φ and are therefore added to the independent term b, such as known source terms, boundary conditions, or Φ-dependent terms calculated for a previous timestep.

The diffusive term is linearly approximated as shown in Equation 3.10 where the f subindex represents that the magnitude is evaluated at a face f of a given cell, S is the surface area of the face and $\frac{\partial\phi}{\partial n}$ is the projection of the gradient in the normal direction $\vec{n}$, which is calculated through first grade linear approximation for internal faces.

$$\int_{\partial D} \Gamma_\phi \nabla\phi.\vec{n}dS \approx \sum_f \Gamma_\phi S_f \left.\frac{\partial\phi}{\partial n}\right|_f \tag{3.10}$$

The approximation is presented at Equation 3.11, where the subindexes i and j indicate the cells separated by the face f, d_{ij} is the distance between the cells (uncorrected linear Laplacian scheme).

$$\left.\frac{\partial\phi}{\partial n}\right| \approx \frac{\Phi_j - \Phi_i}{d_{ij}} \tag{3.11}$$

Using this scheme, the diffusive term adds coefficients to the matrix A, $a_{ij} = -\Gamma_\phi S_f/d_{ij}$ for the neighbouring cells and $a_{ii} = \Gamma_\phi S_f/d_{ii}$ for the central cell.

Source term modeling varies from equation to equation. Outside the tur-

bulence quantities, source term contribution is explicit only, as air age and particle count sources are fixed, heat generation is zero, buoyancy force, and pressure gradient are calculated considering temperature and pressure fields as input data for the momentum equation. The source term is therefore approximated using Equation 3.12, where V_i is the volume of the i cell and $S_{\phi i}$ is the source term evaluated at the center of the cell. This kind of source term adds an explicit term $b_i = V_i S_{\phi i}$.

$$\int_D S_\phi dV \approx V_i S_{\phi i} \tag{3.12}$$

Both turbulent kinetic energy and dissipation rate equations contain advective terms, which are modeled implicitly. Furthermore, the turbulence dissipation rate equation includes linearly ε-dependent terms, which are evaluated directly at the cell center and modeled implicitly as $a_{ii} = V_i \rho \left(C_1 \frac{\varepsilon_i G_i}{k_i} - C_2 \frac{\varepsilon_i^2}{k_i} \right)$.

The convective term for momentum and particle count equations requires special consideration. For the momentum equation, the convective term is non-linear. To avoid non-linear equations, OpenFOAM creates the flux field Ψ, stored at cell faces. This flux field is calculated from the velocity field at the previous time or iteration step, as shown in Equation 3.13.

$$\int_{\partial D} \rho \phi \vec{v}.\vec{n} dS \approx \rho \sum_f (S_f \vec{V}.\vec{n}) \Phi_f = \rho \sum_f \Psi_f \Phi_f \tag{3.13}$$

Upwind schemes are implemented to approximate Φ_f. Figure 3.2 presents the concept of how the upwind scheme works. If $\vec{v} \cdot \vec{n} > 0$, then $\Phi_f = \Phi_c$; otherwise, $\Phi_f = \Phi_n$, where $\Phi_c = \Phi_i$ and Φ_n is evaluated at the center of neighboring cells Φ_j (for non-boundary faces). Equation 3.14 displays the contribution of the convective term to the implicit matrix A.

$$\begin{cases} a_{ii} = \rho \sum_f \Psi_f, & \forall f / (\vec{v_f}.\vec{n_f}) > 0 \\ a_{ii} = 0, & \forall f / (\vec{v_f}.\vec{n_f}) \leq 0 \\ a_{ij} = \rho \sum_f \Psi_f, & \forall f / (\vec{v_f}.\vec{n_f}) < 0 \\ a_{ij} = 0, & \forall f / (\vec{v_f}.\vec{n_f}) \geq 0 \end{cases} \tag{3.14}$$

The modified drift-flux model incorporates the particle settling speed into the velocity field, thereby altering the advective term in the particle concentration

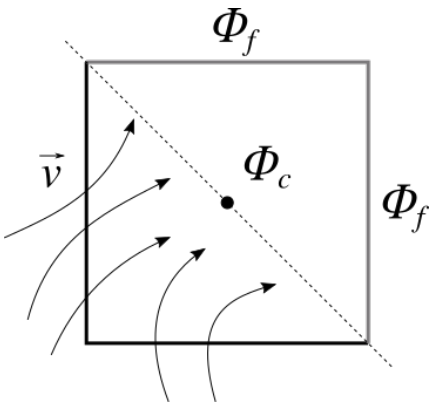

Figure 3.2: Upwind schema.

equation. An additional settling flux field was created for the numerical simulation. Equation 3.15 is employed to approximate the convective term for the particle concentration equation.

$$\int_D \nabla.(\vec{v}+\vec{v}_s)CdV = \underbrace{\int_{\partial D} C\vec{v}.\vec{n}dS}_{\text{Velocity flux}} + \underbrace{\int_{\partial D} C\vec{v}_s.\vec{n}dS}_{\text{Settling flux}} \approx \sum_f (\Psi_f + \Psi_{sf})C_f \quad (3.15)$$

Given that Ψ_s depends on particle and fluid properties, it can be calculated and added as a contributor to the implicit matrix A. Using the upwind approximation, Ψ_{sf} is incorporated into Ψ_f in Equation 3.14.

The Euler scheme is implemented to approximate the accumulation term (Equation 3.16), where the superscript p represents the current time step, and $p-1$ indicates the previous time step. This scheme adds a coefficient $a_{ii} = \frac{\rho V_i}{\Delta t}$ to the implicit matrix A and an explicit term $b_i = -\frac{V_i \rho \Phi_i^{p-1}}{\Delta t}$. The time step Δt is limited by continuously monitoring the maximum Courant number to ensure solution stability.

$$\int_D \rho \frac{\partial \phi}{\partial t} dV \approx V_i \rho \frac{\Phi^p - \Phi^{p-1}}{\Delta t} \quad (3.16)$$

Up until this point, the approximation criteria (such as the upwind scheme for advective terms) have been introduced for inner cells. Cells where one or more of their faces coincide with the domain boundary are classified as boundary cells. Field or gradient values at boundary faces are set through boundary conditions. Two types of boundary conditions are present for the simulations

in this work: Neumann boundary conditions (gradient boundary conditions) and Dirichlet boundary conditions (field boundary conditions). Whenever a gradient or field value is known due to a boundary condition, instead of adding the corresponding entry to the implicit matrix, an explicit term is obtained.

3.3.2. Implemented Algorithms

The simulation process is divided into two stages. The first stage results in the velocity field. During this stage, the temperature, velocity, pressure, and turbulence fields are solved using the *buoyantBoussinesqPimpleFoam* solver. In the second stage, the particle concentration and air age fields are calculated using the velocity field and turbulence diffusivity as input data, employing a custom solver. Velocity and particle concentration are calculated independently, as the influence of the particle-air interaction is assumed to be negligible for air motion.

Two algorithms are implemented in the simulation, each associated with the different stages. The *PIMPLE* algorithm, represented in Figure 3.3, is used in the first stage for solving the equation system, resulting in the temperature, pressure, momentum, and turbulence fields. For every timestep, the *PIMPLE* algorithm starts by solving the energy equation for T. The momentum equation is then used to obtain an approximation for the velocity field $\vec{v}$, using the last pressure field calculated. Inside the *PIMPLE* loop, the *Pressure-Implicit with Splitting of Operators (PISO)* loop starts by solving the mass conservation equation (derived into the pressure equation), updating the pressure field p. Both the velocity field $\vec{v}$ and the flux at each face are then coupled with the pressure field using a momentum corrector $H(\vec{v})$, as defined in Equation 3.17. The momentum corrector is then used to update the velocity field by substituting Equation 3.17 into the momentum version of Equation 3.2 (Navier-Stokes), obtaining the pressure-velocity coupling in Equation 3.18 Greenshields and Weller, 2022.

$$A_u.\vec{v} - H(\vec{v}) \equiv \frac{\partial \vec{v}}{\partial t} + \nabla.(\vec{v}.\vec{v}) - \nabla.(\nu \nabla \vec{v}) - \beta(T - T_0)\vec{g} \tag{3.17}$$

$$A_u.\vec{v} - H(\vec{v}) = -\nabla p \tag{3.18}$$

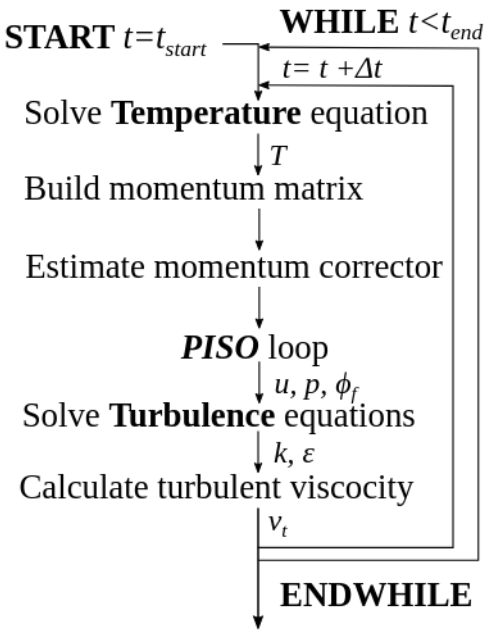

Figure 3.3: First stage algorithm (*PIMPLE*) logic.

The PISO loop restarts at this point, iterating until the convergence criteria are met. Afterwards, the turbulence kinetic energy k and dissipation rate ε are calculated, updating the turbulent viscosity ν_t, thus closing the PIMPLE loop. The loop then restarts with the updated values of Ψ_f, p, T, k, ε, ν_t, and $\vec{v}$, and continues until the convergence criteria are satisfied. Once convergence is achieved for a given timestep, the simulation advances to the next timestep, provided that the current time value is still smaller than the specified time limit.

The energy, momentum, and pressure equations are under-relaxed, which means that the amount of change in each variable is limited at every iteration step. This technique helps maintaining stability for higher Courant numbers by ensuring the diagonal dominance of the implicit matrix A, thus preventing divergence during the simulation process.

The first stage focuses on converging the velocity field, which ultimately influences the contamination concentration and air age fields, used to measure air quality in this work. Once the velocity field and turbulent diffusion coefficients have converged, a secondary solver with its own algorithm is applied to calculate air quality parameters. This secondary solver only solves for contam-

ination concentration and air age, without updating the velocity, momentum, turbulence, or temperature for a given time step. Since no coupling is required, the algorithm does not need iterations. Its logic is illustrated in Figure 3.4. The two-stage approach—determining the velocity field and air quality parameters separately—can be consistently implemented because transient situations are not the focus of this work.

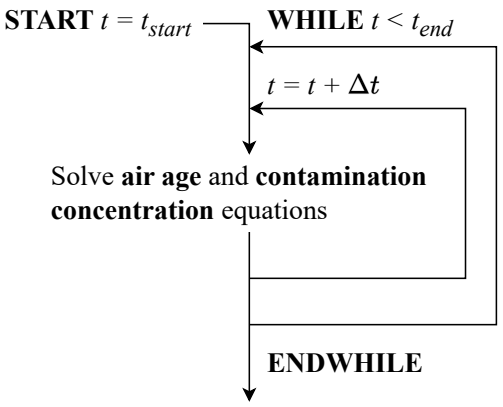

Figure 3.4: Second stage algorithm logic.

It is important to clarify that within the OR, personnel movements, door openings, and other events disrupt the airflow balance. However, the effect of these dynamic events is beyond the scope of this work.

3.4. Validation

Air quality parameter fields, such as BCP concentration and air-age, are the result of a two-stage simulation (as explained in Section 3.3). The first stage, or momentum stage, approximates the momentum, temperature, and turbulence fields until a stationary regime is reached. The second stage, or contamination stage, uses the turbulent diffusion coefficient and stationary average velocity field to approximate the particle concentration and air age fields. Both simulation stages employ different solvers and algorithms, which require validation.

To validate the mathematical model and numerical implementation, the heated cavity experiment by Limane et al., 2015 and the two-zone chamber particle

transport experiment by Lu et al., 1996 are simulated. The heated cavity experiment specifically serves to validate the momentum solver. In this experiment, a prismatic rectangular cavity is uniformly heated from the floor, while airflow is injected near the ceiling level and extracted from the opposite side at floor level, as illustrated in Figure 3.5. This experiment was chosen due to the significant velocity gradients and buoyancy forces present.

The comparison with the two-zone chamber experiment further validates the momentum solver and provides validation for the second contamination solver. Initially, a contaminant is uniformly distributed in the first zone of the chamber. Airflow is then forced from zone one to the outside of the chamber through the second zone for 26 minutes. Contaminant concentration is measured at one-minute intervals for both zones, allowing for comparison with the simulation results.

This Section presents the simulation parameters of each of the validation experiments, as well as the main results, and a brief analysis of parameters.

3.4.1. Heated cavity

The heated cavity test is selected to evaluate the accuracy of the numerical implementation in predicting velocity fields with temperature gradients. The cavity scheme is presented in Figure 3.5. The velocity profile at $(y = W/2, x = 2H)$ was recorded by Limane et al., 2015, and a comparison between the reference measurements and the simulation results is used to validate the momentum equation. A 2D regular mesh is employed to reduce computational cost, as the reference measurements are located away from the front and back of the cavity. The inlet boundary conditions are set to a uniform speed of $\vec{v} = (15.2\,,\,0\,,\,0)$ at a uniform temperature of $T_i = 295.15\,\mathrm{K}$, with a turbulence intensity of $I = 5\%$. A fixed temperature gradient of $\nabla T = 20230\,\mathrm{K/m}$ is imposed on the bottom surface to represent the constant heat flux $\dot{q}'' = 563\,\mathrm{W/m^2}$ (given the air conductivity $\kappa = 0.0278\,\mathrm{W/mK}$). The right, top, and left walls are set to $\nabla T = 0$ and $\nabla k = 0$. Epsilon wall functions are implemented to model the ε boundary conditions. The outlet is set to a uniform pressure of 0, with zero gradients for k, T, ε, and $\vec{v}$. After conducting simulation experiments, the final simulation time was set to 10 seconds, with a write interval

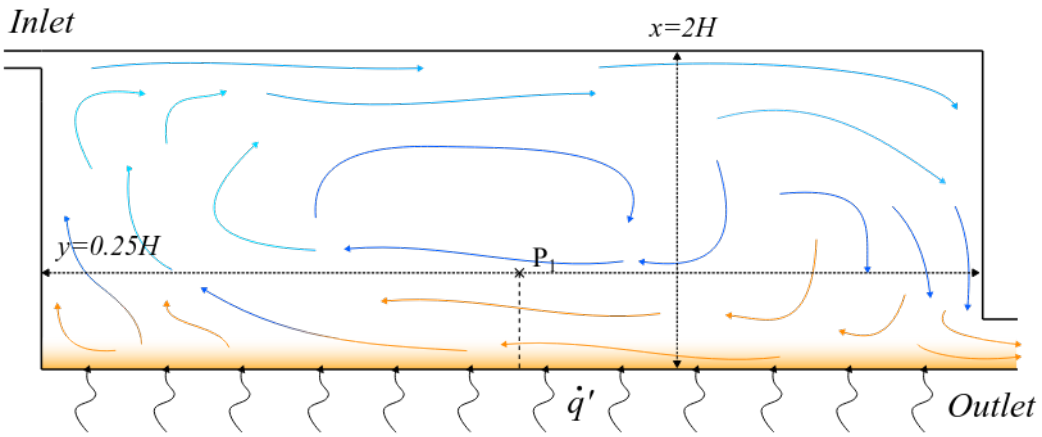

Figure 3.5: Heated cavity descriptive schema.

of 0.01, and the time step was adjusted to maintain stability.

A mesh convergence test is conducted using the temperature at $y = 0.25H$ and the velocity at $x = 2H$ as indicators. Three meshes are evaluated: coarse, fine, and finer. The principal characteristics of these meshes are presented in Table 3.2, where the h_{ref} value is used to calculate the number of divisions in each direction. The fine and finer meshes are graded, reducing the distance

Table 3.2: Heated cavity meshes.

Mesh	#Cells	Type	Grading	h_{ref}
Coarse	12464	Structured	No	2.50
Fine	19570	Structured	Yes	2.00
Finer	50020	Structured	Yes	1.25

between each cell centroid and the wall distance in both the y and x directions, as shown in Figure 3.6. Grading was implemented with an expansion ratio of $e = 4$, meaning the side length of the largest cell is four times that of the smallest cell. Additionally, an unequal distribution of cells was employed, increasing the number of near-wall cells to better represent the gradients near the wall.

The comparison between the three meshes is displayed in Figure 3.8. Although the velocity does not vary significantly across the meshes, a notable difference exists in the temperature profiles, particularly between the coarse mesh and the fine and finer meshes.

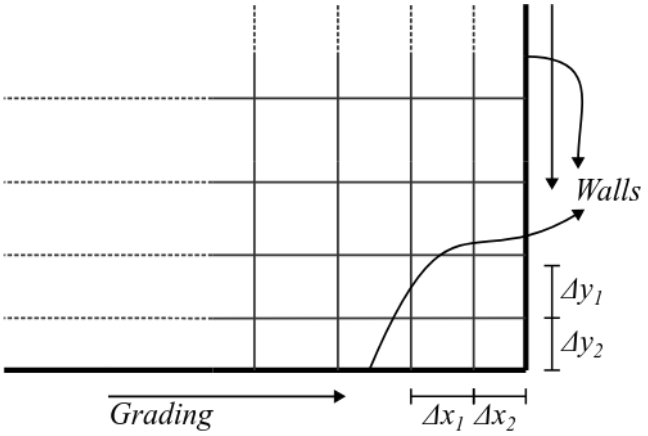

Figure 3.6: Mesh grading schema

The results for temperature and velocity show minimal variation between the fine and finer meshes. Given the difference in computational cost, further analysis is conducted using the fine mesh.

To compare simulation results with the reference data, it is essential to assess the steady state. The evolution of temperature, velocity, and pressure is evaluated at p_1 ($x = 191\,\text{mm}$, $y = 37.5\,\text{mm}$). The temperature, which is observed to be the last field to stabilize, ceases to change after a few seconds, as illustrated in Figure 3.7. A steady state appears to be well established after $t = 5\,\text{s}$.

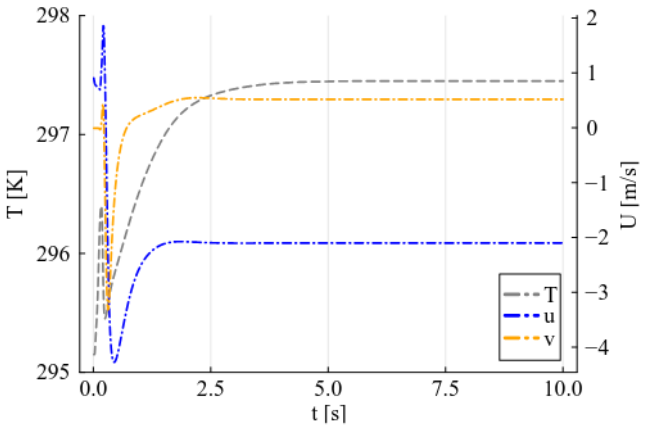

Figure 3.7: Temperature evolution at p_1 Figure 3.5.

The comparison between experimental data and simulated results is graph-

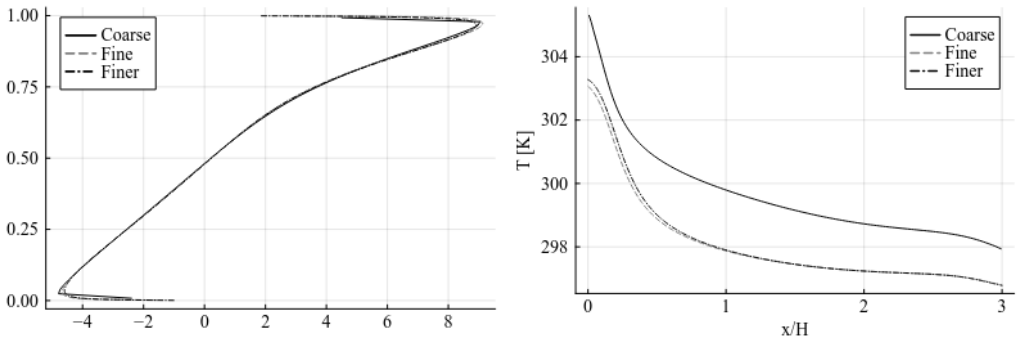

(a) x-velocity profile at $x = 2H$. **(b)** Temperature profile at $y = 0.25H$.

Figure 3.8: Result comparison for the different meshes.

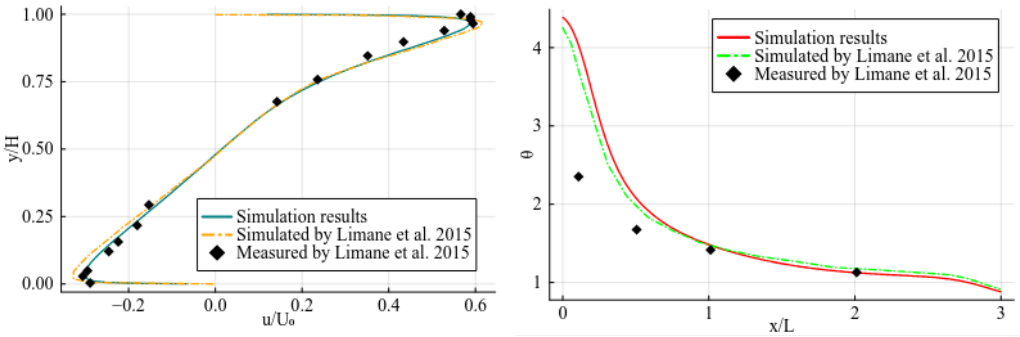

(a) Horizontal velocity at $x = 2H$. **(b)** Temperature at $y = 0.25H$.

Figure 3.9: Simulation results compared with reference simulation results and experimental data.

ically presented in Figure 3.9a. A high degree of agreement can be observed between the simulated velocity profile and the reference data. Additionally, the adimensional temperature profile $\theta = \frac{T - T_{ref}}{T_{in} - T_{ref}}$, where T_{ref} is the average outlet temperature, is compared against experimental and simulated data from Limane et al., 2015 at $y = 0.25H$ (Figure 3.9b). While the temperature measurements appear to differ from the simulated results for $x/H < 1$, both simulation results are consistent with each other and follow the trends of the measured data.

3.4.2. Two-zone chamber particle transport

The two-zone chamber experiment proposed by Lu et al., 1996 investigates airflow and particle concentration within a chamber composed of two identical zones: Zone 1 and Zone 2. Air enters the chamber through Zone 1 near

ceiling level and flows to Zone 2 through a door located at its midpoint. The air then exits the chamber through the outlet, situated in Zone 2 near ground level. The geometry of the two-zone chamber is presented in Figure 3.10. Initially, Zone 1 is filled with a uniformly distributed gaseous contaminant and is hermetically sealed from Zone 2 (closed door), which is initially clean. At the start of the experiment, air is forced into Zone 1, and the door is opened, allowing both air and the gaseous contaminant to pass into Zone 2.

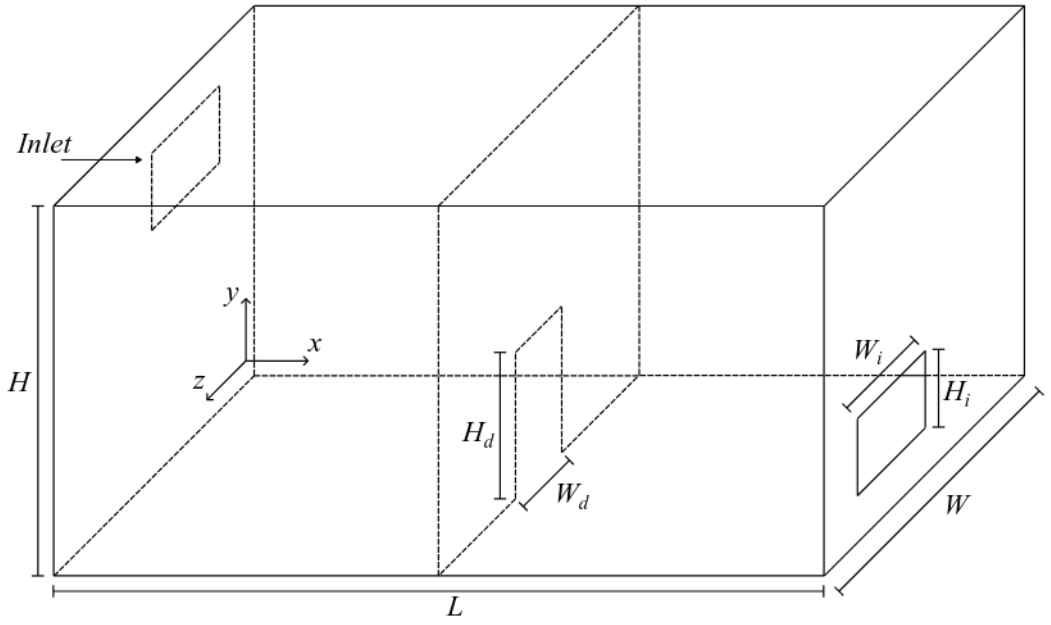

Figure 3.10: Two zone chamber geometry diagram.

The chamber is designed as a rectangular prism with dimensions $L = 5\,\text{m}$, $H = 2.4\,\text{m}$, and $W = 3\,\text{m}$. The zones are connected through a door with dimensions $W_d = 0.7\,\text{m}$ and $H_d = 0.95\,\text{m}$. The dimensions of Zone 1's inlet and Zone 2's outlet are $W_i = 1\,\text{m}$ and $H_i = 0.5\,\text{m}$, respectively. The differences in the x, y, and z axes between the inlet and outlet lead to a three-dimensional flow, where no velocity component can be omitted or considered insignificant compared to the others. Thus, a 3D analysis is necessary.

One of the most well-known disadvantages of RANS modeling is its inaccuracy in capturing unsteady structures in turbulent flows. The two-stage solver algorithm (explained in Section 3.3.2) is designed to address this issue. Two cases with different methodologies for calculating particle concentration

are compared. Case "A1" solves all equations simultaneously (temperature, momentum, pressure, turbulence, particle concentration, and air age). In contrast, Case "A2" solves the temperature, momentum, and turbulence equations until a time-invariant velocity field is achieved; thereafter, the equations for particle concentration and air age are solved using the stationary velocity field. It is important to note that, from the steady state onward, the velocity field is identical for both cases A1 and A2, as the effect of particles on air velocity is considered negligible.

Validating fully developed velocity fields is required, as the velocity fields inside ORs in this work are considered unaffected by personnel and patient movement, and ventilation systems are initialized hours before operations to ensure adequate airflow. However, simulations starting from $t = 0$ are still compared to the experimental results, solving all equations simultaneously. Given the absence of thermal loads in the camber, temperature calculations are omitted for this validation scenario.

The inlet boundary conditions are set to uniform $u = 0.09216\,\mathrm{m/s}$, $v = 0$, and $w = 0\,\mathrm{m/s}$ to match the experimental conditions; turbulence intensity is set to $I = 5\%$. The walls are assigned a "*No slip*" condition (null velocity at boundary corresponding cell faces) for the velocity field, and a "*Zero gradient*" condition for pressure and turbulent kinetic energy fields. Epsilon wall functions are implemented for the dissipation rate boundary conditions. For the outlet boundary conditions, all fields are set to "*Zero gradient*" except for the pressure field, which is fixed at a uniform $p = 0\,\mathrm{m^2/s^2}$.

Initial conditions differ between both cases: In Case A1, the particle concentration is set to match the experiment at $C = 10^5\,\mu\mathrm{g/m^3}$ inside zone 1, and $C = 0$ elsewhere. In Case A2, the initial conditions for particle concentration are set to $C_1 = 5.2 \times 10^3\,\mu\mathrm{g/m^3}$ (uniform concentration in zone 1) and $C_2 = 3.0 \times 10^4\,\mu\mathrm{g/m^3}$ (uniform concentration in zone 2).

Boundary conditions are set to $C = 0$ for the inlet, as the air entering the room does not carry any gaseous contaminant. For every wall, $C = 0$ is also set, meaning that once a particle touches a wall, it permanently leaves the domain (particles do not rebound or resuspend) (Chen et al., 2006). The outlet

boundary condition is set to $\nabla C = 0$, allowing air to exit the room.

To represent particle size effects, particle concentrations are calculated for representative particle sizes C_Φ, where the overall particle concentration C is the average of these representative sizes. Concentrations for particles of sizes $\Phi = 1\ \mu m$, $\Phi = 5\ \mu m$, and $\Phi = 10\ \mu m$ are calculated independently. However, since the gaseous contaminant used for the two zone chamber experiment diameter ranges from 0.5 to 5 μm, the representative concentration is only computed by averaging the concentrations of particles with sizes $\Phi = 1\ \mu m$ and $\Phi = 5\ \mu m$, giving $C = \frac{1}{2}(C_1 + C_5)$. To achieve better agreement between data and simulation, different turbulent Schmidt numbers are tested, with $Sc_t \approx 0.3$ yielding the best results.

A mesh convergence test is conducted using the x and y components of the average steady-state velocity field (u and v, respectively). Since steady state is achieved and only the velocity is evaluated, the mesh convergence test is valid for the velocity fields of both cases "A1" and "A2." The u profiles across the y axis are graphed within the chamber after confirming steady state. Three meshes are evaluated, named coarse, fine, and finer, with their principal characteristics presented in Table 3.3. All tested meshes are structured and graded, with cell sizes decreasing as the distance to the chamber walls decreases, as shown in Figure 3.6. The expansion rate for this simulation is set to $e = 4$ (see subSection 3.4.1).

Table 3.3: Two zone chamber meshes.

Mesh	#Cells	Type	Grading	Base cell size
Coarse	296.512	Structured	Yes	5 cm
Fine	580.300	Structured	Yes	4 cm
Finer	1.351.622	Structured	Yes	3 cm

The results of the convergence tests are illustrated in Figure 3.11. Figures 3.11a, 3.11b, and 3.11c present the speed profiles $u(y)$ at $\mathcal{L}_1(y) = (x_1, y, z_1)$, located at the inlet level of zone 1, $\mathcal{L}_2(y) = (x_2, y, z_1)$ in zone 2, and $\mathcal{L}_3(y) = (x_1, y, z_2)$, where $x_1 = 1.25\,\text{m}$, $z_1 = 1\,\text{m}$, $x_2 = 3.75\,\text{m}$, and $z_2 = 1.5\,\text{m}$. The vertical speed profiles $v(x)$ are shown in Figures 3.11d and 3.11e, which display speed profiles in zones 1 and 2, respectively. Both graphs correspond to the line segment $\mathcal{L}_3(x) = (x, y_0, z_1)$, where $y_0 = 1.2\,\text{m}$. The fine mesh is

selected for further experimentation, as its computational costs are lower than those of the finer mesh, while both yield similar results.

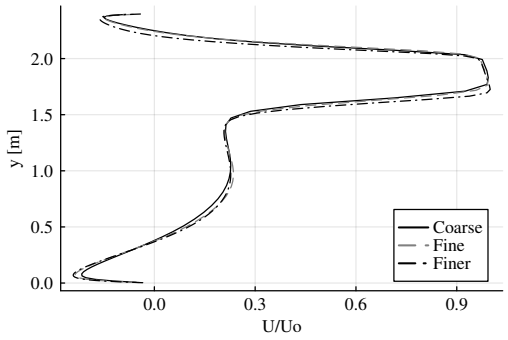

(a) u Profile at $x = 1.25\ m$, $z = 1\ m$.

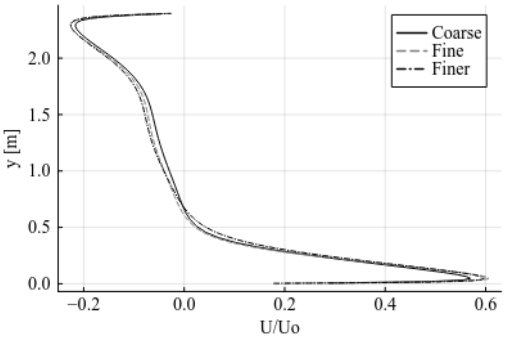

(b) u Profile at $x = 3.75\ m$, $z = 1\ m$.

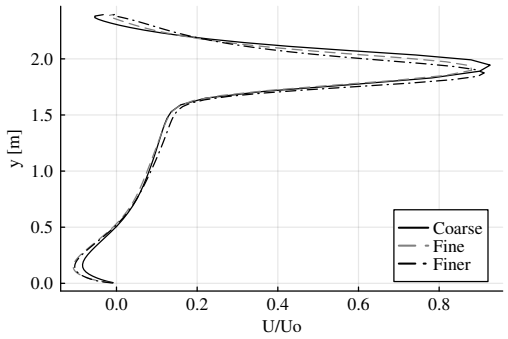

(c) u Profile at $x = 1.25\ m$, $z = 1.5\ m$.

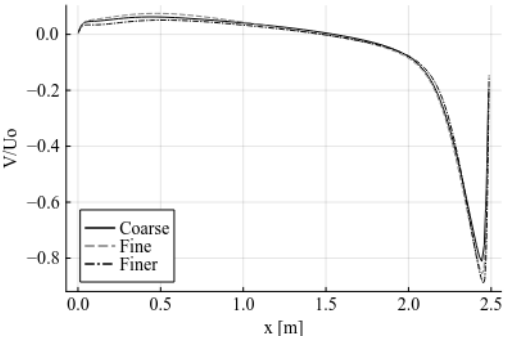

(d) Zone 1 v profile at $y = 1.2\ m$, $z = 1\ m$.

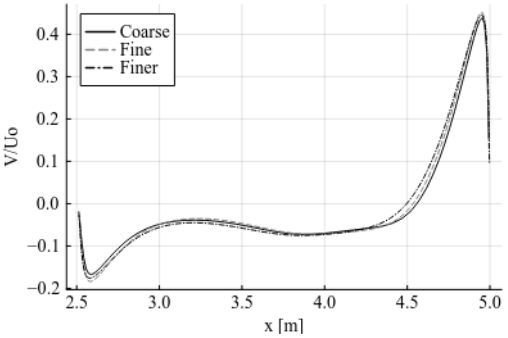

(e) Zone 2 v profile at $y = 1.2\ m$, $z = 1\ m$.

Figure 3.11: Result comparison for the different meshes.

The fine and finer meshes generate similar results, while the coarse mesh shows notable discrepancies near walls and in high-gradient zones. Therefore, further analysis is conducted using the fine mesh, which has minimal differences from the finer mesh and reduced computational costs. The velocity field at $z = 1\,\text{m}$ is qualitatively compared to the results obtained by Lu et al., 1996, as illustrated in Figure 3.12. The simulated velocity field closely resembles that reported in the reference work.

To obtain a better flow characterization, streamlines passing through the

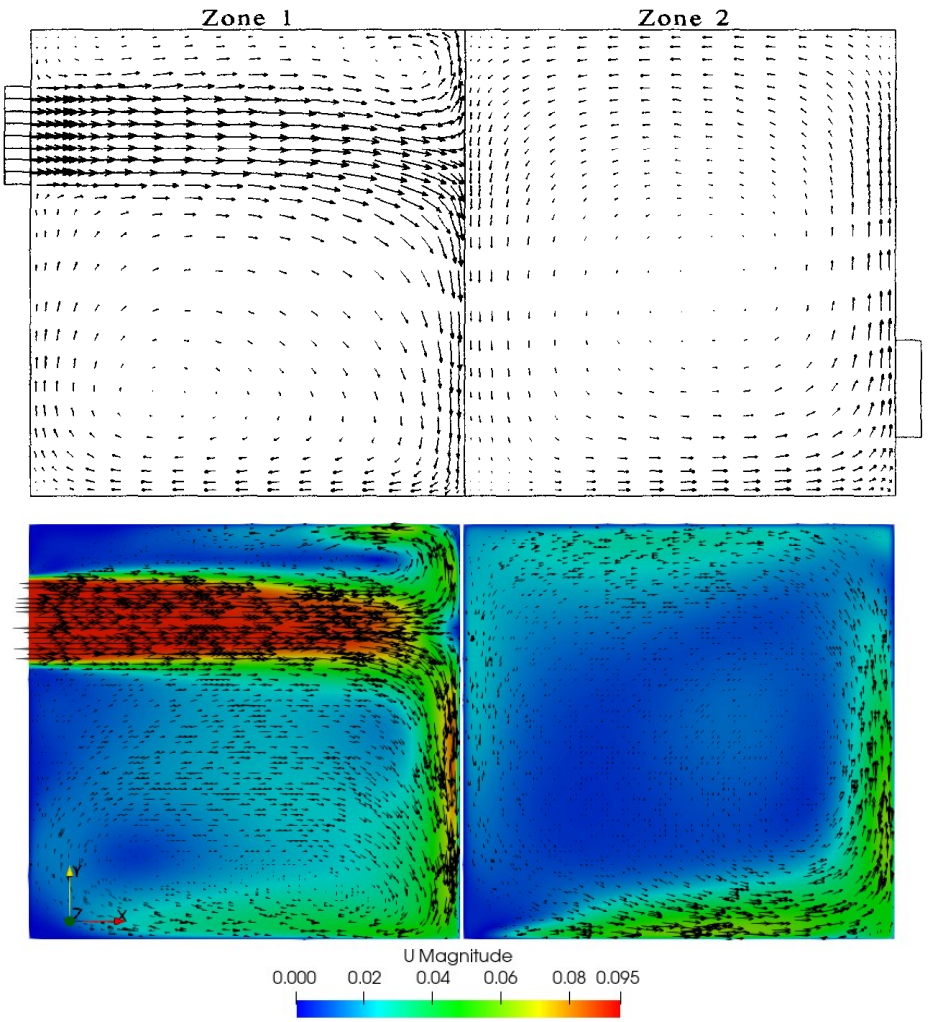

Figure 3.12: Velocity field comparison with Lu et al., 1996 simulation.

inlet are plotted in Figure 3.13. The flow in both zones of the cavity is characterized by a three-dimensional velocity field with areas of high vorticity. In zone 1, the airflow appears to traverse a large portion of the cavity before transitioning to zone 2. Once inside zone 2, the air seems to move more directly out of the cavity, resulting in larger areas of stagnant air. Consequently, air in zone 1 is expected to be better ventilated (with a lower air age) and cleaner (with a lower particle concentration), while zone 2 is anticipated to exhibit significant differences in concentration and air age between the air passing through the separating door and the stagnant air within zone 2.

The results for case A1 are presented in Figure 3.14. A significant degree of disagreement can be observed between the simulated and experimental data;

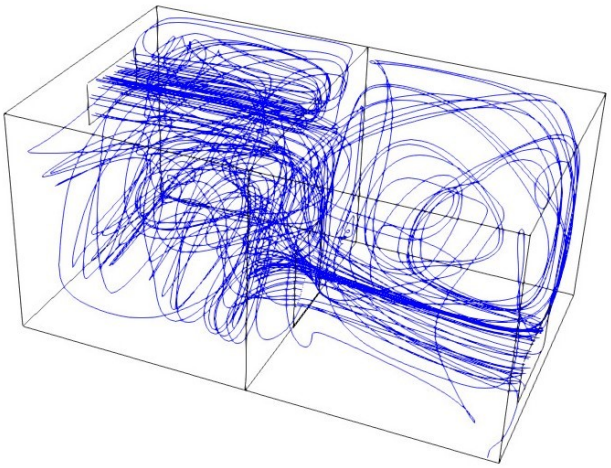

Figure 3.13: Two zone chamber streamlines through separating door.

however, the time tendencies appear similar. The initial discrepancies can be attributed to unsteady velocity field variations that are not accurately represented by URANS modeling.

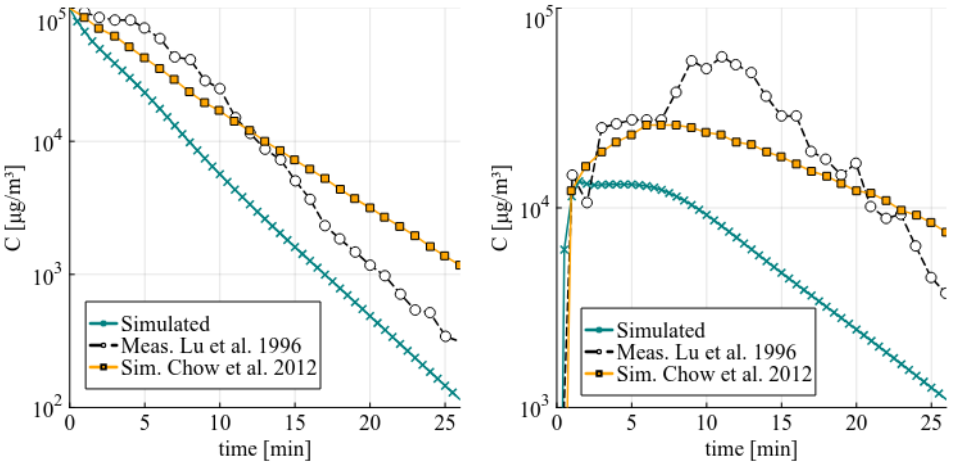

(a) Zone 1. **(b)** Zone 2.

Figure 3.14: Particle concentration comparison between full duration experiment and simulations.

Case A2, which implements the two-stage solver, shows better correlation with the experimental data. Starting from a fully developed velocity field and assuming a uniform distribution, the rate at which contamination decays closely matches the experimental results, as shown in Figure 3.15.

Particle concentration is higher inside zone 2 primarily due to the lower

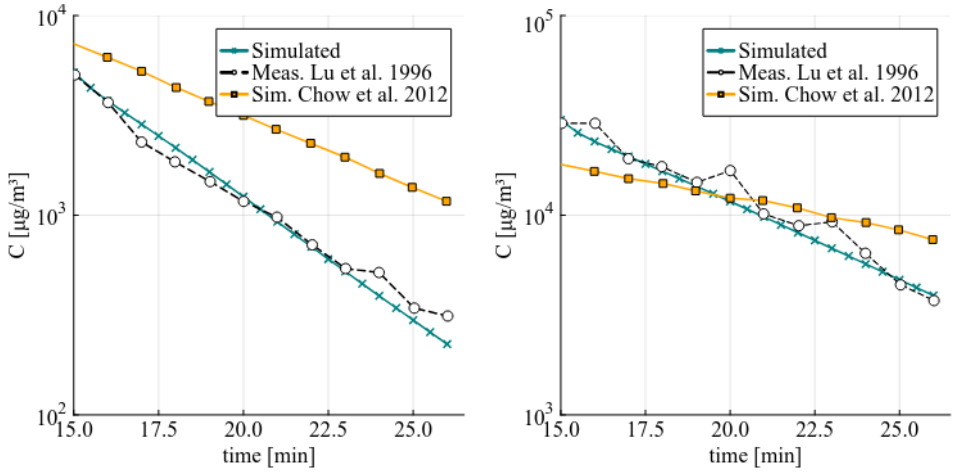

(a) Zone 1. **(b)** Zone 2.

Figure 3.15: Fully developed velocity field contaminant concentration evolution against measured data.

degree of mixing. This reduced mixing is confirmed by observing Figure 3.16a, which displays the distribution of PM_5 concentration across three planes inside the cavity at $t = 27$ min. The particle concentration distributions align closely with the air age distributions (Figure 3.16b), confirming that poorly ventilated air tends to carry more contaminants. Poorly ventilated zones with stagnant air are found in zone 1, away from the inlet and the internal door, as well as in zone 2, away from the outlet and the internal door.

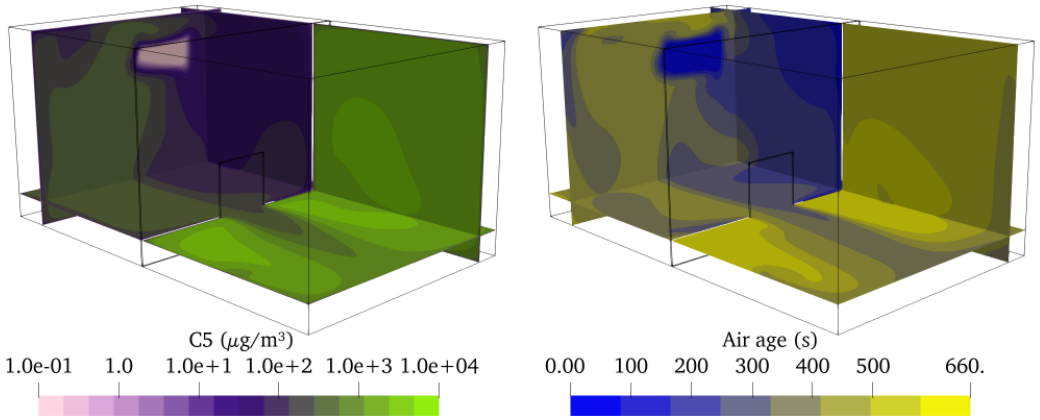

(a) Particle concentration $\phi = 5\ \mu m$. **(b)** Air age.

Figure 3.16: Two zone chamber air quality distribution visualization planes.

Although the air-age and particle concentration fields exhibit a strong cor-

relation, the effect of particle size is evident in the particle concentration y profiles, with relatively lower concentrations of heavier particles observed near the roof level. Air stagnation in the upper regions of the cavity does not correspond with heavy particle concentration, as shown in Figure 3.17.

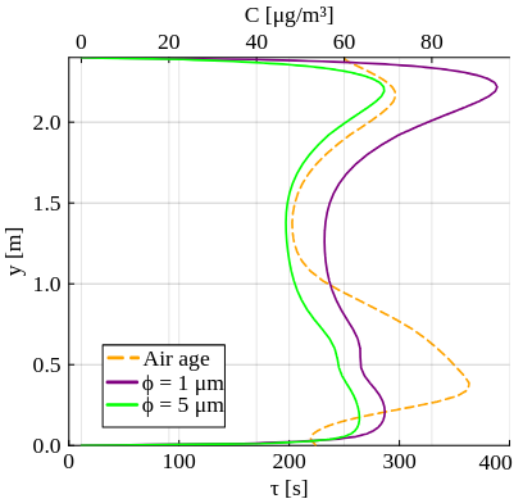

Figure 3.17: Differences between air age and different particle size distributions at zone 1.

3.5. Conclusions

The proposed model simplifies and approximates the conservation equations of momentum, energy, mass, and other relevant properties for air within the control volume. Turbulence is modeled using the RANS $k-\varepsilon$ approach, which calculates the average air velocity while accounting for all scales of turbulence. By employing a RANS turbulence model and disregarding the effects of particles on the air velocity field, the distribution of contaminants can be calculated independently over a stationary velocity field. Accordingly, a two-step resolution algorithm is proposed: the first step computes the fields of velocity, pressure, temperature, and turbulence, while the second step determines the air quality fields, specifically air age and contaminant concentration, utilizing the precomputed velocity field and turbulent diffusion coefficient.

To validate the implemented model, the "heated cavity" case by Limane et al., 2015 and the "two-zone chamber" case by Lu et al., 1996 were selected.

These cases evaluate the model's effectiveness in simulating air movement in both the presence and absence of temperature gradients, in two and three dimensions, and in transporting contaminants. The proposed resolution algorithm is assessed by comparing it with an algorithm that resolves both steps simultaneously. The heated cavity case simulates airflow within a chamber with an air inlet and outlet, uniformly heated from its bottom surface. The objective is to evaluate the model's capability to simulate thermal, flow, and buoyancy dynamics. The model satisfactorily captures the velocity fields within the chamber, achieving good coherence with experimental data. Although the temperature results show significant deviations from the reference measurements, the obtained temperature distributions closely align with other simulation results reported in the literature.

The two-zone chamber experiment simulates the transport of a gaseous contaminant within a chamber, initially comprising a contaminated zone (zone 1) and a clean zone (zone 2). At the onset of the experiment, air flows from the exterior into zone 1 and subsequently into zone 2, thereby cleaning the air within the chamber. This case builds on the heated cavity scenario by evaluating the model's precision in simulating 3D flows, accurately representing contaminant transport, and assessing the resolution algorithm. Results from the scenario where all equations are solved simultaneously show significant discrepancies from the contaminant concentration measurements within the chamber, a trend also observed in other reference simulations. However, when contaminant distribution is calculated over a converged velocity field, the model's ability to predict contaminant concentrations improves substantially. This is particularly significant, as ORs typically operate with stationary velocity fields, with ventilation systems running well before operations commence to ensure proper airflow.

While the model requires further evaluation and validation through measurements within the actual OR to enhance its credibility, it is concluded that the model is suitable for evaluating the proposed study case. Specifically, it is effective for simulating airflow within an OR with a stationary velocity field, where air movement is independent of interactions with contaminants.

Chapter 4

Case Study: Effect of the partial wall at ceiling level

4.1. Introduction

The contents of Chapter 4 bring together some of the conclusions of Chapter 2, using the model proposed in Chapter 3 to carry out a more detailed analysis of air quality on more specific real situations than what was studied in the questionnaire in Section 2.5. Vertical laminar airflow systems have traditionally been utilized in critical surgery ORs. However, outdated layouts featuring curtains between the operating table and ceiling-level air inlets have been observed to disrupt surgical practices. Some surgical teams have removed these curtains, potentially leading to "short-circuiting" of airflow from the inlet to peripheral ceiling outlets, compromising necessary airflow distribution for room cleanliness. To mitigate this issue, installing a partial wall at ceiling level to block direct airflow exit has been proposed as an alternative solution. The OR of the "Centro Nacional de Quemados" (CENAQUE) which stands for national burned center, is selected as the case study room. The selection of the case study is made for three main reasons:

- It is one of the rooms where the curtains were removed, and after the suggestion replaced with a partial separating wall between the inlet and ceiling level outlets.
- As this is a burn patient care room, visits to the room can be coordinated in advance to take measures, without interrupting the emergency nature of the service.

- The maintenance and operation team of the room show good will and enable the room so that the necessary measures can be carried out.

As stated in Chapter 3 the use of CFD to simulate OR airflow distributions has rapidly grown in the latest years, with the reduction of computational costs and increase of resources. Some simulation focus on evaluating different ventilation systems and dispositions; Memarzadeh and Manning, 2002 used CFD to evaluate 11 ventilation systems inside an OR (evaluating them at different air changes per hour ACH), concluding that systems with laminar airflow provide better contamination control. C. Wang et al., 2018a Compared the contamination reduction efficiency of vertical and horizontal LAF systems using CFD, concluding that the selection between VLAF and Horizontal Laminar Airflow (HLAF) depends on the obstacles, and object distribution inside the room. Alsved et al., 2018 and C. Wang et al., 2018b used CFD to compare the TCAF system against the LAF and TMA systems. both concluded that LAF and TCAF are more efficient at removing bacteria from the air at wound level when compared to TMA, with TCAF reducing energy consumption.

Movement impact inside the room has been evaluated, Brohus et al., 2006 examined the impact of staff movement from less clean to ultra clean zones through smoke visualization and CFD. Staff movement was simulated using distributed momentum and turbulence sources and was found to impact velocity and contamination fields. T. T. Chow and Wang, 2012 designed a dynamical simulation to measure the impact of staff bending over the operating bed with a variable particle release rate due to physical activity. Their simulation resulted in BCP concentrations over 10 CFU/m^3 in the critical zone when the staff bent over. The effect of opening and closing the OR sliding door was evaluated using CFD by Zhou et al., 2018. Two cases were evaluated, one where the temperature inside the OR is lower than the anteroom and one where it is higher. They found that, when the temperature inside the OR is higher than the anteroom, contamination intrusion rate and depth are lesser than when the temperature is lower.

Other investigations focus on the effect of different design parameters on comfort and contamination risk. Thermal comfort and contaminant removal efficiency was tested by Ho et al., 2009 using CFD, variating the position of

the supply and exhaust grilles. Supply temperature $19^oC < T < 22^oC$ and velocity $0.1m/s < v_i < 0.2m/s$ were simulated by Ufat et al., 2018, particle count was found to decrease at lower temperatures and high supply velocities, with surgical teams preference being $v_i = 0.1\ m/s$ and $T_i = 19^oC$.

Considering studies about air quality in ORs, this work focuses on air quality parameters such as concentration of contaminants C in CFU/m^3 and air age τ in min for three scenarios. Scenario 1 simulates air quality parameters within a representatio of the CENAQUE OR with the installed partial wall, Scenario 2 with a shorter partial wall and Scenario 3 without it. Partial wall installation effectiveness is evaluated by comparing air quality near surgical staff members and patient with and without it.

4.2. Case study description

The simulated room emulates the surgery room of the CENAQUE which stands for national burn treatment center, where procedures are performed on patients with burned skin. The room has a laminar flow system with air recirculation. According to discussions with the room's maintenance and operation personnel, the ventilation system starts working hours before operation. Unlike other ORs, patient admission is predictable well in advance as burned skin patients must go through a surgical bath before. Said nature of operation allows measures to be taken without stopping its operation.

As mentioned in Chapter 2, air temperature and relative humidity inside burned units are fixed due to procedure requirements (thermal comfort of the surgical team can not be aimed for). Burned skin treatment requires heat loss from the patient to be as small as possible, and sweating should be avoided. Supply temperature of the CENAQUE OR is controlled to be above 30ºC, airflow is introduced through a single inlet at ceiling level at an average velocity of 0.26 m/s (see Figure 4.1). Photos of the actual room are presented in Figure 4.2. Photos display tables for instruments and material disposal containers, among other elements. In order to simplify the simulation said elements are not considered, only including the surgical bed, surgical lamp, partial wall and an element of surgical equipment (which corresponds to the anesthesia machine). The main dimensions of the geometry and a diagram of

the air inlets and outlets are shown in Figure 4.1. The maximum length of the room is $L = 6.36\ m$ for the x direction and $B = 6\ m$ for the y direction. Room height differs between the periphery $H = 2.37\ m$ and under the laminar flow $H + h_1 = 2.51m$. The partial wall depth is $h_1 + h_2$. The installed partial wall length is 0.425 m, in order to study the effect of partial wall length, three scenarios are simulated, Scenario 1, using the real partial wall length $h_2 = 28.5\ cm$, Scenario 2 with a shorter partial wall $h_2 = 17\ cm$ and Scenario 3 without a partial wall.

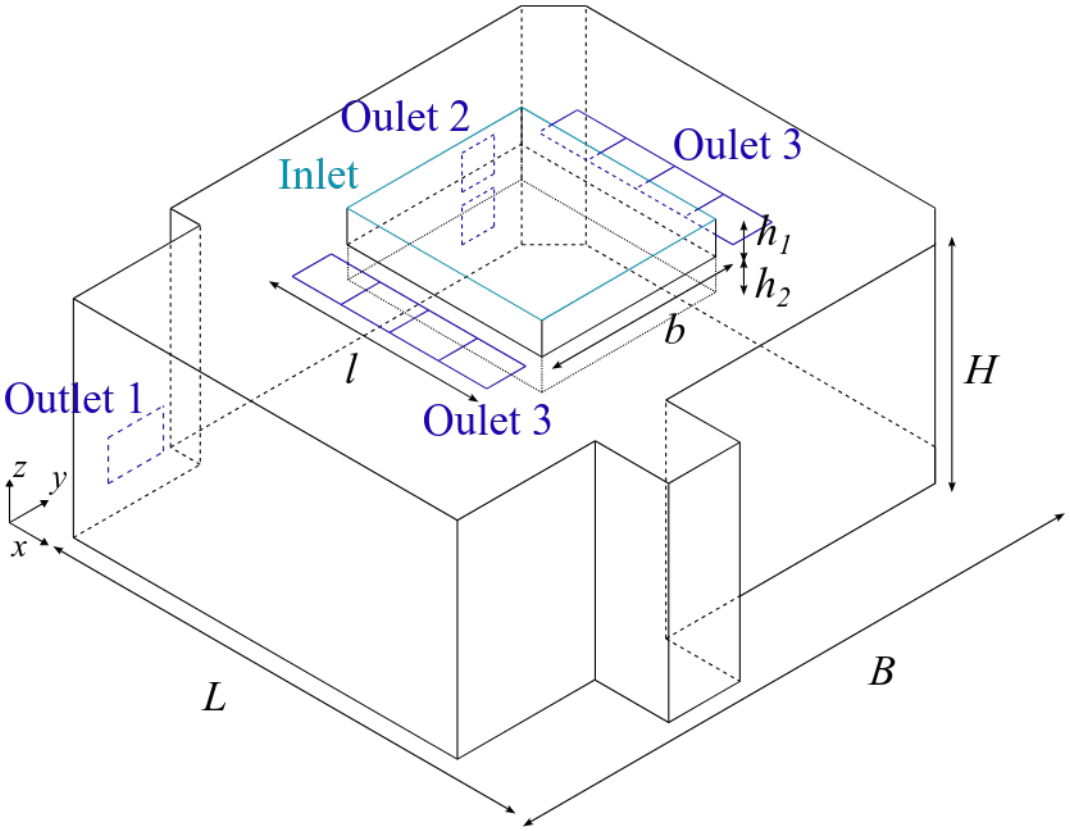

Figure 4.1: CENAQUE OR scheme, main dimensions, inlet and outlets.

Inlet supply area is the Section between two concentric rectangles, the outer rectangle dimensions are $l = 3.22\ m$ and $b = 3.03\ m$, and the inner rectangle dimensions are $l_i = 0.31\ m$ and $b_i = 0.42\ m$. Outlets are separated into three groups. Outlet 1 is one damper of length $b_{o1} = 0.56\ m$ and height h_{o1}. Outlet 2 is composed of two sqaure dampers of side $a_{o2} = 0.55\ m$. Outlet 3 is composed of two groups of four grids of length $l_{o3} = 0.4m$ and width $b_{o3} = 0.3\ m$. In every Scenario the room is assumed to be occupied by seven surgical staff team

members around a patient who is laying on the surgical bed.

(a) View 1.

(b) View 2.

(c) Surgical lamp and partial wall.

Figure 4.2: CENAQUE OR.

4.2.1. Particle considerations

Particle flux from surgical staff, the patient and other possible surgical procedures is modelled as a source term affecting a box-like volume $\mathcal{B}$ named "Contamination area" around the operating table, defined by $P_1 = (2.1,\ 2.5,\ 0.8)$, $P_2 = (3.6,\ 5.2,\ 1.7)$ and $P_3 = (2.1,\ 5.2,\ 0.8)$, presented in Figure 4.3. This approach of particle generation is similar to what lagrangian transport studies do, like C. Wang et al., 2018b, where the particles are point generated, however, initial velocity is not considered in passive scalar models, hence the region where particles are generated is enlarged. The particle concentration source term is set to $\Gamma_C = 3.67$ PM/m$^3 s$ for every particle size $\phi_{PM} = \{1, 5, 10\}\ \mu m$. Contaminant field is calculated as the average of the different particle concentration fields. This approach results in only the particles that are categorized as CFU being simulated, as by averaging the fields (not adding them directly) the source term corresponds to 100 cfu/min per person inside the contamination area $\mathcal{B}$, which is the CFU generation declared by T. T. Chow and Wang, 2012 for people standing still. Particle density is set $\rho_p = 1000\ kg/m^3$, Brownian diffusion coefficient is neglected against turbulent diffusion coefficient $D_{PM} << \varepsilon_p$. Settling speeds are $\vec{v}_s . - \hat{z} = \{3.27 \times 10^{-5}, 7.16 \times 10^{-4}, 2.81 \times 10^{-3}\}\ m/s$ for $\phi_{PM} = \{1, 5, 10\}\ \mu m$ respectively.

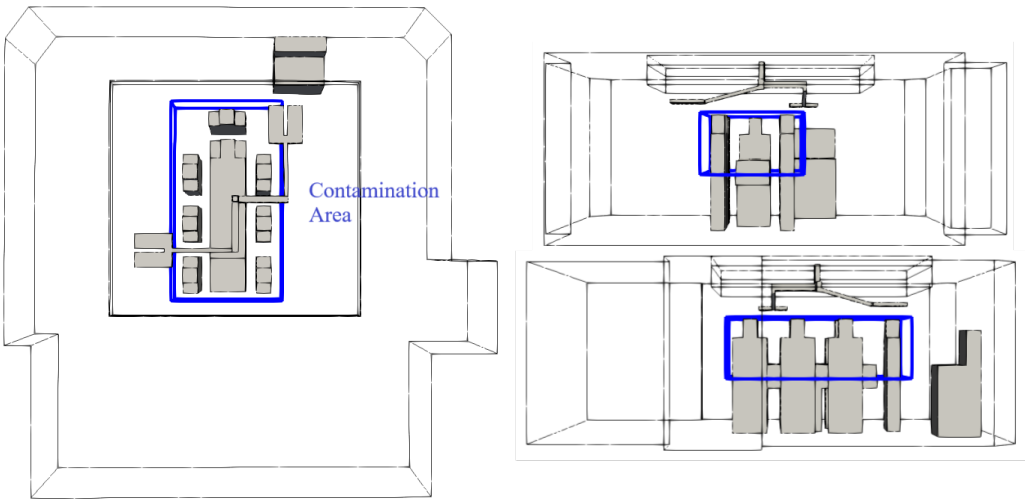

Figure 4.3: Contamination Area $\mathcal{B}$

4.3. Model implementation

The mathematical model, numerical algorithms and implementations are presented and described in depth in Chapter 3. The model approximates the scalar transport equation (Equation 3.2) for velocity, temperature, air age, turbulent kinetic energy and dissipation rate, then couples the velocity and pressure fields with the mass conservation equation. Turbulence is modeled using a turbulent diffusion coefficient, based on the turbulent kinetic energy and dissipation rate (Equation 3.4). The particle concentration field is calculated using the modified drift-flux equation (Equation 3.5), forces exerted by particles towards the air are neglected (zero-coupling).

By neglecting contaminant influence on airflow, the velocity field is independent of the contaminant field, therefore it can be calculated independently. Using this idea and considering the nature of the OR, where the ventilation system starts working long before the operation begins, a two stage approach is implemented for air quality parameter calculations. The first stage calculates the velocity $\vec{v}$, temperature T, pressure p and $p_{rgh} = p + \rho g z$ and turbulence fields k, ε and ν_t, until steady state is verified. The second step calculates the particle concentration C_ϕ with $\phi = \{1, 5, 10\}$ μm) and air age τ fields using the velocity field and turbulent diffusion coefficient resulting from the previous stage as data.

A simplified version of the OR geometry is converted into numerical meshes generated by the ICEM-CFD software. The geometry for which meshes are generated is displayed in Figure 4.4. The room is modeled with seven members of the surgical team, a patient, the operating table, surgical lamp and electrical surgical equipment. Three meshes are evaluated: coarse, fine and finer; mesh details are shown in Table 4.1. Meshes are hexaedrical, created with a combi-

Table 4.1: Tested mesh descriptions.

Mesh	#Cells	Type	Grading	Max cell size
Coarse	477.072	Unstructured	Near boundary	30 cm
Fine	718.587	Unstructured	Near boundary	20 cm
Finer	1.506.154	Unstructured	Near boundary	15 cm

nation of iterative methods included in ICEM software Delaunay and Octree.

The Octree method uses the output generated by the Delaunay and refines the mesh. Element size regulation is carried by imposing a maximum global and surface specific cell size. Surfaces are defined as different mesh elements which coincide with the OR elements such as surgical lamp, partial wall and surgical staff between others, afterwards, a maximum edge length is defined for each mesh element (near boundary grading), a cut plane of Fine mesh is presented in Figure 4.5.

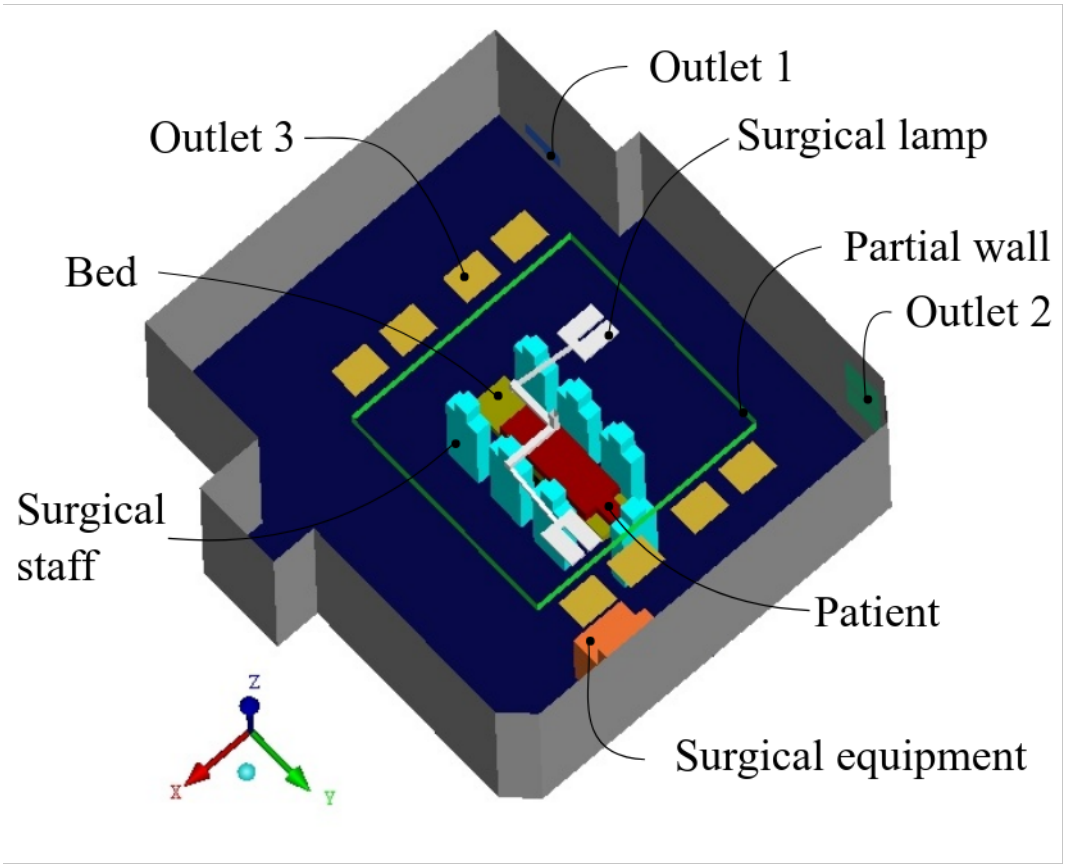

Figure 4.4: Simulated OR arrangement.

4.3.1. Boundary and initial conditions

Velocity Boundary conditions are set to $\vec{v} = \vec{0}$ for every boundary aside from the inlet and outlets, where its set to uniform velocity $u = v = 0\ m/s$, $w = -0.26\ m/s$ and null gradient respectively. Every pressure boundary but the outlets are set to zero gradient boundary condition, outlet pressure is fixed $p = 0\ m^2/s^2$ for every outlet. It should be noted that the pressure at each outlet is not necessarily the same. However, due to a lack of specific information

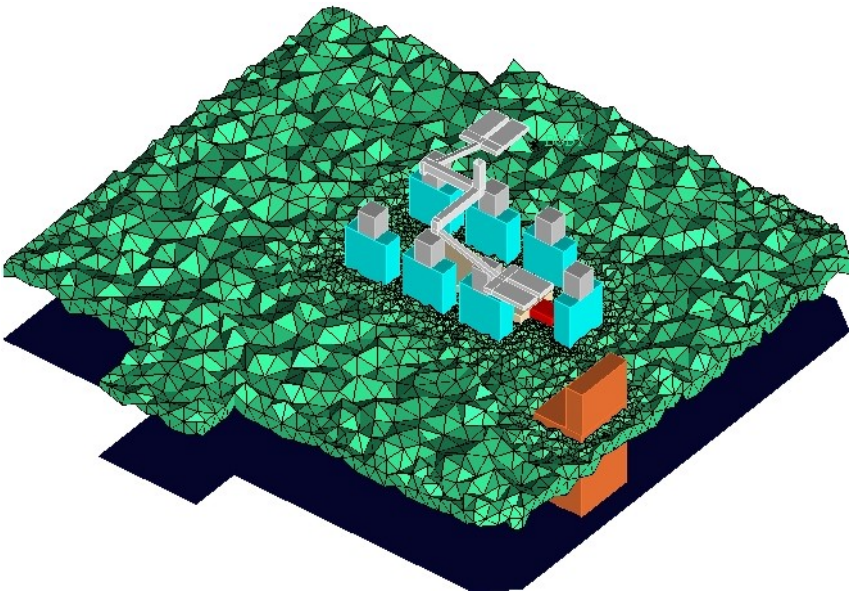

Figure 4.5: Fine mesh cut plane at patient level.

regarding the pressure, or pressure drop at each outlet, they were assumed to be equal. This assumption may exaggerate the short-circuit effect if the actual pressure at Outlet 3 is higher than that at Outlets 1 and 2. Kinetic turbulent energy k is calculated from turbulence intensity, which is estimated as $I = 2\%$ at the inlet, and its gradient is set to zero for every other boundary. Solid boundary turbulence dissipation rate ε and turbulent diffusion coefficient ν_t are calculated through wall functions ("OpenFOAM", n.d.), outlet boundary conditions are set to $\nabla\varepsilon.\vec{n} = 0$ and $\nabla\nu_t.\vec{n} = 0$ respectively, inlet boundary condition for ε is calculated from I, ν and turbulence length, estimated as $l_\varepsilon = 2.37 \times 10^{-7}\ m^2/s^3$, with sliding velocities of $u^* \approx 1 - 5 \times 10^{-3}\ m/s$, turbulent diffusivity is calculated from k and ε. Age of air τ is set to $\tau = 0\ s$ which stands for new air entering the OR, and $\nabla\tau.\vec{n} = 0\ s/m$ for every other surface. Thermal and particle count boundary conditions for each surface are presented in Table 4.2. The inlet boundary condition for particle count $C^*_\phi = 0$ as air enters the domain without contaminants, solid surface $C^*_\phi = 0$ represents no rebound boundary condition (Chen et al., 2006).

Initial conditions are set to null velocity and pressure, uniform $T = 31^oC$, $k = 0.01\ m^2/s^2$, $\varepsilon = 1 \times 10^{-6}\ m^3/s^2$, $\nu_t = 0\ m^2/s$, $C_\phi = 0$ and $\tau = 0\ s$.

Table 4.2: Temperature and particle count Boundary conditions

Boundary	Temperature	Particle count
Inlet	$T = 30^oC$	$C_\phi = 0$ cfu$/m^3$
Outlets	$\nabla T.\vec{n} = 0\frac{^oC}{m}$	$\nabla C_\phi.\vec{n} = 0$ cfu$/m^4$
Walls	Adiabatic	$C_\phi = 0$ cfu$/m^3$
S. Staff and patient	$T = 36^oC$	$C_\phi = 0$ cfu$/m^3$
Lamp lights	$\dot{q}'' = 250\ \frac{W}{m^2}$	$C_\phi = 0$ cfu$/m^3$
S. Equipment	$T = 42^oC$	$C_\phi = 0$ cfu$/m^3$

4.3.2. Simulation evaluation

The mathematical and numerical model presented in Chapter 3 is implemented and evaluated with a grid independence test, and a steady state assessment test. All tests are carried for Scenario 3, which simulates the room without the partial wall separating ceiling inlet and outlets. Time Independence is assessed by registering temperature and velocity components at 69 points inside the OR. Velocity magnitude and temperature evolution over 20 minutes at 69 points inside the OR are shown in Figure 4.6. Velocity and temperature change at grater rates during the first five minutes of simulation, afterwards, most evaluated points start to stabilize, reaching a partial steady state at around 15 minutes. From that point onward, some little oscillations in both temperature and velocity can be observed, however said cyclical time dependence is neglected.

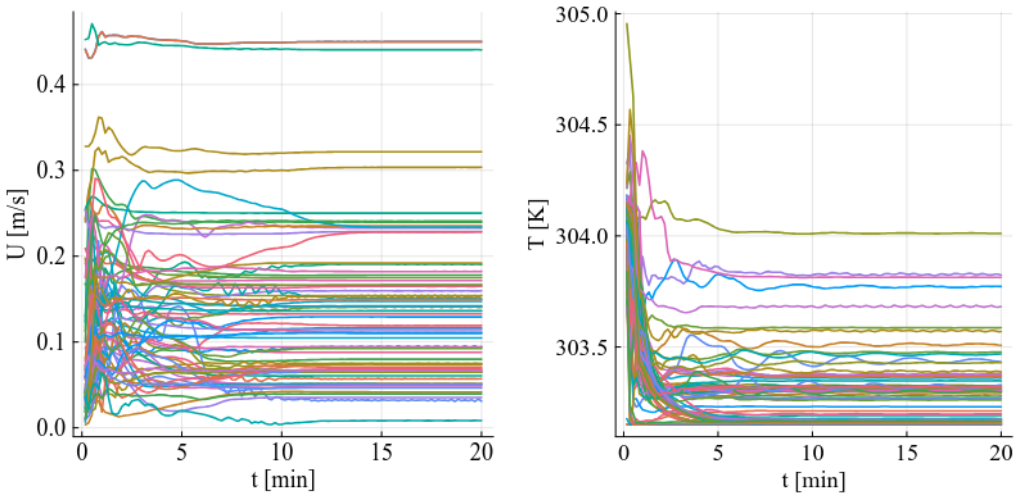

(a) Velocity magnitude U. **(b)** Temperature T.

Figure 4.6: Velocity magnitude and temperature evolution.

Grid independence is compared over average velocity and temperature fields, from 15 min to 20 min, by running the first stage of the simulation and comparing velocity and temperature profiles at $\mathcal{L}_1(x) = (x, y_1, z_1)$, $\mathcal{L}_2(x) = (x, y_1, z_2)$ and $\mathcal{L}_3(y) = (x_1, y, z_1)$ where $x_1 = 2.81\ m$, $y_1 = 3.18\ m$, $z_1 = 1.2\ m$ and $z_2 = 1.8\ m$. Grid independence test results are presented in Figure 4.7, $\mathcal{L}_3$ intersects a surgical teams body near $y = 5\ m$, as can be seen in figures 4.7e and 4.7f, where no data is registered around that point. The fine mesh is selected for further analysis given the reduced computational costs when compared to the finer mesh. Even though results are similar for fine and finer meshes, results could vary for meshes with higher mesh density, specifically at the room periphery.

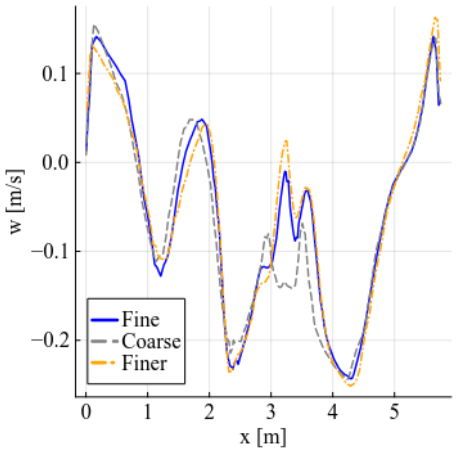

(a) Vertical velocity profile $w(x)$ at $\mathcal{L}_1$.

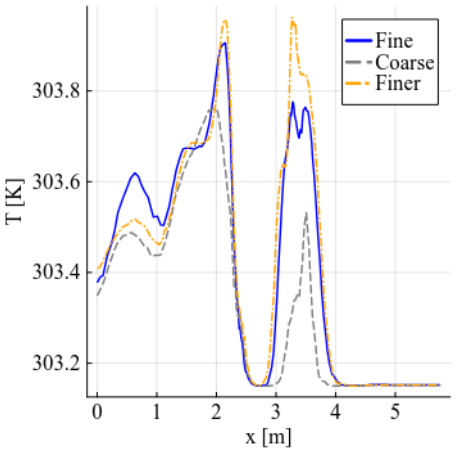

(b) Temperature Profile $T(x)$ at $\mathcal{L}_1$.

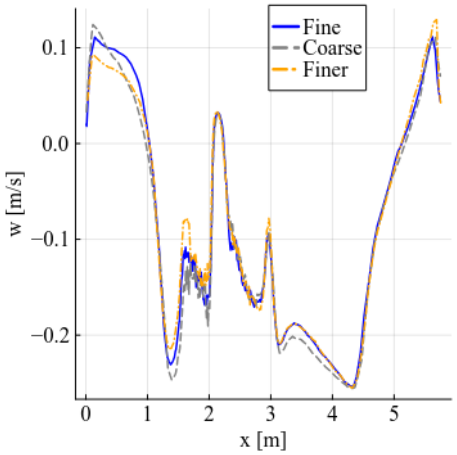

(c) Vertical velocity profile $w(x)$ at $\mathcal{L}_2$.

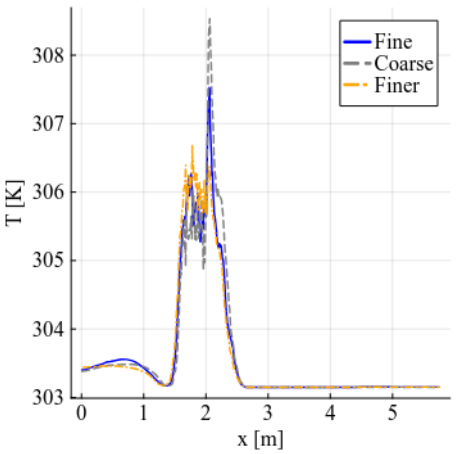

(d) Temperature Profile $T(x)$ at $\mathcal{L}_2$.

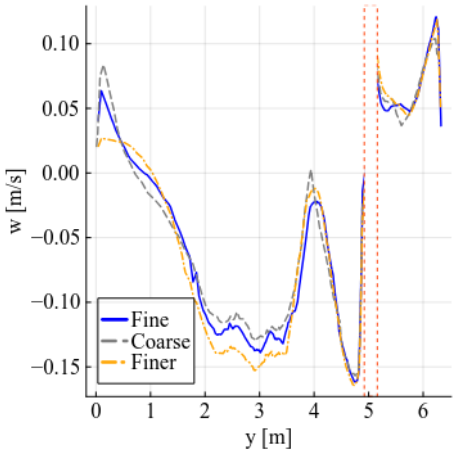

(e) Vertical velocity profile $w(y)$ at $\mathcal{L}_3$.

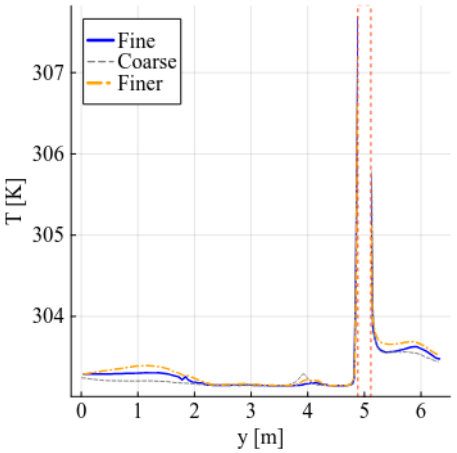

(f) Temperature profile $T(y)$ at $\mathcal{L}_3$.

Figure 4.7: Time average result comparison for the different meshes.

4.4. Results and discussion

4.4.1. Airflow and temperature distribution

Average streamlines are plotted in Figure 4.8 for the no partial wall case following various inlet points in order to visualize the velocity field and airflow distribution. The flow enters from the entrance in the ceiling and descends towards the OR, sweeping from the interior of the room towards the periphery. The majority of the flow leaves the room through the outlets at ceiling level (outlet 3), while a smaller portion exits through the side outlets. Flow is observed to be considerably asymmetric due to the element arrangement inside of it. Two hypotheses are verified; the first is the existence of a downward flow from the inlet that sweeps the air from the center of the room to the periphery. The second hypothesis is the existence of a "short circuit" between a portion of the air inflow with the ceiling level outlet (outlet 3).

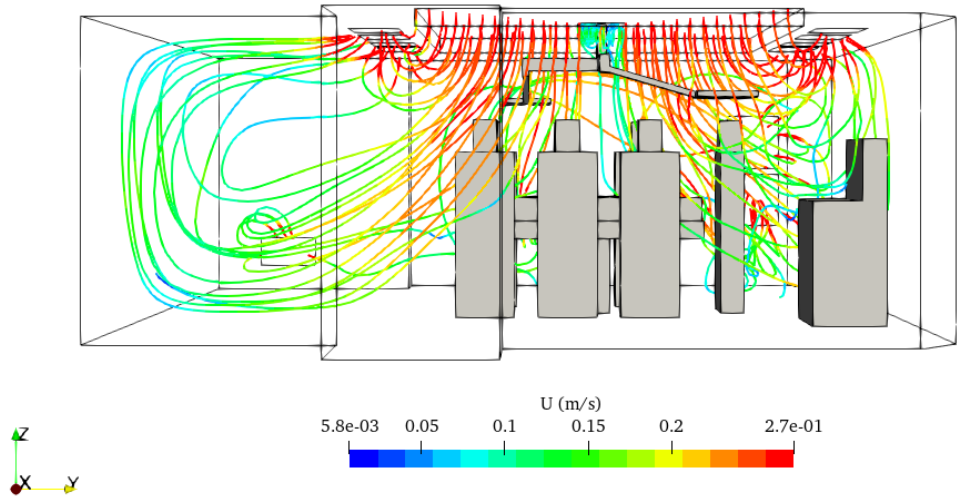

Figure 4.8: Simulated Stream lines without partial wall.

The velocity fields are compared between scenarios 1 and 3 (real and no partial wall). Broadly speaking, both velocity fields are similar, as shown in Figure 4.9. A portion of the inflow leaves quickly through outlet 3 for both cases. Although the amount of "short-circuited" air is sensitive to the boundary condition $p = 0\ m^2/s^2$, which is fixed for every outlet, the effect of the partial wall can be observed when comparing the streamlines for both cases. Streamlines tendencies towards the outlet are reduced with the installation of the partial wall, resulting in a more vertically dominant flow. Furthermore,

"short-circuited" air trajectories are larger when the partial wall is present. Streamline comparison is presented in Figures 4.10 and 4.11, the blue streamlines are obtained with the partial wall, the black streamlines without it.

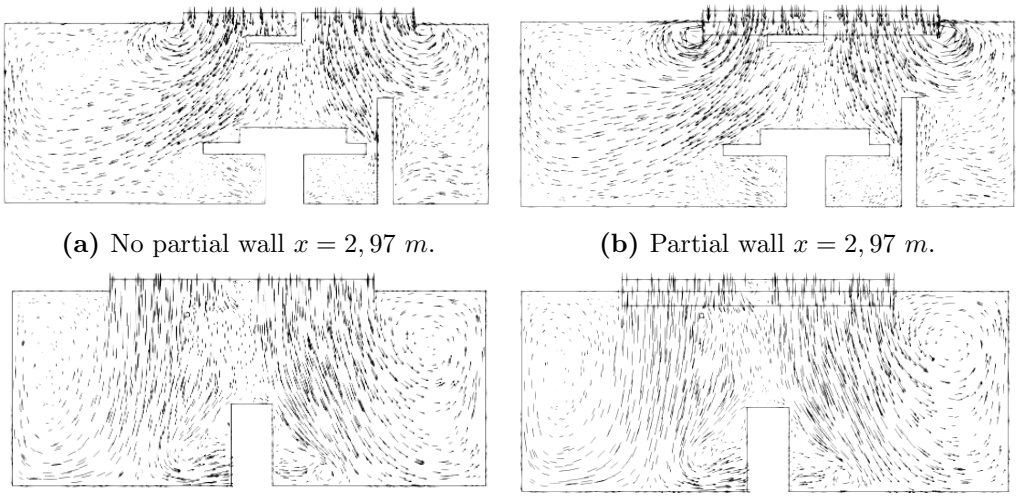

(a) No partial wall $x = 2,97\ m$. **(b)** Partial wall $x = 2,97\ m$.

(c) No partial wall $y = 3.90\ m$. **(d)** Partial wall $y = 3.90\ m$.

Figure 4.9: Velocity field comparison without partial wall (a) and (c) and with the partial wall (b) and (d), for central perpendicular planes.

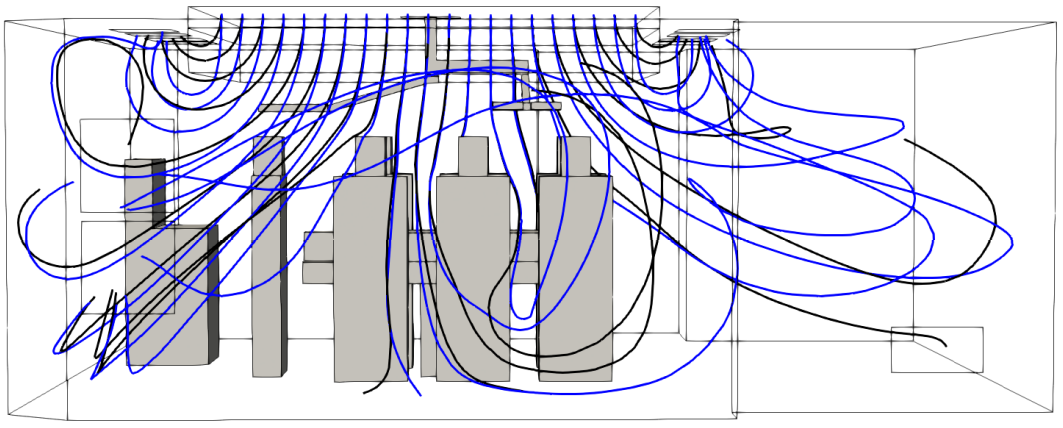

Figure 4.10: Streamline differences with (blue) and without (black) partial wall. Variable distance with ceiling outlet y. Fixed depth x

Streamline observed in Figure 4.10 suggest that the installation of a partial wall not only increases the amount of clean air reaching the work area but also favors that the air arrives in a more orderly manner, aligning better with the intended air distribution for the workspace.

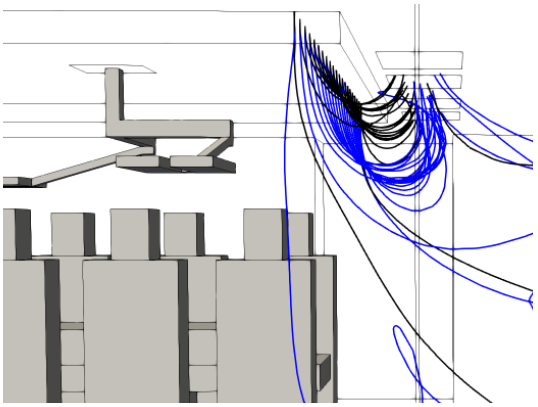

Figure 4.11: Streamline differences with (blue) and without (black) partial wall y. Fixed distance (near) towards ceiling outlet, variable depth x.

Velocity distributions at different heights above the contamination zone remark the effect of the partial wall in airflow direction, vertical velocity profiles at $x = 2\ m$ and at different heights $z = 2.3\ m$, $z = 2.0$ and $z = 1.7\ m$ are presented in Figure 4.12. The plane defined by $x = 2\ m$ intersects the inlet and a roof outlet at each side of the room. At $z = 2.3$ the vertical component of the velocity below the inlet presents a good degree of uniformity. At this height airflow has not yet left the partial wall for scenarios 1 and 2,unlike Scenario 1 where part of the airflow has already left the injection zone. As airflow advances and reaches $z = 2.0\ m$ it becomes less uniform due to the lack of partial wall (for every scenario) and incidence of obstacles such as the surgical lamp. Scenario 1 presents a particular shape at this height, as airflow has just abandoned the partial wall. Velocity increases near the inlet border $y = 2,34\ m$ and $y = 5.37\ m$ due to the pressure gradient generated by the outlet boundary condition. The effect of the partial wall decreases with height from this point onward, a notable difference still remains at $z = 1.7\ m$, where despite having similar shapes, the vertical velocity modules for the scenarios 1 and 2 are higher than Scenario 3, representing higher airflow reaching the contamination zone.

The vertical flow below the air inlet has the particular importance of being the flow that enters the contamination area B. The air flow below the injection is defined as "sweep flow". The velocity profiles in Figure 4.12 provide notion on the evolution of the sweep flow as the air advances in the OR, however, since the velocity profile is in a straight line segment, it is not completely represen-

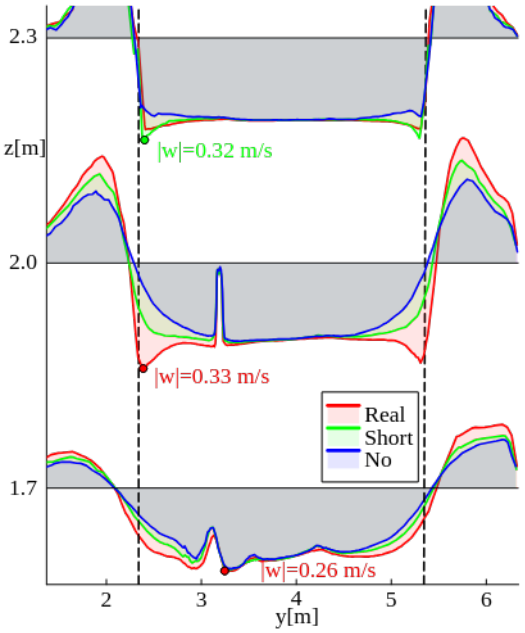

Figure 4.12: Velocity profiles at different heights and $x = 2\ m$, for al three scenarios: Scenario 1 (Real), Scenario 2 (Short) and Scenario 3 (No).

tative of it. The sweep flux is calculated as the numerical surface integral of the scalar product between the velocity and the versor -$\hat{z}$ at different heights z, its distribution for the three simulated scenarios is represented in Figure 4.13. Results show that sweep flow decreases less for cases with partial wall, with the real partial wall Scenariokeeping the highest simulated sweep flows, with a relative difference to the no partial wall sweep flow of about 12.5% more volume at staff head level (z=1.67 m). Therefore simulation results suggest that the incorporation of the partial wall increases the amount of clean air that sweeps the work area.

The incidence angle (angle formed between the velocity vector and the z-axis) is analyzed within a rectangle of inlet size $z = 1.75\ m$, situated between the surgical lamp and the heads of the personnel. The distribution of the incidence angle for the Scenario with the real partial wall is illustrated in Figure 4.14a. Incidence angle is near perpendicular at the plane segment center, incidence angle stays roughly perpendicular when moving away from the center through the x direction, angle tends to increase the further the y-distance from the plane center. The surgical lamp disrupts the flow at this level, as incidence angles near 90^{o} are observed resembling the shape of the surgical

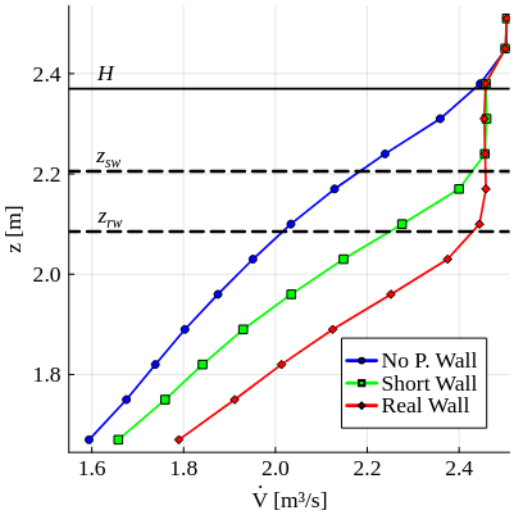

Figure 4.13: Flow comparison below inlet.

lamp.

Flow direction tends to be horizontal (near 90° incidence angles) towards the borders of the plane Section studied, mainly in the y direction as pressure gradient imposed by the outlet boundary conditions force airflow towards it. Comparing the approximate angle distributions for the three scenarios, it is verified that the air reaches the work area in a more orderly manner with the real partial wall, and in a less orderly manner without the partial wall (Figure 4.14b), as higher incidence angles frequency increases with the absence of a partial wall.

Parallel to the calculation of the velocity field, the temperature field is calculated. The temperature fields with or without the partial wall do not present major differences. Three plains with relevant temperature gradients are presented in Figure 4.15. The greatest temperature gradients occur near the lamp lights and surgical equipment. Despite some local temperature differences, the temperature field inside the OR is approximately homogeneous and for the most part very similar to the air inlet temperature. The absence of important temperature variations in the simulation results is favored by two main factors. Firstly, the operating condition of the room indicates an inlet flow of 2.50 m^3/s, which corresponds to 106.6 ACH, which is well above recommended and usual ventilation values for these rooms. Cold airflow dilute the

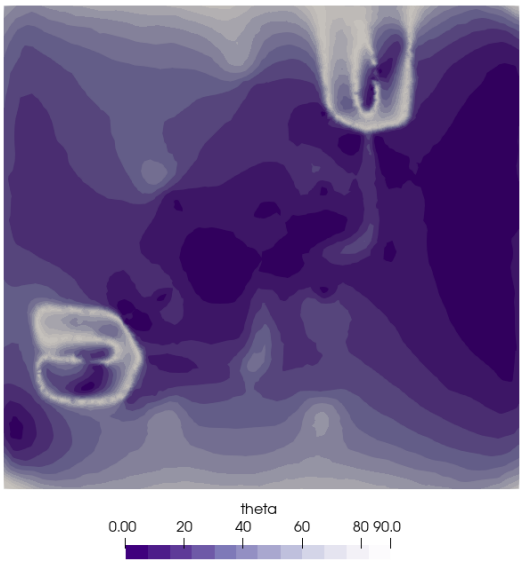

(a) Incidence angle for Scenario 1

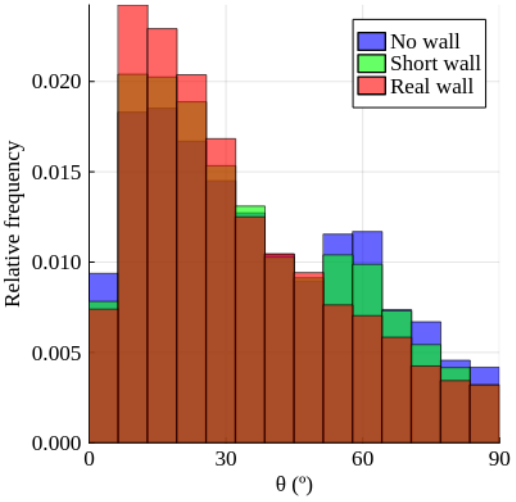

(b) Horizontal angle relative frequency histogram for the the three scenarios.

Figure 4.14: Incidence angle at 1,75 m.

temperature differences between the heated air, therefore inlet and outlet temperature differences tend to become smaller. To a lesser extent, the proposed model simplifies the heat transfer within the room, ignoring, for example, the sensible heat that comes from people's breathing. Due to the high airflow, it is estimated that the consideration of additional heat loads will not significantly affect the temperature distribution.

4.4.2. Air quality parameters

To analyze the partial wall impact on air quality parameters τ and C, the results are divided into two sections: results for the entire room volume and results for contamination zone $\mathcal{B}$.

4.4.2.1. Entire room

Using the velocity and turbulence fields as input data, the air quality, CFU concentration C_ϕ, and air age fields τ are calculated. An overview of the air quality fields is presented in Figure 4.16. The contaminant concentration C is computed as the average of the contaminant concentrations for each particle size: C_1, C_5, and C_{10}

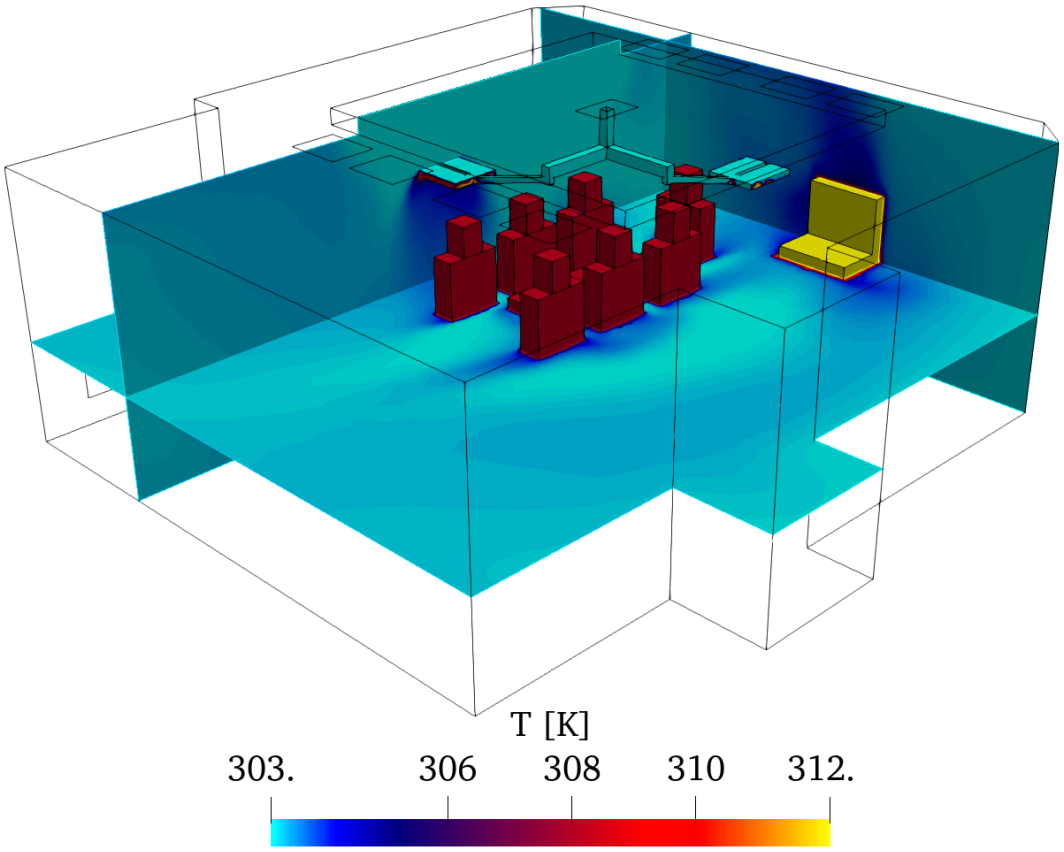

Figure 4.15: Temperature field ploted over three plains inside the OR, $\hat{z}$ normal at $z = 0.9\ m$, which shows heat transfer of patient and surgical staff, $\hat{x}$ normal at $x = 1.75\ m$ which shows the effect of the surgical lamp on air temperature, and $\hat{y}$ normal at $y = 6\ m$, which displays the effect of the surgical equipment.

Higher concentrations of CFUs are observed around the patient and surgical equipment, where the downward flow is obstructed. The concentration of contaminants diffuses as the air moves away from the operating area, being carried towards the peripheral and ceiling outlets.

The air age exhibits significant asymmetry along the x-axis, tending to be higher on the side without extraction points in the OR. Air in this area has lower velocities compared to the rest of the room, resulting in longer egress times. The air age increases with height z in the periphery, away from the operating area, excluding the air short-circuit zone. Inside the operating area (below the air inlet) air age is relatively low as air flows from the inlet, through the operating area to the periphery. Highest air age values inside the operating area are found in stagnation zones, such as the back of the surgical staff or

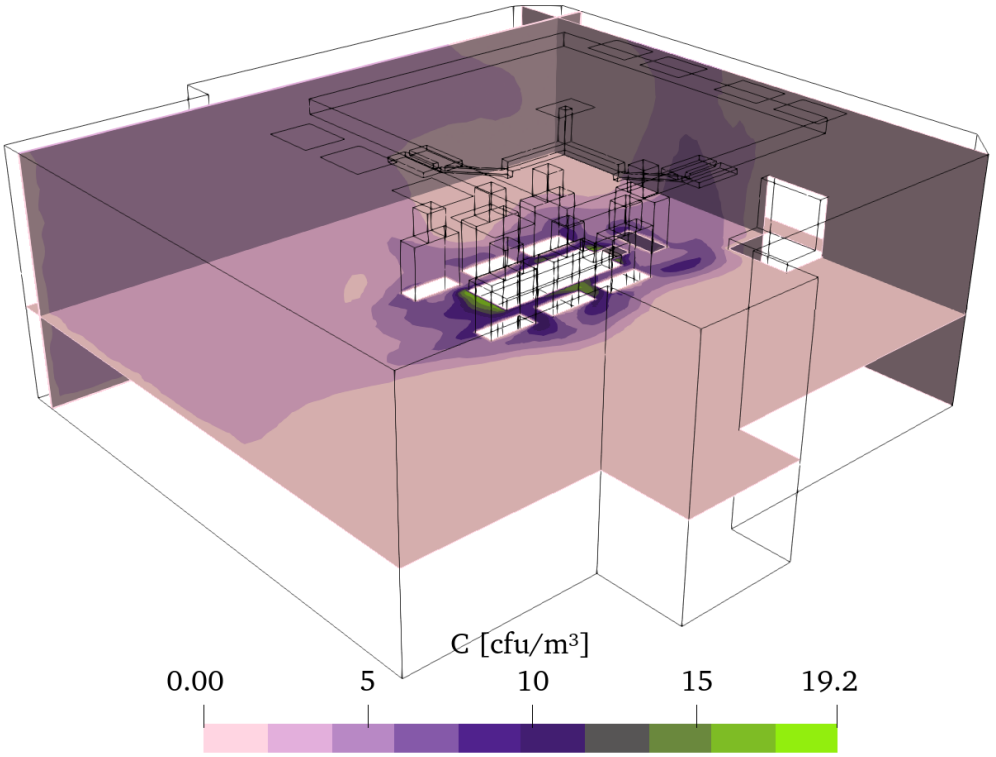

(a) CFU concentration inside the CENAQUE OR.

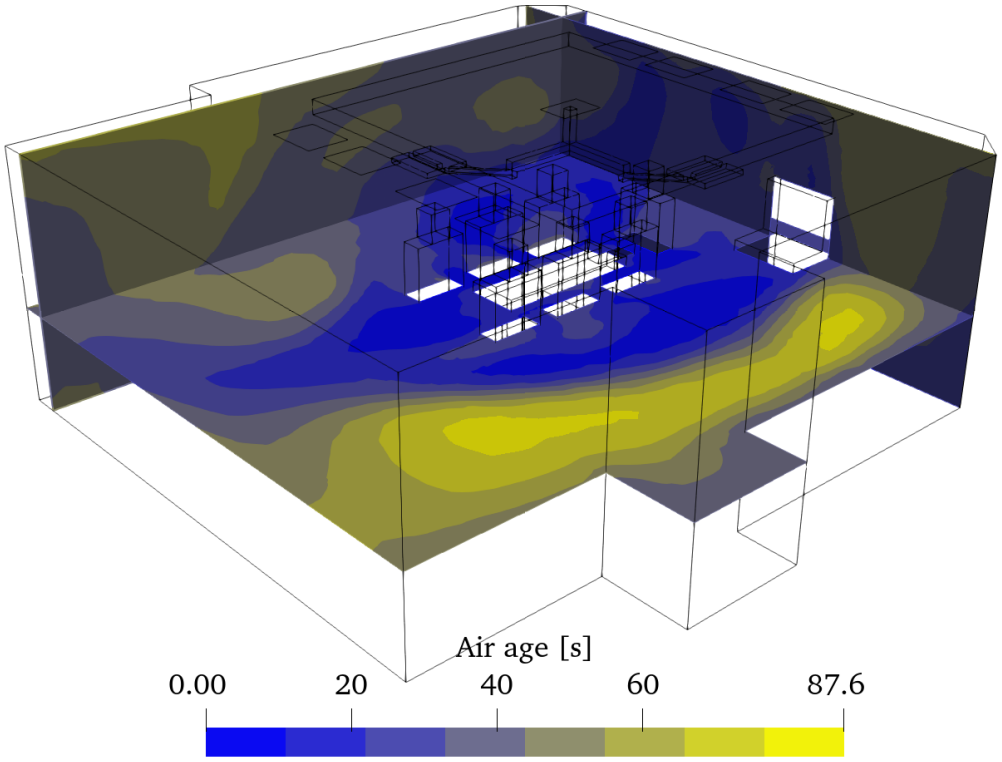

(b) Air age inside the CENAQUE OR.

Figure 4.16: Visualisation of CENAQUE OR air quality fields with the real partial wall, (a) CFU concentration and (b) air age.

above and below the surgical bed.

In contrast to the observations in the validation cases presented in Chapter 3, areas with high air age do not appear to indicate zones of high CFU concentration. However, these differences can be explained by understanding the differences between both physical situations. As a reminder, the two-zone chamber experiment carried out and simulated by Lu et al., 1996 is one of the reference cases used to evaluate the implemented particle transport model. The experiment studies the transport of particles in a chamber composed of two identical zones, zone 1 and zone 2, which are initially separated from each other. Within zone 1 there is a uniformly distributed contaminant gas, whose initial concentration is known, while zone 2 is completely clean. The average contaminant concentration is recorded throughout the experiments for both zones.

At the start of the experiment, the door separating zones 1 and 2 is opened and a flow of air from the outside of the chamber (clean of gaseous contaminants) is mechanically forced into zone 1. The clean air pushes the contaminated air from zone 1 to zone 2 and towards the outside of the chamber, so as time passes the total concentration of contaminants in the chamber decreases. Due to the geometry of the chamber, stagnation zones form inside (high air age zones), where the concentration of contaminants accumulates.

Particle transport inside the OR is different, as air is initially clean, and contaminants are generated inside the room, increasing the concentration over time. On the other hand, the results of the OR simulations do not show stagnation zones like those observed in the simulation of the two-zone chamber experiment, reaching a steady state for the air age field at about 5 minutes, as shown in Figure 4.17. Since contaminants are generated in areas of low air age and then diffuse throughout the room, it makes sense that the highest concentrations occur in areas of low air age.

Achieving a steady-state air age indicates that within the control volume, the air has reached its maximum residence time. Analyzing the maximum and average air age for the three scenarios reveals that the presence of the partial wall results in fresher air within the volume. The maximum and average

CFU concentration and air age throughout the OR for the three scenarios are presented in Table 4.3, the averages shown in Table 4.3 are volume-weighted, while the maximum values are associated with cell centroid values of τ and C. To quantify the relative importance of air age changes in the OR, a fictitious Scenarioin which air is renewed uniformly is defined as a reference.

The reference fictitious situation is defined as an equivalent room where the air flows from the inlet to the outlet at a constant and uniform speed without obstructions and with equal air renewals to the evaluated OR. The equivalent room is shaped as an extruded surface, where air flows uniformly form the base surface to the end of the extrusion. For the equivalent situation, the age of air at the exit can be calculated according to Equation 4.1, and since the air is evacuated uniformly, the average age of the air in the reference situation is half that at the exit. The average air age in the reference situation is defined as the reference air age, which allows defining an idea of ventilation efficiency $\eta_{\tau u}$ that compares the time that the air resides within the OR against a uniform situation without obstacles, air shorts or stagnation (Equation 4.2).

$$\tau_u = \frac{1}{\text{ACH}} \times 3600 = 33.8\ s \tag{4.1}$$

$$\eta_{\tau u} = \frac{\tau_u}{2\overline{\tau}} \tag{4.2}$$

Both the average air age and CFU concentration decrease from Scenario 3 to Scenario 2, and from Scenario 2 to Scenario 1. Simulation results suggest that, on average, the air quality within the room improves with the installation of the partial wall. Particularly noteworthy is a 10.7% reduction in the average global contaminant concentration within the OR as well as a 9.8% increase in ventilation efficiency. Additionally, the maximum values for both air quality parameters are reduced, indicating that the air is being used more efficiently in the scenarios with the partial wall compared to those without it.

Table 4.3: Global OR maximum and average air quality parameters for the three simulated scenarios.

Scenario	C_{max} $(\frac{cfu}{m^3})$	$\overline{C}$ $(\frac{cfu}{m^3})$	τ_{max} (s)	$\overline{\tau}$ (s)	$\eta_{\tau u}(\%)$
1. No P. Wall	20.1	1.87	126.8	40.5	41.7
2. Short P. Wall	20.1	1.78	105.2	37.9	44.6
3. Real P. Wall	18.9	1,67	93.6	32.8	51.5

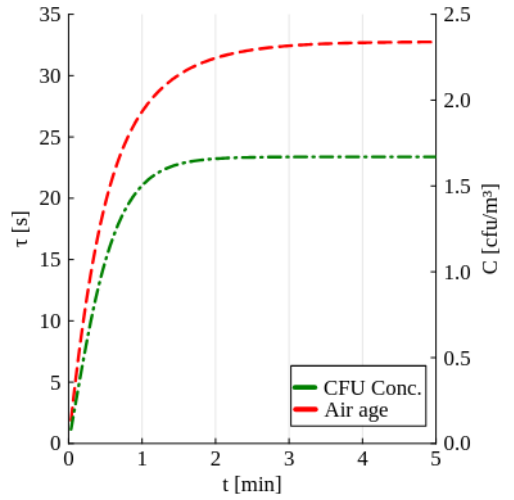

Figure 4.17: Room average air quality parameters over time, air age τ and CFU concentration C.

Further evidence of the reduction in short-circuiting effect is found by studying the contaminant flows through the air outlets. At "Outlet 3," both the air age and the removal of CFUs from the OR increase when the partial wall is installed, indicating that older air carrying more contaminants is being expelled. The average values of air age and CFU concentration, as well as the airflow and CFU flow are shown on Table 4.4. The effect of the partial wall is most pronounced at Outlet 3 when comparing scenarios without the partial wall and with the real partial wall. For said Scenariocomparison the average air age , $\overline{\tau}$, increases from 30.8 seconds to 34.1 seconds (air is 10.71% older), and the contaminant flow, $\dot{C}$, increases from 5502 CFU/h to 6338 CFU/h, enhancing contaminant evacuation through Outlet 3 by 15.19%.

To highlight the effect of installing the partial wall in the OR, a parameter E_τ can be defined, calculated according to Equation 4.3, which represents the proportional excess air age with which the air leaves the OR from each outlet, compared against a Scenariowhere airflow leaves a room at the same ACH rate, with an uniform flow distribution, meaning air leaves the room with an air-age equal to τ_u (Equation 4.1).

$$E_\tau = \frac{\overline{\tau} - \tau_u}{\tau_u} \times 100 \tag{4.3}$$

The calculation of the excess air age shows that when the partial wall is in-

stalled, the air leaves the OR at a more uniform air age. The majority of the air leaves the OR through Outlet 3, whose excess air age increases, going from a negative value of -8.9% to 0.9%, which suggests a reduction in the short circuit phenomenon. On the other hand, the excess for the other two Outlets decreases, indicating that the air reaches the OR outlet through them with less stagnation.

Table 4.4: Principal outlet results with and without partial wall

No P. Wall	$A\ (m^2)$	$\dot{V}\ (\frac{m^3}{h})$	$\overline{\tau}\ (s)$	$\overline{C}\ (\frac{\text{cfu}}{m^3})$	$\dot{n}\ (\frac{cfu}{h})$	$E_\tau(\%)$
Out. 1	0.157	605	51.7	3.56	2155	53.0
Out. 2	0.605	2319	34.0	2.16	5017	0.6
Out. 3	1.600	5981	30.8	0.92	5502	-8.9
Short Wall	$A\ (m^2)$	$\dot{V}\ (\frac{m^3}{h})$	$\overline{\tau}\ (s)$	$\overline{C}\ (\frac{\text{cfu}}{m^3})$	$\dot{n}\ (\frac{cfu}{h})$	$E_\tau(\%)$
Out. 1	0.157	598	47.7	3.51	2101	41.1
Out. 2	0.605	2299	33.0	2.08	4779	-2.4
Out. 3	1.600	5978	33.1	0.99	5932	-2.1
Real Wall	$A\ (m^2)$	$\dot{V}\ (\frac{m^3}{h})$	$\overline{\tau}\ (s)$	$\overline{C}\ (\frac{\text{cfu}}{m^3})$	$\dot{n}\ (\frac{cfu}{h})$	$E_\tau(\%)$
Out. 1	0.157	602	43.4	3.40	2046	28.4
Out. 2	0.605	2311	31.7	1.89	4371	-6.2
Out. 3	1.600	5950	34.1	1.06	6338	0.9

4.4.2.2. Contamination zone $\mathcal{B}$

Simulation results indicate an improvement in the overall air quality parameters for the entire OR volume. However, this does not necessarily imply that air quality improves uniformly throughout the space. Variations in air age and contaminant distribution in the area directly beneath the air inlet are particularly important as it is where the patient and surgical team are positioned for extended periods, making it the zone where infection risk is highest.

The "contamination zone" $\mathcal{B}$, defined in Section 4.2.1, serves as a reference for the air in the infection risk area. Within this zone, the air age and contaminant concentration are analyzed across the three scenarios. The infection risk zone is characterized by the generation of contaminants, the presence of several obstacles to airflow such as surgical equipment, the patient, and the bed, as well as its location directly beneath the air inlet, allowing clean air with low air age to enter from above. Due to these factors, the air within the

contamination zone exhibits relatively low air ages and relatively high contaminant levels, as shown when comparing Figure 4.18 with Figure 4.16.

Contamination zone results show the same trend of decreasing the proportion of contaminants in the air with the installation of the partial wall (Table 4.5). The real partial wall simulation instalation resulted in a reduction of about a second of air age inside the contamination area and almost 10% cfu concentration reduction. "Ventilation efficiency" η_τ is calculated from Equation 4.4 using average air age inside the contamination area $\mathcal{B}$. Additionally, the air age within the contamination area decreases when the partial wall is installed. Said air age reduction is attributed to the reduced short-circuiting of the air, allowing more fresh air to reach the surgical team and patient. A reference aire age value τ_{ref} can be defined in order to mesure ventilation efficiency. The reference air age for the contamination area $\mathcal{B}$ is defined as the time needed to travel in a straight line from inlet height to the medium $\mathcal{B}$ height, at inlet average velocity $w = 0.26$ m/s, which is $\tau_{ref} = 4.85$ s. Comparison with this reference value equates to a comparison against a fully uniform and unidirectional flow from inlet to each point inside $\mathcal{B}$, without any obstruction or flow loss from outlets, surgical staff, surgical lamps and other.

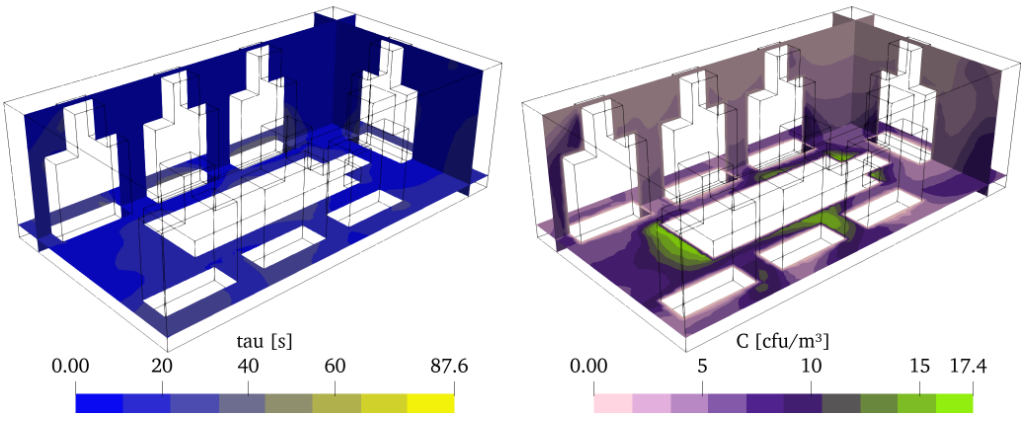

(a) Air age **(b)** CFU concentration

Figure 4.18: Contamination area air age and CFU concentration distribution visualization for Scenario 1, with the real partial wall.

Observing the contamination zone in more detail, it is noted that contaminant concentration appears to increase as height decreases, with maximum concentration values near the center of the zone. This phenomenon is attributed to two main causes: First, the low velocities in the center (due to

the obstruction from the lamp and the geometry of the air injector) cause the residence time of the air within the contaminant generation zone to be greater for the air descending through the center than for the air descending through the periphery. Second, the air descending through the center is surrounded by contaminated air (the center of the contaminant generation zone). This second cause is a direct consequence of how particle generation is modeled in the implemented physical model.

Additionally, it is observed that the areas of lower velocity near the surgical table are where the maximum CFU concentrations are reached, as presented in Figure 4.19. This phenomenon is explained by the fact that the air in this area has already traveled through the entire contaminant generation zone and struggles to exit due to the low velocities, resulting in increased contaminant concentration.

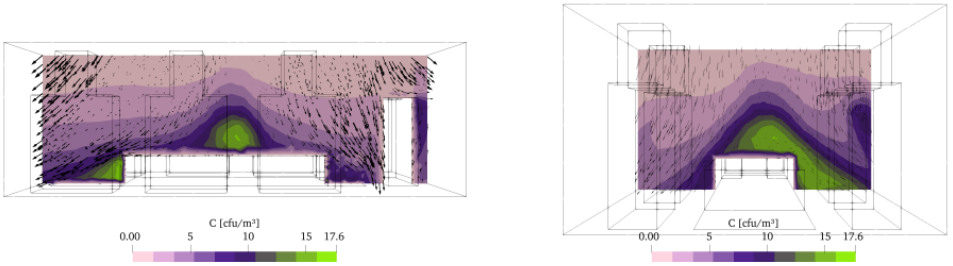

(a) Contamination area middle x-plane **(b)** Contamination area middle y-plane

Figure 4.19: Contamination distribution visualization plotted with average speed values.

$$\eta_\tau = \frac{\tau_{ref}}{\overline{\tau}} \tag{4.4}$$

Table 4.5: Contamination area average air quality parameters for the three simulated scenarios.

Scenario	$\overline{C}$ $(\frac{cfu}{m^3})$	$\overline{\tau}$ (s)	τ_{min} (s)	τ_{max} (s)	η_τ (%)
1. Real P. Wall	4.30	9.9	3.2	43.5	49.0
2. Short P. Wall	4.50	10.3	3.2	43.7	47.1
3. No P. Wall	4.69	10.8	3.2	51.7	44.9

4.5. Conclusions

In this section, the mathematical model explained in Chapter 3 is applied to simulate the ventilation within the CENAQUE OR. The CENAQUE room simulated features a VLAF-type ventilation system, with extractions on the side walls and ceiling. Inside the room, it is assumed there are seven people (six standing and one lying down), a surgical lamp, and heat-dissipating equipment. Before studying the results, a mesh convergence analysis is performed, and the convergence of the velocity and temperature fields is evaluated.

To evaluate the impact of installing the partial wall between injection and roof extraction, three scenarios were defined: Scenario 1 with the partial wall installed, Scenario 2 with a shorter partial wall and Scenario 3 without the partial wall. For the three scenarios, the velocity fields, the concentration of pollutants and the age of the air are studied.

Installation of the partial wall results in an increase of the sweep flow by 12.5%. Moreover, results indicate that when the partial wall is installed, the flow arrives in a more orderly manner with the presence of the partial wall. The air short circuit effect can be observed in the simulation of the three scenarios, however, the results suggest that the installation of the partial wall reduces the portion of the air that leaves the OR through the extraction that is at ceiling level.

Air quality (represented by the concentration of contaminants and the age of air) is evaluated by sectioning the volume of the room, differentiating between results that cover the entire room with results within contamination area B.

The results of the simulations indicate that the average contaminant concentration of the OR decreases by 10.7% when installing the partial wall. Furthermore, the ventilation efficiency referred to an equivalent situation of uniform flow increases from 41.7% without the partial wall to 44.6% with the short wall and up to 51.5% with the real-size partial wall.

The average air age in the roof extraction increases, increasing the excess

time spent inside the OR from negative values of -8.9% and -2.1% for Scenarios 3 and 2 respectively, to a positive value of 0.9% for Scenario 1. That is, by installing the partial wall, a portion of the air that previously left the OR with a residence time less than expected in a uniform situation, now remains longer inside the OR. The increase in excess residence time, accompanied by the reduction in flow in the extraction at ceiling level, indicates a decrease in the short circuit of air.

Inside the contamination zone $\mathcal{B}$, the installation of the partial wall reduces average contamination concentration in 8,32% compared to Scenario 1, without partial wall. Ventilation efficiency improves from 44,9% without the partial wall, to 47,1% with a shorter partial wall and up to 49,0% with the real partial wall.

The results suggest that the installation of a partial wall improves the air quality in the room. Moreover, they indicate that a longer wall provides a greater improvement in air quality compared to a shorter wall.

Chapter 5

Conclusions

This Chapter compiles the thesis main conclusions, more specific conclusions are presented in Chapters 2, 3 and 4.

Air quality in ORs is strongly linked to the success of the operation and the patient's risk of contracting an SSI. Temperature, RH, differential pressure, ventilation and particle concentration were identified as the most important parameters related to air quality in ORs. Some of these parameters, such as temperature, relative humidity and air speed, mainly influence the thermal comfort of the inhabitants of the OR. Other parameters mainly influence sepsis, such as ventilation and particle concentration. Particle concentration and specifically PM_1-PM_{10} is directly related to SSI risk, as bacteria use PM of this size range to become airborne.

At an international level, standards are used to define the ranges of temperature, humidity, differential pressure, air renewals and total ventilation. The ranges defined for the parameters in the standards are usually compromises of different phenomena, such as temperature, which is a compromise between the comfort of the patient and the surgical team. At the national level, no enforceable standard equivalent to those evaluated in this thesis was found.

The most usual way to control the air quality parameters inside the OR is to condition the incoming air, using an AHU. The AHU can dictate the amount of air entering the OR, as well as its temperature and RH. In addition, upstream of the OR, filter banks are installed with the aim of reducing the concentration

of contaminants. The ventilation schemes used inside the rooms can be separated into two large families, diffusion-based systems (TMA) and sweep-based systems (LAF). Studies have shown that LAF systems are more effective at creating a protective area within the OR, making them the preferred choice for ORs performing higher-risk procedures. In contrast, TMA systems are less complex to operate and require less ventilation, making them suitable for ORs where a lower level of air cleaning is adequate.

At national level, analysis of reports generated by the IIMPI team for 41 rooms used by IMAEs reveals that key air quality parameters such as total ACH, outdoor ACH, temperature, RH, and differential pressures are not commonly known by ventilation system supervisors. As interactions between the IMAEs, the FNR and the room managers continue, it is anticipated that information on these air quality parameters will become more widely available.

An OR used for the treatment of patients with burned skin is defined as a case study to analyze using CFD. In these OR, which has a LAF ventilation system, a partial wall was recently installed separating the air inlet from the outlets that are at ceiling level. Three scenarios are proposed for airflow and air quality CFD analysis, one with the partial wall installed, another with a shorter partial wall and finally a scenario without the partial wall.

A CFD code was designed capable of calculating velocity distributions and air quality parameters in indoor environments. The proposed model simplifies and approximates the conservation equations of momentum, energy, mass, and other relevant properties for air within the control volume. Turbulence is modeled using the RANS $k - \varepsilon$ approach, which calculates the average air velocity while accounting for all scales of turbulence. By employing a RANS turbulence model and disregarding the effects of particles on the air velocity field, the distribution of contaminants can be calculated independently over a stationary velocity field. Accordingly, a two-step resolution algorithm is implemented: the first step computes the fields of velocity, pressure, temperature, and turbulence, while the second step determines the air quality fields, specifically air age and contaminant concentration, utilizing the precomputed velocity field and turbulent diffusion coefficient. The code is implemented in OpenFOAM, which is free software capable of solving differential equations

using the finite volume method.

To validate the implemented model, the "heated cavity" case by Limane et al., 2015 and the "two-zone chamber" case by Lu et al., 1996 were selected. These cases evaluate the model's effectiveness in simulating air movement in both the presence and absence of temperature gradients, in two and three dimensions, and in transporting contaminants. The proposed resolution algorithm is assessed by comparing it with an algorithm that resolves both steps simultaneously.

The heated cavity case simulates airflow within a chamber with an air inlet and outlet, uniformly heated from its bottom surface. The objective is to evaluate the model's capability to simulate thermal, flow, and buoyancy dynamics. The model satisfactorily captures the velocity fields within the chamber, achieving good coherence with experimental data. Although the temperature results show significant deviations from the reference measurements, the obtained temperature distributions closely align with other simulation results reported in the literature. The two-zone chamber experiment examines the model capabilities of predicting contaminant transport on a 3D chamber. Simulations show better correlation to experimental data when the two step algorithm is implemented. The two stage algorithm could be applied to OR simulations, as the flow is fully developed before operations starts.

The mathematical model is implemented to simulate the ventilation within the burned skin treatment OR. The simulated OR features a VLAF-type ventilation system, with extractions on the side walls and ceiling. Inside the room, it is assumed there are seven people (six standing and one lying down), a surgical lamp, and heat-dissipating equipment. The results of the simulations indicate that the average contaminant concentration of the OR decreases by 10.7% when installing the partial wall. Furthermore, the ventilation efficiency referred to an equivalent situation of uniform flow increases from 41.7% without the partial wall to 44.6% with the short wall and up to 51.5% with the real-size partial wall.

The average air age in the roof extraction increases, increasing the excess time spent inside the OR from negative values of -8.9% and -2.1% for Scenar-

ios 3 and 2 respectively, to a positive value of 0.9% for Scenario 1. That is, by installing the partial wall, a portion of the air that previously left the OR with a residence time less than expected in a uniform situation, now remains longer inside the OR. The increase in excess residence time, accompanied by the reduction in flow in the extraction at ceiling level, indicates a decrease in the short circuit of air.

Inside the contamination zone $\mathcal{B}$, the installation of the partial wall reduces average contamination concentration in 8,32% compared to scenario 3, without partial wall. Ventilation efficiency improves from 44,9% without the partial wall, to 47,1% with a shorter partial wall and up to 49,0% with the real partial wall.

The results suggest that the installation of a partial wall improves the air quality in the room. Moreover, they indicate that a longer wall provides a greater improvement in air quality compared to a shorter wall.

Future research

Some possibilities to continue the line of research proposed by this work are:

- Monitor air quality in the rooms associated with the IMAEs that interact with the FNR, observing how the availability of information and compliance with international standards changes, as more audits are carried out.
- Detail a first draft of regulations equivalent to international standards applicable to Uruguay with regard to air quality in ORs.
- Create sensibility analysis scenarios for simulation parameters, such as the definition of the contamination area, and the pressure boundary conditions
- Further validation of the results through field measurements
- Expand simulated scenarios to include a full-length wall separating contamination area from room periphery (original conditions), and simulation of "air curtain" where a secondary air injection works as separation between the contamination area and the periphery.

Bibliographic references

Alsved, M., Civilis, A., Ekolind, P., Tammelin, A., Andersson, A. E., Jakobsson, J., Svensson, T., Ramstorp, M., Sadrizadeh, S., Larsson, P. A., Bohgard, M., Šantl-Temkiv, T., and Löndahl, J. (2018). Temperature-controlled airflow ventilation in operating rooms compared with laminar airflow and turbulent mixed airflow. *Journal of Hospital Infection*, *98*, 181–190. https://doi.org/10.1016/j.jhin.2017.10.013

Angelova, R. A., and Velichkova, R. (2020). Thermophysiological comfort of surgeons and patient in an operating room based on pmv-ppd and phs indexes. *Applied Sciences (Switzerland)*, *10*. https://doi.org/10.3390/app10051801

Armellino, D. (2017). Minimizing sources of airborne, aerosolized, and contact contaminants in the or environment. *AORN Journal*, *106*, 494–501. https://doi.org/10.1016/j.aorn.2017.09.012

ASHRAE. (2021). *Ansi/ashrae/ashe standard 170-2021*. www.ashrae.org/technology.

Asociación Española de Normalización. (2005). *Une 100713 instalaciones de acondicionamiento de aire en hospitales*.

Asociación Española de Normalización. (2020). 171340: 2020. validación y cualificación de salas de ambiente controlado en hospitales.

Balaras, C. A., Dascalaki, E., and Gaglia, A. (2007). Hvac and indoor thermal conditions in hospital operating rooms. *Energy and Buildings*, *39*(4), 454–470. https://doi.org/https://doi.org/10.1016/j.enbuild.2006.09.004

Balocco, C., and Petrone, G. (2015, October). Microclimate and indoor air quality in an operating theatre under real use conditions — an experimental and numerical investigation. InTech. https://doi.org/10.5772/59671

Barrasa-Villar, J. I., Aibar-Remón, C., Prieto-Andrés, P., Mareca-Doñate, R., and Moliner-Lahoz, J. (2017). Impact on Morbidity, Mortality, and

Length of Stay of Hospital-Acquired Infections by Resistant Microorganisms. *Clinical Infectious Diseases*, *65*(4), 644–652. https://doi.org/10.1093/cid/cix411

Brandt, C., Hott, U., Sohr, D., Daschner, F., Gastmeier, P., and Rüden, H. (2008). Operating room ventilation with laminar airflow shows no protective effect on the surgical site infection rate in orthopedic and abdominal surgery. *Annals of surgery*, *248*(5), 695–700.

Brewster, L., Tarrant, C., and Dixon-Woods, M. (2016). Qualitative study of views and experiences of performance management for healthcare-associated infections. *Journal of Hospital Infection*, *94*, 41–47. https://doi.org/10.1016/j.jhin.2016.01.021

Brohus, H., Balling, K. D., and Jeppesen, D. (2006). Influence of movements on contaminant transport in an operating room. *Indoor Air*, *16*, 356–372. https://doi.org/10.1111/j.1600-0668.2006.00454.x

Chen, F., Yu, S. C., and Lai, A. C. (2006). Modeling particle distribution and deposition in indoor environments with a new drift-flux model. *Atmospheric Environment*, *40*, 357–367. https://doi.org/10.1016/j.atmosenv.2005.09.044

Cho, J. (2019). Investigation on the contaminant distribution with improved ventilation system in hospital isolation rooms: Effect of supply and exhaust air diffuser configurations. *Applied Thermal Engineering*, *148*, 208–218. https://doi.org/https://doi.org/10.1016/j.applthermaleng.2018.11.023

Chow, T. T., and Wang, J. (2012). Dynamic simulation on impact of surgeon bending movement on bacteria-carrying particles distribution in operating theatre. *Building and Environment*, *57*, 68–80. https://doi.org/10.1016/j.buildenv.2012.04.010

Chow, T.-T., and Yang, X.-Y. (2004). Ventilation performance in operating theatres against airborne infection: Review of research activities and practical guidance. *Journal of Hospital Infection*, *56*(2), 85–92.

Cornejo-Juárez, P., Vilar-Compte, D., Pérez-Jiménez, C., Ñamendys-Silva, S., Sandoval-Hernández, S., and Volkow-Fernández, P. (2015). The impact of hospital-acquired infections with multidrug-resistant bacteria in an oncology intensive care unit. *International Journal of Infectious Diseases*, *31*, 31–34. https://doi.org/https://doi.org/10.1016/j.ijid.2014.12.022

Davies, C. N. (1945). Definitive equations for the fluid resistance of spheres. *Proceedings of the Physical Society*, *57*(4), 259. https://doi.org/10.1088/0959-5309/57/4/301

de Lissovoy, G., Fraeman, K., Hutchins, V., Murphy, D., Song, D., and Vaughn, B. B. (2009). Surgical site infection: Incidence and impact on hospital utilization and treatment costs. *American Journal of Infection Control*, *37*, 387–397. https://doi.org/10.1016/j.ajic.2008.12.010

DIN. (2008). Din 1946-4 ventilation and air conditioning - part 4: Vac systems in buildings and rooms used in the health care sector.

Djamila, H., Chu, C.-M., and Kumaresan, S. (2014). Effect of humidity on thermal comfort in the humid tropics. *Journal of Building Construction and Planning Research*, *02*, 109–117. https://doi.org/10.4236/jbcpr.2014.22010

Ferguson, J. C., and Martin, C. J. (1991). A study of skin temperatures, sweat rate and heat loss for burned patients. http://iopscience.iop.org/0143-0815/12/4/007

Gaever, R. V., Jacobs, V. A., Diltoer, M., Peeters, L., and Vanlanduit, S. (2014). Thermal comfort of the surgical staff in the operating room. *Building and Environment*, *81*, 37–41. https://doi.org/10.1016/j.buildenv.2014.05.036

Gambogi, R., Fernández, G., Ausqui, C., Baldizzoni, M., Chifflet, L., Cichero, M., Focone, Á., Leiva, G., and Wald, I. (2020). Estándares de evaluación y seguimiento para la mejora de la calidad de los centros y servicios de alta especialización.

Greenshields, C., and Weller, H. (2022). *Notes on computational fluid dynamics: General principles*. CFD Direct Ltd.

Ho, S. H., Rosario, L., and Rahman, M. M. (2009). Three-dimensional analysis for hospital operating room thermal comfort and contaminant removal. *Applied Thermal Engineering*, *29*, 2080–2092. https://doi.org/10.1016/j.applthermaleng.2008.10.016

Limane, A., Fellouah, H., and Galanis, N. (2015). Thermo-ventilation study by openfoam of the airflow in a cavity with heated floor. *Building Simulation*, *8*(3).

Liu, Z., Liu, H., Yin, H., Rong, R., Cao, G., and Deng, Q. (2021). Prevention of surgical site infection under different ventilation systems in operating

room environment. *Frontiers of Environmental Science and Engineering*, *15*. https://doi.org/10.1007/s11783-020-1327-9

Liu, Z., Yin, D., Niu, Y., Cao, G., Liu, H., and Wang, L. (2022). Effect of human thermal plume and ventilation interaction on bacteria-carrying particles diffusion in operating room microenvironment. *Energy and Buildings*, *254*. https://doi.org/10.1016/j.enbuild.2021.111573

Lu, W., Howarth, A. T., Adamf, N., and Riffatj, S. B. (1996). Modelling and measurement of airflow and aerosol particle distribution in a ventilated two-zone chamber.

Memarzadeh, P. E. F., and Manning, A. P. (2002). Comparison of operating room ventilation systems in the protection of the surgical site.

Mičko, P., Nosek, R., Hrabovský, P., and Hečko, D. (2023). The effect of airflow velocity through a laminar airflow ceiling (lafc) on the assessment of thermal comfort in the operating room. *Applied Sciences*, *13*, 4860. https://doi.org/10.3390/app13084860

Nastase, I., Croitoru, C., Vartires, A., and Tataranu, L. (2016). Indoor environmental quality in operating rooms: An european standards review with regard to romanian guidelines. *Energy Procedia*, *85*, 375–382. https://doi.org/10.1016/j.egypro.2015.12.264

National Collaborating Centre for Women's and Children's Health (UK). (2008). *Surgical site infection clinical guideline*. www . nice . org . uk / guidance/ng125

NHS England. (2021). *Health technical memorandum 03-01 specialised ventilation for healthcare premises part a: The concept, design, specification, installation and acceptance testing of healthcare ventilation systems classification: Official publications approval reference: Par38*.

Nightingale, F. (1863). Notes on hospitals.

Openfoam. (n.d.). https://www.openfoam.com/

Schillaci, E., Vera i Fernández, J., Morozova, N., and Rigola Serrano, J. (2022). A numerical set-up for the simulation of infection probability from sars-cov-2 in public transport vehicles. *Collection of papers presented at the 8th European Congress on Computational Methods in Applied Sciences and Engineering (ECCOMAS Congress 2022)*.

Tang, J. W. (2009, December). The effect of environmental parameters on the survival of airborne infectious agents. https://doi.org/10.1098/rsif.2009.0227.focus

U S Department of Health and Human Services and Centers for Disease Control. (2019). *Guidelines for environmental infection control in healthcare facilities recommendations of cdc and the healthcare infection control practices advisory committee (hicpac)*.

Ufat, H., Kaynakli, O., Yamankaradeniz, N., and Yamankaradeniz, R. (2018). Investigation of the number of particles in an operating room at different ambient temperatures and inlet velocities. *International Journal of Ventilation*, *17*, 209–223. https://doi.org/10.1080/14733315.2017.1392107

Vonci, N., Marco, M. F. D., Grasso, A., Spataro, G., Cevenini, G., and Messina, G. (2019). Association between air changes and airborne microbial contamination in operating rooms. *Journal of Infection and Public Health*, *12*, 827–830. https://doi.org/10.1016/j.jiph.2019.05.010

Wang, C., Holmberg, S., and Sadrizadeh, S. (2018a). Numerical study of temperature-controlled airflow in comparison with turbulent mixing and laminar airflow for operating room ventilation. *Building and Environment*, *144*, 45–56.

Wang, C., Holmberg, S., and Sadrizadeh, S. (2018b). Numerical study of temperature-controlled airflow in comparison with turbulent mixing and laminar airflow for operating room ventilation. *Building and Environment*, *144*, 45–56. https://doi.org/10.1016/j.buildenv.2018.08.010

Wang, F., Permana, I., Rakshit, D., and Prasetyo, B. Y. (2021). Investigation of airflow distribution and contamination control with different schemes in an operating room. *Atmosphere*, *12*. https://doi.org/10.3390/atmos12121639

Whyte, W., Hodgson, R., and Tinkler, J. (1982). The importance of airborne bacterial contamination of wounds. *Journal of Hospital Infection*, *3*(2), 123–135.

World Health Organization. (2018). Global guidelines for the prevention of surgical site infection.

World Health Organization. (2022). *Global report on infection prevention and control*.

Yang, C., Yang, X., and Zhao, B. (2015). The ventilation needed to control thermal plume and particle dispersion from manikins in a unidirectional ventilated protective isolation room. *Building Simulation*, *8*, 551–565. https://doi.org/10.1007/s12273-014-0227-6

Zhang, Y., Cao, G., Feng, G., Xue, K., Pedersen, C., Mathisen, H. M., Stenstad, L. I., and Skogås, J. G. (2020). The impact of air change rate on the air quality of surgical microenvironment in an operating room with mixing ventilation. *Journal of Building Engineering*, *32*. https://doi.org/10.1016/j.jobe.2020.101770

Zhang, Z., and Chen, Q. (2006). Experimental measurements and numerical simulations of particle transport and distribution in ventilated rooms. *Atmospheric Environment*, *40*, 3396–3408. https://doi.org/10.1016/j.atmosenv.2006.01.014

Zhou, B., Ding, L., Li, F., Xue, K., Nielsen, P. V., and Xu, Y. (2018). Influence of opening and closing process of sliding door on interface airflow characteristic in operating room. *Building and Environment*, *144*, 459–473. https://doi.org/10.1016/j.buildenv.2018.08.050